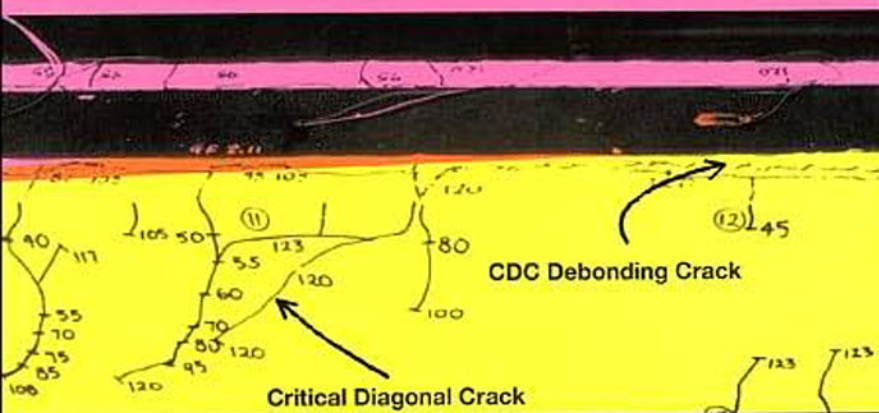
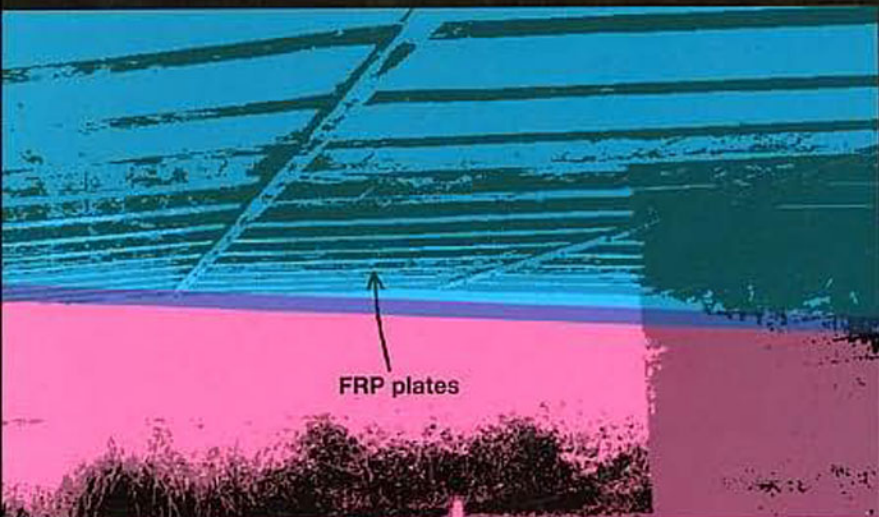




Design of FRP and Steel Plated RC Structures

Retrofitting Beams and Slabs for Strength, Stiffness and Ductility

Deric John Oehlers and Rudolf Seracino



Design of FRP and Steel Plated RC Structures

**Retrofitting Beams and Slabs for
Strength, Stiffness and Ductility**

Elsevier Internet Homepage - <http://www.elsevier.com>

Consult the Elsevier homepage for full catalogue information on all books, journals and electronic products and services.

Elsevier Titles of Related Interest

- | | |
|--|--|
| ANSON <i>et al.</i>
Advances in Building Technology (ABT2002)
ISBN: 008 044100 9 | OEHLERS & BRADFORD
Composite Steel and Concrete Structural
Members
ISBN: 008 041919 4 |
| CHAN <i>et al.</i>
Advances in Steel Structures (ICASS '02)
ISBN: 008 044017 7 | TENG
FRP Composites in Civil Engineering
ISBN: 008 043945 4 |
| FRANGOPOL <i>et al.</i>
Reliability and Optimization of Structural
Systems
ISBN: 008 042826 6 | WANG <i>et al.</i>
Shear Deformable Beams and Plates
ISBN: 008 043784 2 |
| HOLLAWAY & HEAD
Advanced Polymer Composites and Polymers in
the Civil Infrastructure
ISBN: 008 043661 7 | |

Related Journals/Products

Free specimen copy gladly sent on request. Elsevier Ltd, The Boulevard, Langford Lane, Kidlington, Oxford, OX5 1GB, UK

CAD
Composites Part A: Applied Science and Manufacturing
Composites Part B: Engineering
Composite Structures
Computer Methods in Applied Mechanics and Engineering
Computers and Structures
Construction and Building Materials
Engineering Failure Analysis
Engineering Structures
International Journal of Solids and Structures
Journal of Constructional Steel Research
Mechanics of Materials

To Contact the Publisher

Elsevier welcomes enquiries concerning publishing proposals: books, journal special issues, conference proceedings, etc. All formats and media can be considered. Should you have a publishing proposal you wish to discuss, please contact, without obligation, the publisher responsible for Elsevier's civil and structural engineering programme:

Keith Lambert Materials Science and Engineering Elsevier Ltd The Boulevard, Langford Lane Kidlington, Oxford OX5 1GB, UK	Phone: +44 1865 843411 Fax: +44 1865 843920 E-mail: k.lambert@elsevier.com
---	--

General enquiries, including placing orders, should be directed to Elsevier's Regional Sales Offices – please access the Elsevier homepage for full contact details (homepage details at the top of this page).

Design of FRP and Steel Plated RC Structures

Retrofitting Beams and Slabs for
Strength, Stiffness and Ductility

by

DERIC JOHN OEHLERS and RUDOLF SERACINO

*School of Civil and Environmental Engineering,
The University of Adelaide, Australia*



ELSEVIER

2004

Amsterdam - Boston - Heidelberg - London - New York - Oxford - Paris
San Diego - San Francisco - Singapore - Sydney - Tokyo

ELSEVIER B.V. Sara Burgerhartstraat 25 P.O. Box 211, 1000 AE Amsterdam, The Netherlands	ELSEVIER Inc. 525 B Street Suite 1900, San Diego CA 92101-4495, USA	ELSEVIER Ltd. The Boulevard Langford Lane, Kidlington, Oxford OX5 1GB, UK	ELSEVIER Ltd. 84 Theobalds Road London WC1X 8RR UK
--	--	--	---

© 2004 Elsevier Ltd. All rights reserved.

This work is protected under copyright by Elsevier Ltd., and the following terms and conditions apply to its use:

Photocopying

Single photocopies of single chapters may be made for personal use as allowed by national copyright laws. Permission of the Publisher and payment of a fee is required for all other photocopying, including multiple or systematic copying, copying for advertising or promotional purposes, resale, and all forms of document delivery. Special rates are available for educational institutions that wish to make photocopies for non-profit educational classroom use.

Permissions may be sought directly from Elsevier's Rights Department in Oxford, UK: phone (+44) 1865 843830, fax (+44) 1865 853333, e-mail: permissions@elsevier.com. Requests may also be completed on-line via the Elsevier homepage (<http://www.elsevier.com/locate/permissions>).

In the USA, users may clear permissions and make payments through the Copyright Clearance Center, Inc., 222 Rosewood Drive, Danvers, MA 01923, USA; phone: (+1) (978) 7508400, fax: (+1) (978) 7504744, and in the UK through the Copyright Licensing Agency Rapid Clearance Service (CLARCS), 90 Tottenham Court Road, London W1P 0LP, UK; phone: (+44) 20 7631 5555; fax: (+44) 20 7631 5500. Other countries may have a local reprographic rights agency for payments.

Derivative Works

Tables of contents may be reproduced for internal circulation, but permission of the Publisher is required for external resale or distribution of such material. Permission of the Publisher is required for all other derivative works, including compilations and translations.

Electronic Storage or Usage

Permission of the Publisher is required to store or use electronically any material contained in this work, including any chapter or part of a chapter.

Except as outlined above, no part of this work may be reproduced, stored in a retrieval system or transmitted in any form or by any means, electronic, mechanical, photocopying, recording or otherwise, without prior written permission of the Publisher.

Address permissions requests to: Elsevier's Rights Department, at the fax and e-mail addresses noted above.

Notice

No responsibility is assumed by the Publisher for any injury and/or damage to persons or property as a matter of products liability, negligence or otherwise, or from any use or operation of any methods, products, instructions or ideas contained in the material herein. Because of rapid advances in the medical sciences, in particular, independent verification of diagnoses and drug dosages should be made.

First edition 2004

Library of Congress Cataloging in Publication Data

A catalog record is available from the Library of Congress.

British Library Cataloguing in Publication Data

A catalogue record is available from the British Library.

ISBN: 0-08-044548-9

Ⓢ The paper used in this publication meets the requirements of ANSI/NISO Z39.48-1992 (Permanence of Paper).
Printed in The Netherlands.

Working together to grow
libraries in developing countries

www.elsevier.com | www.bookaid.org | www.sabre.org

ELSEVIER

BOOK AID
International

Sabre Foundation

Preface

Retrofitting is a major growth area in civil engineering simply because the infrastructure is forever expanding and aging and more of the available resources are being used to maintain it. Hence, it is imperative to develop inexpensive and efficient retrofitting techniques, and tests have shown that bonding longitudinal plates to the surfaces of reinforced concrete structures can be economical, efficient and unobtrusive. However, these tests have also shown that the plates can debond prematurely so that much high quality research has been done around the world on identifying and quantifying these debonding mechanics. It may be worth noting that because plated structures exhibit unique forms of failure, they should be treated as a new form of structure.

This book covers all forms of longitudinal plating reinforced concrete beams and slabs. The plates can be either adhesively bonded or bolted, they can be flat plates or of any shape and size and they can be made from any material such as steel, aluminium or any type of fibre reinforced polymer (FRP). Furthermore, the issues of premature failure and the ultimate strength and ductility which includes moment redistribution are fully addressed. The aim of this book is to provide engineers with a deep understanding of the fundamental behaviour of externally plated structures and, in particular, to provide the design tools so that they can develop their own forms of this retrofitting technique or to develop safe and efficient forms for their specific structural problem.

Chapter 1 describes the numerous forms of longitudinal plating that can be applied, and in particular the unique failure mechanisms associated with all plate materials that have to be designed against and how this affects the choice of plate and form of bonding. Intermediate crack (IC) debonding of adhesively bonded plates is the dominant form of debonding as it directly affects the choice of plate, directly affects the flexural capacity and ductility of the beam and indirectly affects the shear capacity. Hence, it is the starting point of the design procedure and is covered in Chapter 2. Having quantified the IC debonding resistance, it is used in Chapter 3 to quantify both the flexural strength and ductility of adhesively plated beams and slabs. The analysis for the flexural capacity of bolted plated beams is also covered in this chapter as well as the ability to redistribute moment. IC debonding may be considered the dominant form of debonding, but an analysis of published test results has shown that it is not the most common form of debonding which is that due to the formation of critical diagonal cracks (CDC). CDC debonding is covered in both Chapters 4 and 5 where it is shown that the addition of longitudinal plates can substantially increase the shear capacity of beams or slabs without stirrups. However, it is also shown how CDC debonding may prevent the use of adhesively bonded plates in some regions of a beam. In which case bolted plates may have to be used as this is a ductile form of retrofitting that is not affected by the formation of CDCs. The final major debonding mode, that of plate end (PE) debonding, is covered in Chapter 6. This form of debonding rarely controls or limits the design as it can be easily prevented by terminating the plate in regions of low moment. However, it does allow the designer to determine the minimum length of plate required and hence optimise the cost. Finally, comprehensive and detailed design examples are given in Chapter 7 covering virtually all forms of longitudinal plating beams and slabs. Of interest, it is shown how combinations of plating techniques often provide the best solutions, can provide

substantial increases in strength, and how moment redistribution can substantially affect the choice of plating.

It is not the object of this book to prescribe one form of plating or plating material as it is felt that this approach limits the use of plating. For example, the calculations in Chapter 7 clearly show that if the designer is restricted to using adhesively bonded FRP plates then this can severely limit the increase in strength. Whereas, combining adhesively bonded FRP plates with adhesively bonded steel plates or with bolted FRP plates can allow large increases in strength and in turn a much larger use of FRP plates. The authors feel that adhesive bonding FRP plates should typically be the first choice because of its durability and ease of application. However, adhesively bonding FRP whilst having many benefits also has some limitations. For example metal plates can be designed to yield prior to debonding which is not an option available for FRP material which is an elastic brittle material. Hence, FRP plates may have to be restricted to regions of continuous beams where moment redistribution does not occur whilst metal plates can be used in regions where moment redistribution is required. As another example, it may be determined by calculations that it is not possible to adhesively bond plates in negative moment regions of continuous beams where the vertical shear is large and hence where stirrups are required. In which case, metal or FRP plates can be bolted in these negative regions and used in conjunction with adhesively bonded FRP plates in the positive moment regions where the vertical shear is lower. It can now be seen why the object of this book is to provide generic design rules that cover all forms of longitudinal plating so that designers can choose and develop their own unique plating systems.

This book is not meant to be a code or standard; nor has it attempted to summarise the research on plating which has already been done in numerous papers and books; nor has it covered the design of the plate material as it is assumed that the plates are supplied by the manufacturers with guarantees such as against delamination within the FRP plate and durability. Instead, this book is meant to be a design guide that covers all of the major aspects of the mechanical design of plated beams and slabs. It covers the fundamental principles that govern: the major aspects of plate debonding; the shear capacity and flexural capacity of plated beams; and moment redistribution in plated beams. Furthermore, these fundamental principles are described in a form that can be applied to plates of any material, shape or position and have been described in a way that can be applied to new forms of plating such as near surface mounted plates. Near surface mounted plates have the potential to rapidly expand the use of plating due to their large strain capacities which not only provide a more efficient use of the material but more importantly provide much greater ductility. In order to try and cover all of the major aspects of design, we have had to introduce research concepts that are relatively new and in their early stages of development; in particular moment redistribution where we felt that ductility, which is often considered by structural engineers to be as important as strength and often more important, had to be covered from the fundamental principles. Having described the overall governing fundamental principles, we have developed design approaches based on advanced work on IC debonding published by others. However, we have used our own research on PE and CDC debonding as these are generic rules as they can be applied to any plate material, plate shape and plate position.

The first author has been studying plating since the mid eighties during which time he has had the privilege and enjoyment of working with and supervising some outstanding researchers, in particular Dr. M.S. Mohamed Ali Sahib and Dr. Ninh T. Nguyen whose contribution to the fundamental understanding of this field of research

has allowed this book to be written. We would also like to acknowledge with thanks the facilities made available at our University of Adelaide for the writing of this book and the invaluable support provided by Professor Kitipornchai at Hong Kong City University where the first author wrote his portion of the book whilst on study leave. Thanks also to Professor Jin-Guang Teng at Hong Kong Polytechnic University for his close collaboration and providing information and photographs, and above all and in particular the support and encouragement by our wives Bernie and Joanne.

This page is intentionally left blank

Notation

The following notation is used in this book and is first defined where first used in the text. Hence, although in general only one meaning is assigned to each symbol, in cases where more than one meaning is given then the correct one will be evident from the context in which it is used.

A_{int}	= surface area of plate/concrete interface
A_p	= cross-sectional area of plate
A_{rect}	= area of a rectangular section of plate
$(A_{rect})_{sp}$	= A_{rect} of side plate
$(A_{rect})_{tfp}$	= A_{rect} of tension face plate
A_s	= cross-sectional area of reinforcing bar; cross-sectional area of all the longitudinal reinforcing bars crossing the CDC
A_{sc}	= cross-sectional area of the compression reinforcing bars
A_{st}	= cross-sectional area of tension reinforcing bars
AUST	= Australian
BRIT	= British
$(b_{bnd})_{ang}$	= width of the bonded region in an angle bonded to the tension face
b_c	= width of concrete element; effective width of concrete element; width of RC beam; width of slab; width of web of RC beam
b_p	= width of plate
b_{sp}	= width of side plate
b_{tfp}	= width of tension face plate
CDC	= critical diagonal crack
CDC_{plated}	= CDC in plated beam
$CDC_{unplated}$	= CDC in unplated beam
CFRP	= carbon fibre reinforced polymer
c	= distance from tension reinforcing bars to tension face; reinforcing bar cover
d	= effective depth of RC beam measured from compression face
d_{ang}	= distance between angle centroid and neutral axis of cracked plated section
d_e	= depth of the position of the maximum strain in plate from the compression face
d_{na}	= depth to neutral axis from compression face
d_p	= distance of individual plate centroid from the neutral axis of the composite plated beam
d_{ps}	= perpendicular distance of prestressing tendon from focal point; lever arm of prestressing force from the compression face
d_{sp}	= distance of side plate centroid from neutral axis of plated beam
d_{tfp}	= distance of tension face plate centroid from neutral axis of plated beam
d_{ufp}	= distance of underside plate centroid from neutral axis of plated beam
d_y	= depth of the pseudo plastic concrete zone
E	= Young's modulus; material stiffness
E_a	= Young's modulus of adhesive
E_{al}	= Young's modulus of aluminium
E_{CFRP}	= Young's modulus of carbon FRP plate
E_c	= Young's modulus of concrete
$(E_c)_{long}$	= long term Young's modulus of concrete
$(E_c)_{short}$	= short term Young's modulus of concrete
E_{GFRP}	= Young's modulus of glass FRP plate

E_p	= Young's modulus of plate
E_s	= Young's modulus of steel
$(EA)_p$	= axial rigidity of plate
EI	= flexural rigidity of a beam
EI_{constant}	= results when flexural rigidity is assumed constant along beam
EI_{cr}	= flexural rigidity of cracked section
$(EI)_{\text{cr.pl}}$	= flexural rigidity of cracked plated section
EI_{crack}	= results allowing for variations of elastic flexural rigidities EI_{scr} and EI_{hcr}
$(EI_{\text{cracked}})_{\text{long}}$	= long term cracked flexural rigidity of unplated section
$(EI_{\text{cracked}})_{\text{short}}$	= short term cracked flexural rigidity of unplated section
$(EI)_{\text{creep}}$	= long term flexural rigidity of cracked plated section
EI_h	= flexural rigidity of hogging region
EI_{hcr}	= flexural rigidity of elastic cracked plated section in hogging region
EI_{hdeb}	= flexural rigidity of hogging region at plate debonding
$(EI)_{\text{hog}}$	= flexural rigidity of hogging region
$(EI)_{\text{min}}$	= minimum secant flexural rigidity
$(EI)_p$	= flexural rigidity of plate
EI_s	= flexural rigidity of sagging region
$(EI)_{\text{sag}}$	= flexural rigidity of sagging region
EI_{scr}	= flexural rigidity of elastic cracked sagging region; flexural rigidity of cracked plated section in sagging region
EI_{sdeb}	= flexural rigidity of sagging region at plate debonding
$(EI)_{\text{short}}$	= short term flexural rigidity of cracked plated section
EI_{sit}	= flexural rigidity in sagging region for iterative analysis
EI_{ep}	= flexural rigidity at plate strain ϵ_p
EI_{ec}	= flexural rigidity at concrete crushing
EUR	= European
e	= distance of $(W_{\text{da}})_{\text{cr}}$ from focal point
F	= force; resultant force
F_c	= axial force in concrete element
F_n	= resultant force normal to plate in tensile or compressive zone
F_p	= axial tensile force in plate element
$(F_{\text{plate}})_{\text{cr}}$	= force in plate resisting formation of diagonal crack
F_{ps}	= prestressing force
F_s	= axial force in steel reinforcing bars
$(F_{\text{sp}})_{\text{cr}}$	= force in side plate resisting formation of diagonal crack
F_t	= total axial tensile force
$(F_{\text{tp}})_{\text{cr}}$	= force in tension face plate resisting formation of diagonal crack
FRP	= fibre reinforced polymer
f_c	= concrete compressive cylinder strength
f_{cb}	= Brazilian tensile strength of concrete; split tensile strength of concrete; $0.53\sqrt{f_c}$
f_{CFRP}	= carbon FRP fracture stress
f_{FRP}	= FRP fracture stress
f_{GFRP}	= glass FRP fracture stress
f_s	= serviceability plate stress
f_t	= tensile strength of concrete; $0.4\sqrt{f_c}$
f_{tef}	= effective tensile strength of concrete in CDC analysis
f_y	= metal yield stress; yield strength of reinforcing bars
f_{yp}	= yield strength of metal plate

GFRP	= glass fibre reinforced polymer
HK	= Hong Kong
h	= depth of beam
$(h_{\text{bnd}})_{\text{ang}}$	= depth of portion of angle web adhesively bonded to the beam side
$(h_{\text{bnd}})_{\text{sp}}$	= depth of bonded side plate
I	= second moment of area about centroid
I_{ang}	= second moment of area of angle about angle centroid and about axis parallel to bending axis
$(I_{\text{cracked}})_{\text{long}}$	= long term second moment of area of unplated cracked section transformed to concrete
$(I_{\text{cracked}})_{\text{short}}$	= short term second moment of area of unplated cracked section transformed to concrete
$I_{\text{cr,pl}}$	= second moment of area of cracked plated section
I_{p}	= second moment of area of plate about centroid
IC	= intermediate crack
K	= coefficient in PE debonding equations
K_{M}	= parameter of stress resultants at datum point in CDC analysis; moment factor $M_{\text{dat}}/V_{\text{dat}}$
K_{W}	= parameter for applied loads in CDC analysis; load factor $W_{\text{dat}}/V_{\text{dat}}$
$(K_{\text{W}})_{\text{sag}}_{\text{udl}}$	= K_{W} for sagging region in encastre beam with uniformly distributed load with datum at point of contraflexure
$(K_{\text{W}})_{\text{hog}}_{\text{udl}}$	= K_{W} for hogging region in encastre beam with uniformly distributed load with datum at point of contraflexure
k_{u}	= neutral axis depth factor; d_{na}/d
L	= beam span; length of hogging or sagging region; lever arm
L_{anch}	= length of plate required for anchorage approach
L_{CDC}	= length of plate required from CDC analysis
L_{e}	= effective length; minimum length of plate required for full anchorage; minimum anchorage length l_{p} to achieve maximum debonding axial force $(P_{\text{IC}})_{\text{max}}$; full anchorage length
L_{flex}	= length of plate required for flexure
L_{h}	= length of hogging region
L_{hinge}	= hinge length
L_{hog}	= length of hogging region
L_{o}	= length of shear span in CDC analysis; length of free body in CDC analysis
L_{p}	= anchorage length of plate from CDC
L_{pl}	= length of plate per half span
$(L_{\text{p}})_{\text{tfp}}$	= anchorage length of tension face plate
L_{PE}	= length of plate required for PE debonding analysis
L_{poc}	= distance of point of contraflexure from nearest support
L_{rect}	= lever arm from the centroid of the rectangular section to the compression face
$(L_{\text{rect}})_{\text{sp}}$	= L_{rect} side plate
$(L_{\text{rect}})_{\text{tfp}}$	= L_{rect} tension face plate
L_{s}	= length of sagging region
L_{sag}	= length of sagging region
$L_{\text{sh-sp}}$	= length of plate in shear span
l_{b}	= bonded length of plate
M	= moment
M_{beam}	= constant moment in beam
M_{cap}	= moment capacity; maximum moment that can be obtained

$(M_{cap})_{fi}$	= moment capacity from a full interaction analysis
$(M_{cap})_{pi}$	= moment capacity allowing for partial interaction
M_{creep}	= moment due to long term loads and sustained live loads that induce creep
M_{dat}	= moment at datum point
$(M_{dat})_{applied}$	= applied moment at datum point
$(M_{dat})_{cr}$	= moment at datum point when a diagonal crack forms and when $(V_{dat})_{cr}$ is acting
$(M_{dat})_h$	= moment at datum point in the hogging region
$(M_{dat})_{hog}$	= moment at datum point in the hogging region
$(M_{dat})_s$	= moment at datum point in the sagging region
$(M_{dat})_{sag}$	= moment at datum point in the sagging region
$M_{elastic}$	= elastic moment based on constant EI
M_h	= hogging moment; maximum hogging moment; hogging moment at the support
$(M_h)_{Elcracked}$	= hogging moment based on a beam with varying elastic EI of EI_{scr} and EI_{hcr}
$(M_h)_{el}$	= elastic hogging moment
$(M_h)_{test}$	= hogging moment in test
$(M_h)_{pl}$	= hogging moment capacity of plated section
$(M_h)_u$	= ultimate strength of hogging section; ultimate strength of unplated hogging section
M_{hu}	= ultimate strength of hogging section; ultimate strength of plated hogging section
$(M_h)_{un}$	= maximum hogging moment capacity of unplated section
$(M_h)_{u-max}$	= maximum possible hogging moment based on moment redistribution
$(M_h)_{u-plated}$	= moment capacity of plated hogging section
M_{hog}	= moment at supports; maximum hogging moment
$(M_{hog})_{res}$	= support moment to cause residual strains
$(M_{hog})_u$	= hogging moment capacity
M_{max}	= maximum applied moment in beam
M_p	= moment in plate
M_{PE}	= PE debonding capacity
$(M_{PE})_{ang.sp}$	= PE debonding capacity for angle plate beam bonded to the side face of the beam
$(M_{PE})_{ang.tfp}$	= PE debonding capacity for angle plate beam bonded to the tension face of the beam
$(M_{PE})_{cfp}$	= PE debonding capacity for compression face plates
$(M_{PE})_{sp}$	= PE debonding capacity for a side plate beam
$(M_{PE})_{tfp}$	= PE debonding capacity for a tension face plated beam
$(M_{PE})_{ufp}$	= PE debonding capacity for underside of flange plates
M_{plate}	= moment in plate
M_s	= sagging moment; maximum sagging moment
$(M_s)_{el}$	= elastic sagging moment
$(M_s)_{pl}$	= sagging moment capacity of plated section
M_{sag}	= moment at mid-span; maximum sagging moment
$(M_{sag})_u$	= sagging moment capacity
M_{short}	= moment at plate end due to short term loads; moment due to short term loads
M_{static}	= static moment
$(M_{static})_{plated}$	= static moment capacity of plated beam
$(M_{static})_{res}$	= static moment to cause residual strains

$(M_{static})_u$	= theoretical maximum static moment when hogging and sagging sectional capacities achieved
$(M_{static})_{unplated}$	= static moment capacity of unplated beam
$(M_{st})_{pl}$	= static moment capacity of plated beam
$(M_{st})_{un}$	= static moment capacity of unplated beam
$(M_s)_{test}$	= sagging moment in test
M_{su}	= ultimate strength of sagging section; ultimate strength of unplated sagging section
$(M_s)_{un}$	= maximum sagging moment capacity of unplated section
$(M_s)_{u-max}$	= maximum possible sagging moment based on moment redistribution
$(M_s)_{u-plated}$	= moment capacity of plated sagging section
$(M_s)_{un}$	= sectional strength of unplated sagging region
M_{sp}	= moment in side plate
$(M_s)_{pl}$	= moment capacity of plated section in sagging region
M_{tfp}	= moment in tension face plate
M_u	= ultimate moment capacity
$(M_u)_{pl}$	= flexural capacity of plated section
M_x	= variation of applied moment along length of beam
ΔM	= percentage increase in moment capacity due to plating
ΔM_{cap}	= increase in flexural capacity due to plating
ΔM_{st}	= increase in static moment due to plating
m_{long}	= long term modular ratio E_s/E_c
m_p	= modular ration of the plate material stiffness to that of the concrete; E_p/E_c
m_s	= modular ratio E_s/E_c
m_{short}	= short term modular ratio E_s/E_c
%MR	= percentage moment redistribution
N_{long}	= number of bolts in a shear span to resist P_{plate}
N_{vert}	= number of bolts in a shear span to resist the vertical forces induced by M_{plate}
$(n_{crack})_{long}$	= long term elastic neutral axis depth of unplated cracked section
$(n_{crack})_{short}$	= short term elastic neutral axis depth of unplated cracked section
P	= applied load
P_{bar}	= tensile axial force in reinforcing bar
P_{dowel}	= shear transferred by dowel action
P_{IC}	= IC debonding resistance of plate; IC debonding force; $A_p\sigma_{IC}$
$(P_{IC})_{max}$	= maximum IC debonding resistance of fully anchored plate
$P_{IC-tooth}$	= contribution to plate force from an individual concrete tooth
P_{inter}	= compressive force across crack interface; passive normal force; passive compressive interface force
P_p	= axial force in plate
$(P_p)_{max}$	= maximum IC debonding resistance
P_{plate}	= axial force in plate in a beam to cause IC debonding; axial force in plate; maximum force in plate in CDC analysis
$(P_{plate})_{cfp}$	= axial force in compression face plate
$(P_{plate})_{sp}$	= axial force in side plate
$(P_{plate})_{tfp}$	= axial force in tension face plate
$P_{pull-test}$	= IC debonding resistance measured from a pull-push test
P_{sh}	= shear capacity of a single bolt in a bolted plated joint
P_{sp}	= axial force in side plate
$P_{stirrup}$	= axial force in internal steel stirrup
P_{tfp}	= axial force in tension face plate

P_u	= fracture capacity of FRP plate; $A_p f_{FRP}$
P_y	= yield capacity of metal plate; $A_p f_{yp}$
PE	= plate end
RC	= reinforced concrete
t_a	= thickness of adhesive layer
t_{cfp}	= thickness of compression face plate
t_p	= plate thickness
t_{sp}	= side plate thickness
t_{tfp}	= tension face plate thickness
$(t_{tfp})_{ang}$	= plate thickness of angle flange attached to tension face
t_{ufp}	= thickness of plate at underside of flange
udl	= uniformly distributed load
V	= vertical shear force
$V_{applied}$	= applied shear load
$V_{Ay/lb}$	= elastic interface shear stress; VQ/It
V_c	= shear capacity of unplated beam or slab without stirrups; concrete component of the shear capacity
$(V_c)_{code}$	= concrete component of the shear capacity of unplated beams from national standards
V_{conc}	= resistance to shear across diagonal crack
$(V_{conc})_{code}$	= resistance to shear across critical diagonal crack in a plated beam based on code concrete shear resistance
$(V_{conc})_{pl}$	= shear capacity at the weakest or critical diagonal crack in a plated beam
$(V_{conc})_{sp}$	= shear capacity of side plated beam
$(V_{conc})_{tfp}$	= shear capacity of tension face plated beam
$(V_{conc})_{un}$	= shear capacity at the weakest or critical diagonal crack in an unplated beam; concrete component of the shear capacity V_c
$V_{c-plate}$	= shear capacity of plated beam or slab without stirrups; V_c enhanced by plating; shear load to cause CDC debonding
V_{cr}	= shear load to cause cracking
V_{c-unpl}	= concrete shear capacity of unplated beam
V_{dat}	= shear load at any convenient datum point
$(V_{dat})_{applied}$	= design applied shear load at datum point; shear at datum point due to applied loads
$(V_{dat})_c$	= shear load at datum point to cause shear failure in a beam without stirrups; shear load at datum point to cause the critical diagonal crack
$(V_{dat})_{c-mean}$	= shear load at datum point to cause the critical diagonal crack in an unplated beam based on mean approach
$(V_{dat})_{c-plate}$	= shear load at datum point to cause shear failure in a plated beam without stirrups; shear load at datum point to cause CDC debonding
$((V_{dat})_{c-plate})_{full}$	= shear load at datum point to cause shear failure in a fully plated beam without stirrups; shear load at datum point to cause CDC debonding in a fully plated anchored beam
$(V_{dat})_{c-plate-mean}$	= shear load at datum point to cause the critical diagonal crack in a plated beam based on mean approach
$(V_{dat})_{c-unpl}$	= shear load at datum point to cause shear failure in an unplated beam
$(V_{dat})_{cr}$	= vertical shear load at datum point when diagonal crack forms; shear at datum point to cause cracking in unplated beam
$(V_{dat})_{crack}$	= shear load at the datum point to cause a diagonal crack
$[(V_{dat})_{crack}]_{mean}$	= shear load at datum point to cause a diagonal crack based on mean approach
$[(V_{dat})_{crack}]_{pl}$	= shear load at the datum point to cause a diagonal crack in a plated beam

$[(V_{\text{dat}})_{\text{crack}}]_{\text{un}}$	= shear load at the datum point to cause a diagonal crack in an unplated beam
$(V_{\text{dat}})_{\text{crit}}$	= shear load at datum point to cause crack sliding in the critical, that is weakest, diagonal crack
$[(V_{\text{dat}})_{\text{crit}}]_{\text{mean}}$	= shear load at the datum point to cause a critical diagonal crack in a plated beam based on the mean approach
$[(V_{\text{dat}})_{\text{crit}}]_{\text{mean}}^{\text{pl}}$	= shear load at the datum point to cause crack sliding in a fully plate fully anchored beam based on the mean approach
$[(V_{\text{dat}})_{\text{crit}}]_{\text{mean}}^{\text{un}}$	= shear load at the datum point to cause crack sliding in an unplated beam based on the mean approach
$[(V_{\text{dat}})_{\text{crit}}]_{\text{pl}}$	= shear load at the datum point to cause a critical diagonal crack in a plated beam; shear load at datum point to cause CDC debonding
$[(V_{\text{dat}})_{\text{crit}}]_{\text{un}}$	= shear load at the datum point to cause a critical diagonal crack in an unplated beam; shear load at datum point to cause the concrete component of shear failure
$(V_{\text{dat}})_{\text{cr-plate}}$	= shear load at the datum point to cause cracking in the plated beam
$((V_{\text{dat}})_{\text{cr-plate}})_{\text{hog}}$	= shear load at the datum point to cause cracking in the plated beam in the hogging region
$((V_{\text{dat}})_{\text{cr-plate}})_{\text{sag}}$	= shear load at the datum point to cause cracking in the plated beam in the sagging region
$(V_{\text{dat}})_{\text{h}}$	= shear load at datum point in hogging region
$(V_{\text{dat}})_{\text{hog}}$	= shear load at datum point in hogging region
$(V_{\text{dat}})_{\text{mean}}$	= mean of $(V_{\text{dat}})_{\text{cr-plate}}$ and $(V_{\text{dat}})_{\text{u-pres/metal}}$
$((V_{\text{dat}})_{\text{poc}})_{\text{udl}}$	= shear load at point of contraflexure for uniformly distributed load in encastre beam
$(V_{\text{dat}})_{\text{s}}$	= shear load at datum point in sagging region
$(V_{\text{dat}})_{\text{sag}}$	= shear load at datum point in sagging region
$(V_{\text{dat}})_{\text{slide}}$	= shear at datum point to cause crack sliding
$[(V_{\text{dat}})_{\text{slide}}]_{\text{mean}}$	= shear load at the datum point to cause crack sliding in a plated beam based on mean approach
$[(V_{\text{dat}})_{\text{slide}}]_{\text{pl}}$	= shear load at the datum point to cause crack sliding in a plated beam
$[(V_{\text{dat}})_{\text{slide}}]_{\text{un}}$	= shear load at the datum point to cause crack sliding in an un plated beam
$(V_{\text{dat}})_{\text{strength}}$	= shear at datum point to cause failure
$(V_{\text{dat}})_{\text{u}}$	= shear load at datum point to cause shear failure across a diagonal crack; shear load at the datum point to cause crack sliding across a diagonal crack; shear load at datum point to cause crack sliding in unplated beam
$(V_{\text{dat}})_{\text{u-metal}}$	= shear load at datum point to cause shear failure across a diagonal crack based on longitudinal reinforcement approach
$((V_{\text{dat}})_{\text{u-metal}})_{\text{sag}}$	= shear load at datum point to cause crack sliding in a metal tension face plated beam in the sagging region based on the longitudinal reinforcement approach
$((V_{\text{dat}})_{\text{u-metal}})_{\text{hog}}$	= shear load at datum point to cause crack sliding in a metal tension face plated beam in the hogging region based on the longitudinal reinforcement approach
$(V_{\text{dat}})_{\text{u-plate}}$	= shear load at datum point to cause crack sliding in a plated beam
$(V_{\text{dat}})_{\text{u-pres}}$	= shear load at datum point to cause shear failure across a diagonal crack based on passive prestress approach
$(V_{\text{dat}})_{\text{u-pres/metal}}$	= refers to both $(V_{\text{dat}})_{\text{u-pres}}$ and $(V_{\text{dat}})_{\text{u-metal}}$
$((V_{\text{dat}})_{\text{u-pres}})_{\text{hog}}$	= shear load at datum point to cause crack sliding in the hogging region based on the passive prestress approach
$((V_{\text{dat}})_{\text{u-pres}})_{\text{sag}}$	= shear load at datum point to cause crack sliding in the sagging region based on the passive prestress approach
$(V_{\text{incr}})_{\text{pp}}$	= increase in the shear capacity due to passive prestress

V_{\max}	= maximum applied shear in a beam
$(V_{\max})_{Lo}$	= maximum applied shear force at the focal point; distribution of shear due to the applied load
V_p	= volume of plate
V_{plate}	= vertical force in couple to resist M_{plate}
$(V_{pp})_{ACI}$	= concrete component of the shear capacity in a prestressed beam based on ACI approach
$(V_{pp})_{Euro}$	= concrete component of the shear capacity in a prestressed beam based on the Eurocode
V_s	= shear resisted by the internal steel stirrups
$(V_{stirrup})_{transverse}$	= shear resisted by external transverse plates
$(V_{stirrup})_{pl}$	= total shear resisted by internal and external stirrups
V_u	= shear capacity across a diagonal crack; equal to V_c for the CDC in an unplated beam
$V_{u-plate}$	= shear capacity across a diagonal crack in a plated beam
ΔV_{conc}	= increase in the concrete component of the shear capacity due to plating
$(\Delta V_{conc})_{pl}$	= increase in the concrete component of the shear capacity due to plating
$\Delta V_{c-plate}$	= increase in V_c due to plating; increase in the concrete component of the shear capacity due to plating
-ve	= negative; hogging
+ve	= positive; sagging
W_{dat}	= applied load acting on free body in CDC analysis; portion of the applied load, that induces V_{dat} , that is acting on the free body
$(W_{dat})_{cr}$	= resultant of applied loads acting on free body when $(V_{dat})_{cr}$ is acting in deriving the load to cause cracking
$(W_{dat})_h$	= applied load acting on free body in hogging region in CDC analysis
$(W_{dat})_{h\&s}$	= applied load acting on free body that crosses both the hogging and sagging regions in CDC analysis
$(W_{dat})_s$	= applied load acting on free body in sagging region in CDC analysis
$(W_{dat})_u$	= resultant of applied loads acting on free body when $(V_{dat})_u$ is acting in deriving the load to cause crack sliding
w	= uniformly distributed load
w_{fail}	= uniformly distributed load to cause failure
x	= distance from free edge of pull-push specimen; distance from loaded end of concrete prism; horizontal projection of CDC; distance from nearest support
y	= distance from axial force to compression face
z	= distance of focal point from point of contraflexure
α	= coefficient of IC debonding resistance equation
β	= parameter defining position of transition strain ϵ_e
β_p	= plate width parameter $f(b_p/b_c)$
β_L	= plate length parameter $f(l_p/L_c)$
χ	= curvature
χ_{add}	= additional curvature applied after plating adjacent to plate end
χ_c	= curvature at concrete crushing
χ_{cap}	= curvature capacity
$(\chi_c)_{max}$	= maximum curvature when concrete crushing controls
χ_{creep}	= additional curvature applied after plating adjacent to plate end due to concrete creep due to long term loads
$(\chi_{creep})_{plate}$	= creep curvature that occurs after plating
χ_{deb}	= curvature at plate debonding
χ_{max}	= maximum curvature; curvature capacity

χ_{PE}	= curvature to cause PE debonding in an individual plate; PE debonding curvature capacity
χ_{plate}	= curvature in plate
$(\chi_p)_{max}$	= maximum curvature when plate failure controls
χ_{RC}	= curvature in RC beam
χ_{short}	= additional curvature applied after plating adjacent to plate end due to short term loads
$(\chi_{short})_{plate}$	= short term curvature that occurs after plating
χ_{shrink}	= additional curvature applied after plating adjacent to plate end due to concrete shrinkage
$(\chi_{shrink})_{code}$	= shrinkage curvature from national standards
$(\chi_{shrink})_{plate}$	= shrinkage curvature that occurs after plating
χ_u	= curvature at end of plastic plateau; ultimate curvature capacity
χ_y	= curvature at onset of plastic plateau
δ	= deflection
δ_f	= interface slip when τ_{int} reduces to zero
δ_{IC}	= end slip between concrete and plate at loaded end of concrete prism in pull-push specimen; interface slip at intermediate crack
δ_{int}	= interface slip
ϵ	= strain
ϵ_b	= maximum strain in tension reinforcing bar
ϵ_{bar}	= strain in reinforcing bar; strain in reinforcing bars at plate debonding
$(\epsilon_{bar})_{propped}$	= strain in tension reinforcing bar in a propped analysis
$(\epsilon_{bar})_{unpropped}$	= strain in tension reinforcing bar in unpropped analysis
$(\epsilon_{bar})_{res}$	= residual strain in tension reinforcing bar in an unpropped analysis; strain in bar prior to plating
ϵ_c	= concrete crushing strain
$(\epsilon_c)_{max}$	= maximum strain in the concrete at plate debonding; maximum strain in concrete
$(\epsilon_{comp,edge})_{res}$	= residual strain in the concrete adjacent to the compression edge of the plate
ϵ_{CFRP}	= strain at which carbon FRP material fractures
ϵ_{db}	= plate IC debonding strain; IC debonding strain capacity of plate
$(\epsilon_{db})_{anch}$	= IC debonding strain in anchorage approach
ϵ_{deb}	= experimental plate IC debonding strain
ϵ_c	= strain in concrete at transition from elastic to plastic zone
ϵ_f	= maximum plate strain; strain capacity of plate
ϵ_{fract}	= plate fracture strain
ϵ_{FRP}	= FRP strain capacity; strain at which FRP material fractures
ϵ_{GFRP}	= strain at which glass FRP material fractures
ϵ_{IC}	= axial strain in plate at IC debonding
ϵ_p	= plate strain
ϵ_{p-bot}	= strain at bottom edge of plate
ϵ_{p-top}	= strain at top edge of plate
ϵ_{pivot}	= pivotal strain
$(\epsilon_{pivot})_{RC}$	= pivotal strain in the reinforced concrete; pivotal strain in RC beam adjacent to plate that debonds
$(\epsilon_{pivot})_{res}$	= residual strain in the concrete prior to plating at the level of the future pivotal point
ϵ_{pmax}	= maximum strain in plate
ϵ_{rebar}	= fracture strain of reinforcing bar
ϵ_{res}	= residual strain at tension face

ϵ_s	= strain in tension reinforcing bars
ϵ_{sh}	= concrete shrinkage strain; concrete shrinkage strain after plating
ϵ_{sp}	= strain at centroid of side plate
ϵ_{tfp}	= strain at centroid in tension face plate
ϵ_y	= yield strain of steel; yield strain of reinforcing bar
γ	= depth of rectangular stress block factor
γ_0	= cohesive effectiveness factor in shear to resist crack sliding
λ	= coefficient in cohesive effectiveness factor γ_0 ; 1.6
θ	= inclination of the CDC
θ_{hinge}	= hinge rotation
θ_{mean}	= inclination of CDC crack used in mean approach
ρ	= area of all the longitudinal reinforcing bars as a proportion of the cross-sectional area of the concrete element; % longitudinal reinforcing bars; longitudinal reinforcing bar function
ρ_{eq}	= equivalent area of longitudinal reinforcing bar in Blaschko's approach
ρ_{plate}	= longitudinal reinforcement approach function
σ	= stress
σ_{db}	= axial stress at IC debonding
σ_{IC}	= axial stress in plate at IC debonding
σ_n	= stress at interface normal or perpendicular to interface
$\sigma_{p,IC}$	= stress in plate at intermediate crack
σ_{ps}	= mean stress in concrete element due to prestress F_{ps}
σ_{pp}	= mean stress in concrete due to passive prestress of plate
τ	= interface shear stress
τ_f	= peak interface shear stress
τ_{int}	= interface shear stress between plate and concrete
τ_{Rd}	= basic design shear strength in Eurocode

subscripts:

ang	= angle
conc	= shear capacity at formation of weakest or critical diagonal crack
crack	= formation of a diagonal crack
crit	= weakest critical diagonal crack relative to applied shear
cfp	= compression face plate
dat	= datum point
p	= plate
pl	= plated
slide	= rigid body displacement; crack sliding
sp	= side plate
tfp	= tension face plate; tension face plated
un	= unplated

Contents

Preface	v
Notation	ix
Chapter 1: Introduction	1
1.1 Introduction	1
1.2 Forms of plating beams and slabs	2
1.2.1 Bonding or joining techniques	2
1.2.1.1 Bolted and adhesively bonded plates	2
1.2.1.2 Wrapping and mechanical end anchorage	3
1.2.2 Plate position	4
1.2.2.1 Tension face plates	4
1.2.2.2 Side plates	5
1.2.2.3 Compression face plates	5
1.2.3 Plate shapes	6
1.3 Major debonding mechanisms in adhesively bonded plates	6
1.3.1 Intermediate crack (IC) debonding	7
1.3.2 Critical diagonal crack (CDC) debonding	8
1.3.3 Plate end (PE) debonding	10
1.3.4 Interface shear stress (V_{ay}/I_b) debonding	10
1.3.5 Desired form of flexural failure	11
1.3.6 Summary of common debonding mechanisms	12
1.4 Failure of bolted plates	14
1.5 Plate material and geometry	14
1.5.1 Adhesively bonded plates	14
1.5.2 Bolted plates	16
1.6 Commentary of design guides for longitudinal plating	17
1.6.1 Scope of comparison	17
1.6.2 Australian approach	18
1.6.3 Adhesively bonded FRP tension face plate structures	19
1.7 Conclusions	22
1.8 References	22
Chapter 2: Intermediate Crack (IC) Debonding	24
2.1 Introduction	24
2.2 Examples of IC debonding	25
2.2.1 Adhesively bonded longitudinal plates predominantly in flexure	25
2.2.1.1 Tension face plates	25
2.2.1.2 Side plates	26
2.2.2 Adhesively-bonded and bolted longitudinal plates predominantly in flexure	27
2.2.3 IC debonding resistance contribution to vertical shear	28
2.3 IC debonding behaviour	29
2.3.1 IC debonding in pull-push tests	29
2.3.1.1 Pull-push tests	29
2.3.1.2 Global interface behaviour	30

2.3.1.3 Local and fundamental partial-interaction interface behaviour	31
2.3.2 IC debonding in beams	34
2.3.2.1 IC interface crack propagation	34
2.3.2.2 IC interface crack propagation simulations	36
2.4 Comparison of IC debonding rules	37
2.4.1 Effective length or anchorage length concept	37
2.4.2 Effective width concept	37
2.4.3 IC debonding resistances	38
2.4.4 Comparison of IC debonding resistances	40
2.5 IC debonding design philosophies	41
2.5.1 Anchorage design philosophy	42
2.5.2 Hinge design philosophy	43
2.6 Conclusions	44
2.7 References	45
Chapter 3: Flexural Strength and Ductility	46
3.1 Introduction	46
3.2 Ductility	46
3.2.1 Material ductility	46
3.2.2 Sectional ductility	47
3.2.2.1 Moment/curvature	47
3.2.2.2 Maximum curvatures	48
3.2.2.3 Moment/strains	49
3.2.3 Beam ductility	51
3.2.3.1 Moment/deflection	52
3.2.3.2 Moment redistribution concept	53
3.2.3.3 Moment redistribution capacity	55
3.3 Moment redistribution capacities	58
3.3.1 Neutral axis depth approach	58
3.3.2 Flexural rigidity approach	61
3.3.3 Examples of moment redistribution capacities	64
3.3.4 Plating design considerations	68
3.3.4.1 Moment redistribution in unplated beams	69
3.3.4.2 Moment redistribution in plated beams	71
3.4 Sectional flexural strength and ductility capacity	74
3.4.1 Propped structure	75
3.4.1.1 Unplated section	75
3.4.1.2 Adhesively bonded tension face plated beams	76
3.4.1.3 Adhesively bonded shallow FRP side plated beams	78
3.4.1.4 Adhesively bonded deep metal side plated beams	79
3.4.1.5 Bolted side plated beams	80
3.4.2 Unpropped structure	83
3.4.2.1 Adhesively bonded tension face plated beam	83
3.4.2.2 Adhesively bonded side plated beam	85
3.5 Analyses and parametric studies	85
3.5.1 Slab structure with adhesively bonded FRP plates in sagging region	86
3.5.1.1 Slab specifications	86
3.5.1.2 Moment redistribution	87
3.5.1.3 Propped flexural analysis	88
3.5.1.4 Unpropped flexural analysis	90

3.5.2 Beam structure with adhesively bonded plates	90
3.5.2.1 Beam specification	90
3.5.2.2 Tension face plates on underside of flange in hogging region	91
3.5.2.3 Side plates over full depth of web in hogging region	92
3.5.3 Beam structure with bolted plates	93
3.5.3.1 Full interaction flexural analysis	93
3.5.3.2 Bolt forces	94
3.5.4 Moment redistribution in metal plated hinges: flexural rigidity approach	95
3.6 Conclusions	99
3.7 References	99
Chapter 4: CDC Debonding of Tension Face Plates	100
4.1 Introduction	100
4.2 CDC debonding mechanism	101
4.2.1 CDC debonding mechanism	101
4.2.2 Examples of CDC debonding of tension face plates	103
4.3 Concrete shear capacity of unplated beams or slabs	104
4.3.1 Critical diagonal cracks in RC beams	105
4.3.2 Qualitative description of CDC analysis	106
4.3.3 Zhang's iterative approach	107
4.3.3.1 Vertical shear to cause cracking	108
4.3.3.2 Vertical shear to cause crack sliding	109
4.3.3.3 Concrete shear capacity of RC beams and slabs	111
4.4 CDC debonding of tension face plate	111
4.4.1 Iterative CDC analysis	112
4.4.1.1 Position of diagonal crack focal and datum points	112
4.4.1.2 Shear to cause cracking of tension face plated sections	114
4.4.1.3 Shear to cause crack sliding in tension face plated sections – longitudinal reinforcement approach	116
4.4.1.4 Shear to cause crack sliding in tension face plated sections – passive prestress approach	117
4.4.1.5 Shear capacity analysis	118
4.4.2 Design approach for CDC debonding	120
4.4.2.1 CDC design procedure in hinge approach	121
4.4.2.2 CDC design procedure in anchorage approach	123
4.5 Direct CDC debonding analysis	124
4.5.1 Mean approach	125
4.5.1.1 Development of mean approach procedure	125
4.5.1.2 Mean approach analysis	127
4.5.2 Prestressed code approach	128
4.5.3 Comparison with guidelines	129
4.6 Results of CDC analyses	130
4.6.1 Hinge approach with FRP plates in hogging region of beam	130
4.6.2 Anchorage approach with steel plates in sagging region of slab	132
4.7 References	135
Chapter 5: Generic Rules for CDC Debonding	137
5.1 Introduction	137
5.2 Generic CDC debonding analysis	138
5.2.1 Iterative approach	139

5.2.1.1 Shear to cause cracking	141
5.2.1.2 Shear to cause crack sliding	142
5.2.1.3 Critical diagonal crack	144
5.2.1.4 Simplifications	145
5.2.1.5 Interpretation of CDC analysis results	147
5.2.2 Direct approaches	149
5.2.2.1 Mean approach	150
5.2.2.2 Prestressed code approach	151
5.3 Generic design approach for CDC debonding	151
5.3.1 Basic analyses	151
5.3.2 Shear load at datum point V_{dat} to cause CDC debonding	152
5.3.3 Shear capacity V_{conc} to cause CDC debonding	154
5.3.4 Further extension of plate	154
5.4 Further plate combinations and positions	155
5.4.1 Angle and U-sections	155
5.4.2 Short side plates	156
5.4.3 Compression face plates	156
5.5 Enhancement of shear capacity	158
5.5.1 Increase in shear capacity attained by longitudinal plating	158
5.5.2 Shear enhancement design philosophy	160
5.6 Analysis	162
5.6.1 Hinge approach with full depth steel plates in sagging region of beam	162
5.7 References	164
Chapter 6: Plate End (PE) Debonding	165
6.1 Introduction	165
6.2 PE debonding mechanism	165
6.2.1 PE debonding mechanism	165
6.2.1.1 Tension face plates	166
6.2.1.2 Compression face plates	167
6.2.1.3 Side plate with centroid in tensile zone	167
6.2.1.4 Side plate with centroid in compression zone	167
6.2.2 Examples of PE debonding	168
6.2.2.1 Plates bonded to horizontal surfaces	168
6.2.2.2 Plates bonded to vertical surfaces	169
6.3 Generic PE debonding analysis	171
6.3.1 PE debonding curvature capacity	171
6.3.2 Plate end applied curvature	171
6.3.3 Plate end debonding design	172
6.3.3.1 PE curvature capacity and applied curvature	172
6.3.3.2 PE debonding design for short term loads	173
6.3.3.3 PE debonding design for long term effects	174
6.4 PE analysis for bonded interface perpendicular to bending axis	174
6.4.1 Angle plates	175
6.4.2 Side plates	175
6.5 PE analysis for bonded interface parallel to bending axis	176
6.5.1 Angle plates	176
6.5.2 Tension face plates	177
6.5.2.1 Basic analysis	177
6.5.2.2 Comparison of PE debonding rules for tension face plates	177

6.5.3 Compression face plates	178
6.6 Design for PE debonding	179
6.6.1 Generic design approach	179
6.6.2 Interaction between PE, IC and CDC debonding	180
6.7 Examples	181
6.8 References	182
Chapter 7: Design Examples	183
7.1 Introduction	183
7.2 Summary of design procedure	184
7.2.1 Design philosophies available	184
7.2.1.1 Anchorage approach	184
7.2.1.2 Hinge approach	185
7.2.2 Design steps	186
7.2.3 Occurrence of IC, CDC and PE debonding	187
7.3 Continuous slab structure with adhesively bonded plates	189
7.3.1 Detailed slab specifications	189
7.3.1.1 Slab structure	189
7.3.1.2 Reinforced concrete material properties	190
7.3.1.3 Unplated slab mechanical properties	190
7.3.1.4 Plate material properties	191
7.3.2 Plating +ve region only (redistribution from unplated -ve region)	192
7.3.2.1 Strengthening option based on moment redistribution	192
7.3.2.2 Option 1: Hinge approach, FRP plates in sagging region	194
7.3.2.3 Option 2: Anchorage approach, FRP plates in sagging region	196
7.3.2.4 Option 3: Hinge approach, steel plates in sagging region	197
7.3.2.5 Comparison of plating procedures	198
7.3.3 Plating -ve region only (redistribution from unplated +ve region)	199
7.3.3.1 Strengthening option based on moment redistribution	199
7.3.3.2 Option 4: Hinge approach, FRP plates in hogging region	201
7.3.3.3 Option 5: Anchorage approach, FRP plates in hogging region	202
7.3.3.4 Comparison of plating procedures	203
7.3.4 Plating -ve and +ve regions (redistribution from -ve region)	203
7.3.4.1 Strengthening option based on moment redistribution	203
7.3.4.2 Option 6: Steel plating hogging region – hinge approach	204
7.3.4.3 Option 7: FRP plating sagging region – hinge approach	206
7.3.4.4 Moment redistribution based on flexural rigidity approach	206
7.3.5 Summary of all plated slab options	207
7.4 Continuous beam structure with adhesively bonded plates	208
7.4.1 Detailed beam specifications	209
7.4.1.1 Beam structure	209
7.4.1.2 Reinforced concrete material properties	210
7.4.1.3 Unplated beam mechanical properties	210
7.4.1.4 Plate material properties	210
7.4.2 Hinge approach: FRP side plates in +ve and tension face plates in -ve regions	210
7.4.2.1 Strengthening option	210
7.4.2.2 Option 8: Hinge approach, FRP side plates in sagging region	210
7.4.2.3 Option 9: Hinge approach, FRP tension face plates in hogging region	213

7.4.3 Hinge approach: steel side plates in +ve and -ve regions	215
7.4.3.1 Strengthening option	215
7.4.3.2 Option 10: Hinge approach, steel side plates in hogging region	215
7.4.3.3 Option 11: Hinge approach, steel side plates in sagging region	217
7.5 Continuous beam structure with bolted plates	218
7.5.1 Detailed beam specifications	218
7.5.2 Option 12: Side plates bolted to tension zone in hogging region	218
7.5.3 Option 13: Deep side plates bolted in hogging region	221
7.6 References	222
Index	223

Chapter 1: Introduction

1.1 Introduction

Existing reinforced concrete structures are often in need of strengthening, stiffening, improving the ductility or repair. A common form of retrofitting is to adhesively bond plates or sheets to the surfaces. However, tests have shown that these plates are prone to premature debonding, as has occurred to the tension face plate in Fig.1.1, which can inhibit the use of this retrofitting technique. The aims of this book are to:

- provide a comprehensive overview of all types and forms of plating
- provide an insight into the various plate debonding or peeling mechanisms
- compare, comment and apply the numerous design procedures or guidelines that are currently available in Australia, Europe, Hong Kong and the USA
- show where adhesively bonded plates can be safely applied, where they should not be applied and where bolted plates should be used instead of adhesively bonded plates
- clearly distinguish between the behaviours of metal and FRP plated sections
- provide comprehensive information so that retrofitting by plating can be used with safety and confidence and, hence, extend the use of all types of plating
- provide engineers with the design tools to develop their own unique plating systems and to decide on appropriate techniques specific to their retrofitting problems

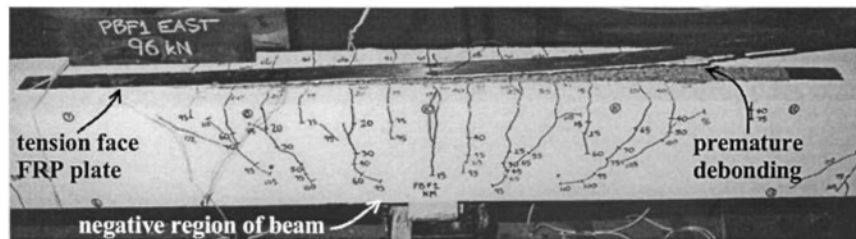


Figure 1.1 Premature failure of adhesively bonded plate

This book covers the mechanics of retrofitting reinforced concrete (RC) beams and slabs using externally bonded longitudinal plates. The plates can be made of FRP, steel, aluminium or any metal; they can have any shape such as flat plates, channels or angle sections; they can be bonded to any surface such as the tension face, sides or compression face; and they can be either adhesively bonded or bolted. Methods of analysis are illustrated and applied to determine the strength, stiffness and ductility of plated structures and design procedures for preventing premature debonding are compared.

In this chapter, the large variety of forms of longitudinal plating available to the designer is first described. This is then followed by a description of the premature failure mechanisms that can occur and have to be designed for, and how these failure mechanisms can affect the choice of plate material and size. Design guides are then compared which shows that there is general agreement on the failure mechanisms.

1.2 Forms of plating beams and slabs

Forces can be transmitted to the external plates from the RC structure through an adhesive bond, through bolts or through wrapping. Plates can be placed on any surface of the beam or slab and they can have any shape such as flat plates, channels or angle sections.

1.2.1 Bonding or joining techniques

1.2.1.1 Bolted and adhesively bonded plates

It is common practice to adhesively bond plates to the tension faces of slab structures as in Fig.1.2(a). Plates can also be adhesively bonded to the sides of beams as in Section A-A in Fig.1.3. However, if a ductile connection is required or if the adhesively bonded plate is prone to premature debonding or peeling, then the plate can be bolted as shown in Figs. 1.2(b) and 1.3. Although plates can be bolted to the tension face as in Fig.1.3, this may be difficult in beams due to congestion of the longitudinal tension reinforcement, in which case the plates can be bolted to the sides of the beam where only the stirrups have to be avoided.

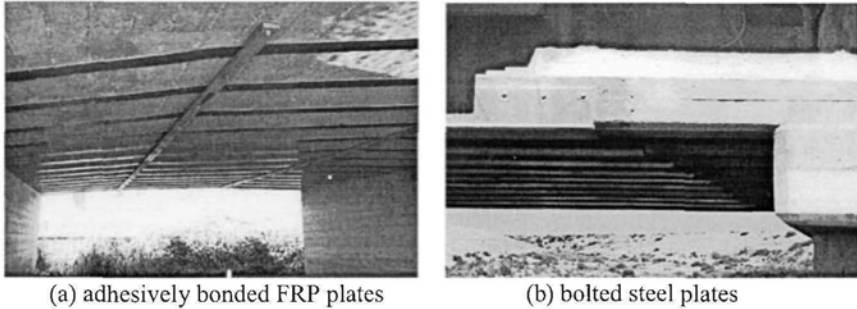


Figure 1.2 Retrofitting bridges

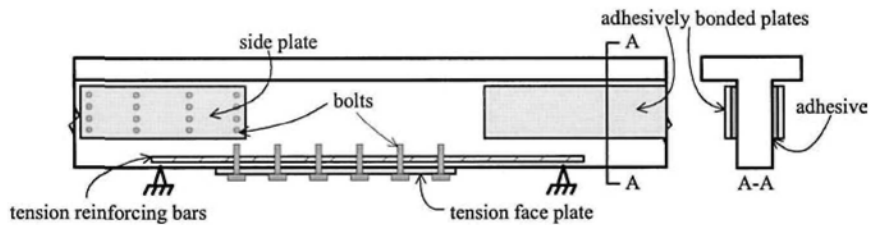


Figure 1.3 Bonding plates by adhesion and/or bolting

Plates can be both bolted and adhesively bonded but it should be remembered that each bonding technique works independently of the other; they do not enhance each other as bolts form a ductile connection that requires slip, whereas, adhesion forms a stiff but brittle connection. For additional safety, a plate can be designed as both bolted and adhesively bonded so that the bolts take over should the adhesive deteriorate. Bolts act as shear connectors in the composite plated structure so that they can be designed using the principles applied to stud shear connectors in composite steel and concrete beams (Oehlers and Bradford 1995, 1999) that are available in

national standards. A bolted FRP plate is probably more expensive to install than an adhesively bonded FRP plate, but bolting does allow the full strength of the plate to be achieved, whereas, adhesively bonded FRP plates often debond at strains between one-quarter to one-third of their fracture strain.

1.2.1.2 Wrapping and mechanical end anchorage

An alternative technique to bolting and/or adhesion for transferring the force into the plate is wrapping as shown in Fig.1.4 where the plate is both adhesively bonded and vertically wrapped around a rounded corner. The most efficient form is to fully wrap the cross-section as shown in A-A. This is a common practice in columns. The vertical wrap neither prevents nor inhibits the plate from debonding but takes over transferring the force, such as at C, after debonding. It is a very efficient system for increasing the vertical shear capacity of a beam with stirrups, as the fully wrapped section has sufficient ductility to allow the stirrups to yield or at least get significantly stressed whilst the wrap is still resisting vertical shear force. However, it is a difficult system to apply as the plate has to penetrate the flange of the beam. An alternative approach is to partially wrap as in B-B but, in this case, the resistance to the force D is generally low and the system is also brittle so that it is likely that the plate will debond before there is any significant stressing of the stirrups. A good compromise is shown at E-E where the plate is bonded within the flange on both surfaces providing a relatively strong joint and a ductile system that may allow some stressing of the stirrups prior to debonding.

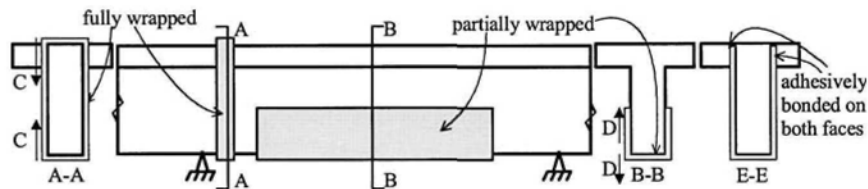


Figure 1.4 Vertically wrapped plates

An example of longitudinal wrapping is shown in Figs.1.5 and 1.6 where the bends in the plate at the ends at positions *A* in Fig. 1.5 act as an anchorage after the adhesively bonded plate has debonded. Anchorage failure can be clearly seen in Fig. 1.6 which was preceded by IC debonding. If possible, wrapping and clamping the plates at the supports such as at *C* in Fig. 1.5 provides an even stronger anchorage after debonding. Bolting the plates at the ends *B* has the same effect as wrapping as the bolts provide anchorage after debonding. It may be worth noting that an adhesively bonded plate or a plate bolted along its length such as in Fig.1.3 can accommodate a variation in longitudinal stress along the plate whereas in end anchored plates as in Fig.1.5 the plates are uniformly stressed along their length which will require a different analysis procedure.

Wrapping and adhesive bonding were applied to strengthening the bridge corbels in Fig.1.7(a) where the plate is adhesively bonded to the top of the corbel and wrapped around the sides. Full size specimens were tested to failure up-side-down in Fig.1.7(b). The *intermediate crack* caused the plate to debond after which the stress in the plate was maintained by the anchorage effect of the wrap until this also failed as shown in Fig.1.8(a). The end anchorage was enhanced with the addition of bolts to the wrap, as in Fig.1.8(b), as an additional safety measure should the adhesive deteriorate

prematurely. These tests clearly showed that the anchorage effect of the wrap was not effective until after debonding and did not affect the load at which debonding occurred.

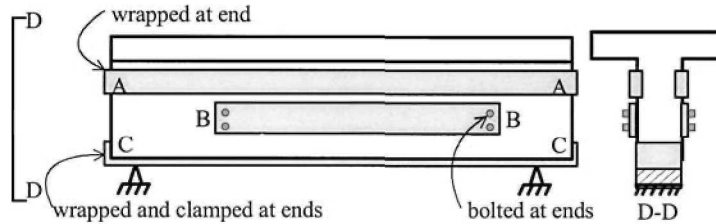


Figure 1.5 Longitudinally wrapped plates

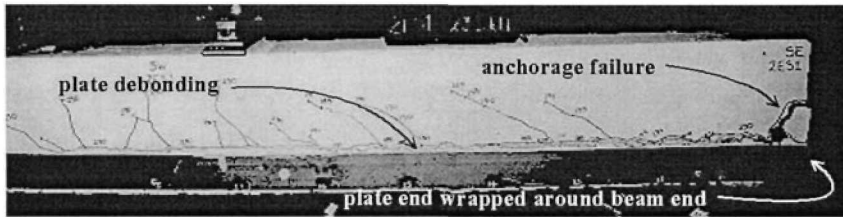


Figure 1.6 Longitudinally wrapped plate after debonding

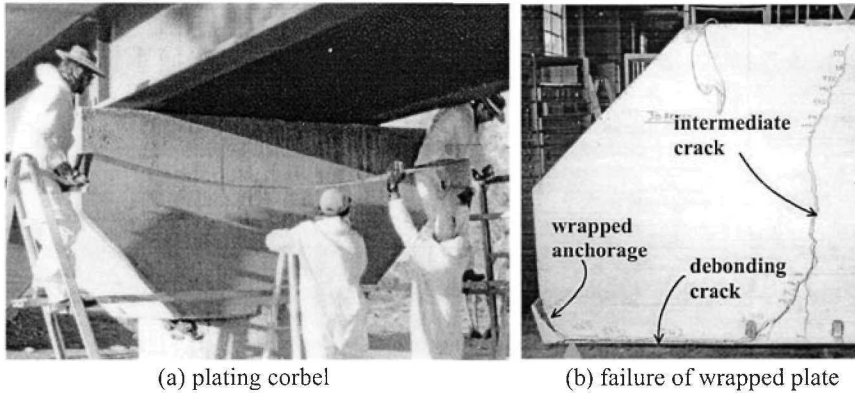


Figure 1.7 Bridge corbel strengthened by wrapping

1.2.2 Plate position

1.2.2.1 Tension face plates

The most commonly used plate position is the tension face, as in Figs.1.2(a) and 1.9, as it maximises the flexural lever arm and, hence, maximises the increase in the flexural capacity due to plating. However, the debonding stress concentrations in the tension face plate tend to interact with those in the adjacent tension reinforcing bars making the tension face plates more susceptible to premature debonding. It is also

worth remembering that the addition of tension reinforcement reduces the ductility of the RC cross-section which may limit the increase in strength that can be achieved with tension face plates. An alternative would be to plate the sides of the beam.

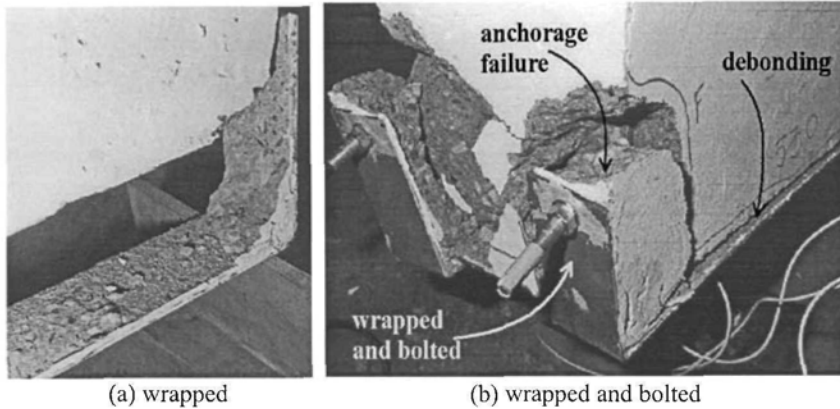


Figure 1.8 End anchorage failure

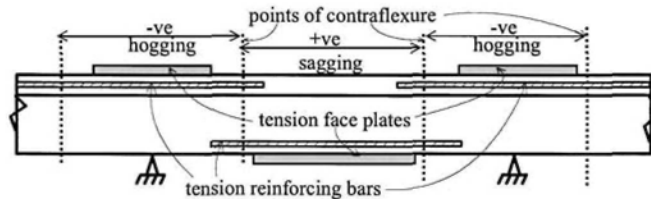


Figure 1.9 Tension face plated beam

1.2.2.2 Side plates

Examples of side plated beams are shown in Figs. 1.2(b) and 1.10. For a given area of plate, side plates are less efficient in increasing the flexural capacity than tension face plates due to the reduced lever arm. However, it may be possible to bond a greater area of plate to the sides than the tension face of the beam; side plated beams tend to be more ductile than tension face plated beams particularly if the plate is extended into the compression region of the web as in plate A in Fig.1.10; adhesively bonded side plates have been found to be less susceptible to debonding as there is little interaction between the debonding stresses and the stresses surrounding the tension reinforcing bars; and adhesively bonded side plates can substantially increase the concrete component of the vertical shear capacity and can substantially increase the total shear capacity when bolted.

1.2.2.3 Compression face plates

Plates can also be bonded to the compression face as in Fig.1.11. Compression face plates such as at position A can be used to increase both the ductility and vertical shear resistance of beams. It is also common practice to extend tension face plates such as at B into the compression faces as this inhibits but does not necessarily prevent debonding. Compression face plates are less susceptible to premature

debonding than tension face plates as there is no interaction between the debonding stresses and those surrounding compression reinforcing bars.

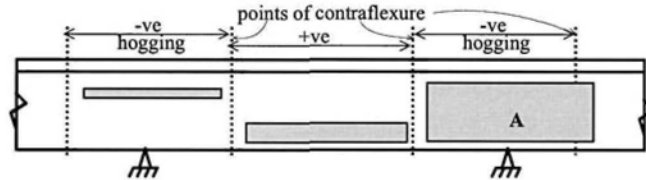


Figure 1.10 Side plated beam

1.2.3 Plate shapes

As well as flat plates, channel or U sections can be used as in Fig.1.12; these shapes are easily formed using the wet lay-up procedure with FRP sheets. Combinations of shapes can also be used as in Fig.1.13 where the U section and side plate are bonded adjacent to the ends of the tension face plate specifically to inhibit debonding of the tension face plate.

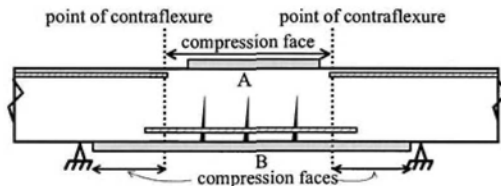


Figure 1.11 Compression face plated beams

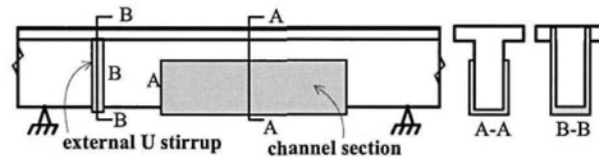


Figure 1.12 Channel or U sections

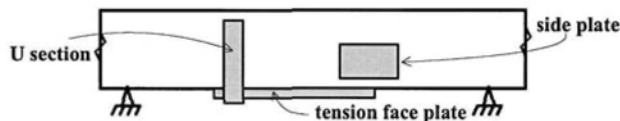


Figure 1.13 Combinations of plates

1.3 Major debonding mechanisms in adhesively bonded plates

In general practice, the adhesive used to bond a plate to a concrete element is much stronger than the tensile strength of the concrete so that debonding or peeling

invariably occurs within the concrete element as shown in Fig.1.8(a). Any crack that intercepts a plate will induce some amount of debonding to relieve the stress concentrations at the intercept. This will be referred to as intermediate crack (IC) interface cracking and generally has little or no effect on the overall strength of the structure. If this IC interface cracking spreads sufficiently to reduce the strains in the plate then this will be referred to as IC debonding. The formation of a critical diagonal crack (CDC), the type of crack commonly associated with the shear capacity of a beam or slab without stirrups V_e , also induces debonding and is referred to as CDC debonding. Furthermore, the curvature in a beam can also cause the plate to debond from the plate ends (PE) inwards and this is referred to as PE debonding. Although not a common debonding mechanism in most retrofitted RC beams or slabs, it is good practice to ensure that the interface shear stresses between the plate and concrete do not cause tensile failure of the concrete and this is referred to as V_Ay/Ib debonding.

In summary, IC debonding is associated with the strains in the plate, CDC debonding is associated with the rigid body shear displacement across a diagonal crack, and PE debonding is associated with the curvature in a beam. All the forms of adhesively bonded plates described in Section 1.2 are susceptible to the following debonding mechanisms in Sections 1.3.1 to 1.3.4.

1.3.1 Intermediate crack (IC) debonding

When an intermediate crack at A-A in Fig.1.14 intercepts a plate, compatibility requires that the plate is subjected to infinite strains across the crack width B-B which of course cannot occur. The accommodation of the intermediate crack is accomplished through some shear straining across the adhesive layer but primarily by the formation of the horizontal interface crack in Fig.1.14 (IC interface crack) such that the deformation in the plate over the length C-C is equal to that in the concrete that incorporates the width of the intermediate crack. As the applied load is increased opening the intermediate crack and increasing the longitudinal strain in the plate, the IC interface crack propagates due to the combination of shear and normal stresses at the crack tip.

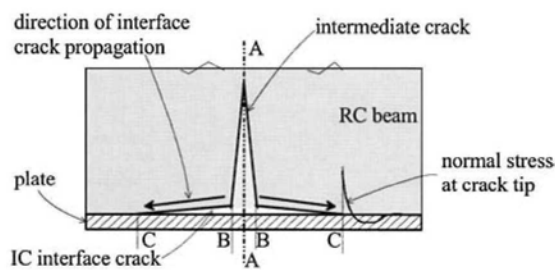


Figure 1.14 IC interface cracking mechanism

The intermediate crack in Fig.1.14 can be any kind of crack such as the flexural crack and flexural/shear cracks in Fig.1.15 or the diagonal cracks in Fig.1.16. It can be seen in both Figs. 1.15 and 1.16 that IC interface cracks initiate at the crack/plate intercept and propagate towards the plate end. They can occur at very low loads and are initially of no significance, as in Figs. 1.15 and 1.16, until they have spread sufficiently to join together and reduce the strains in the plate, in which case IC debonding can be considered to occur. It can be seen that IC debonding is primarily

concerned with the strains in the plate that are required to accommodate the intermediate crack and it is a gradual failure with plenty of warning.

1.3.2 Critical diagonal crack (CDC) debonding

The critical diagonal crack (CDC) debonding mechanism is illustrated in Fig.1.17. The critical diagonal crack is not an inclined shear/flexural crack as in Fig.1.15, nor a diagonal crack as in Fig.1.16, but it is a single inclined crack in a shear span across which rigid body shear displacement occurs. It is the critical diagonal crack associated with the shear failure of beams or slabs without stirrups, that is the CDC associated with the concrete shear capacity of a beam or slab V_c . It is the rigid body sliding action and rotation across the CDC in Fig.1.17 that causes the plate to debond from the root of the crack at B towards the plate end at C as shown. As with all shear failures, failure is very rapid and explosive with virtually no prior warning. Numerous tests have clearly shown that stirrups do not prevent nor inhibit this form of debonding as the plate debonds before the stirrups are stretched to yield.

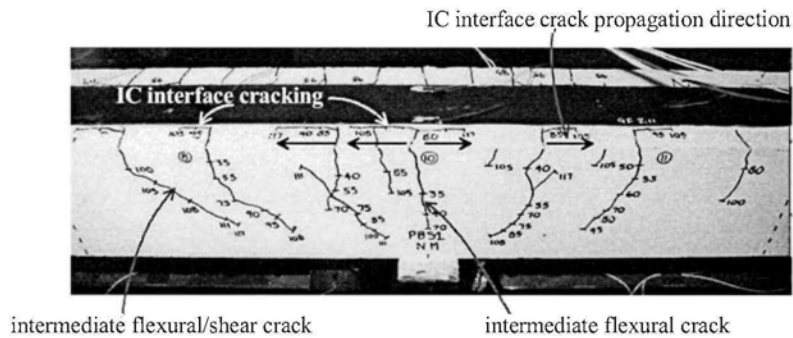


Figure 1.15 IC interface cracking induced by flexural and flexural/shear cracks

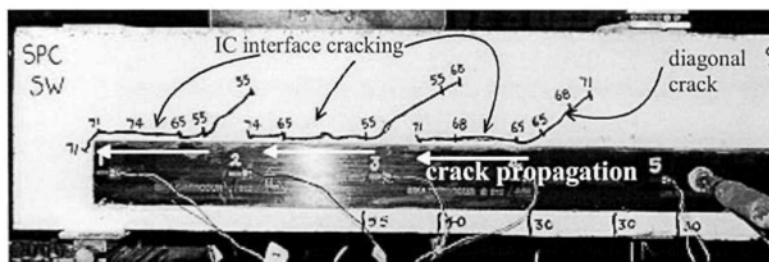


Figure 1.16 IC interface cracking induced by diagonal cracks

Figure 1.18 is a further illustration of the important difference between IC debonding induced by flexural/shear cracks and CDC debonding due to the rigid body displacement across a CDC. As the applied load was being gradually increased in the beam in Fig.1.18, the IC interface cracks induced by the intermediate flexural and shear cracks were gradually propagating in the region over the support. However, suddenly and without any prior warning the critical diagonal crack formed and the

plate debonded from the root of the diagonal crack to the plate end in a region which was uncracked prior to the formation of the critical diagonal crack.

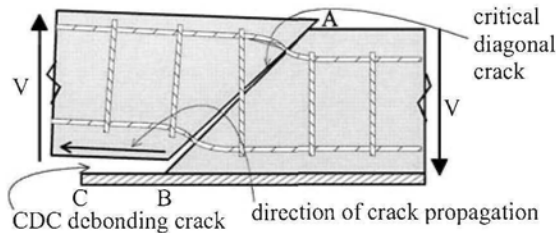


Figure 1.17 Critical diagonal crack (CDC) debonding mechanism

A further example of the rapid and catastrophic nature of CDC debonding is illustrated in Fig.1.19 for a beam with a tension face plate that was terminated near a support. A diagonal crack occurred at an applied load of 100 kN. Virtually nothing happened after that but then at a substantially higher load of 188 kN the critical diagonal crack formed in a previously uncracked region and the rigid body displacement across this crack caused the plate to debond. It can be seen that the critical diagonal crack occurred within the plated region and because of this it caused debonding and also that debonding occurred near to the plate end. In summary, critical diagonal crack debonding is associated with the rigid body shear displacement across a critical diagonal crack and it is a catastrophic failure that occurs without warning.

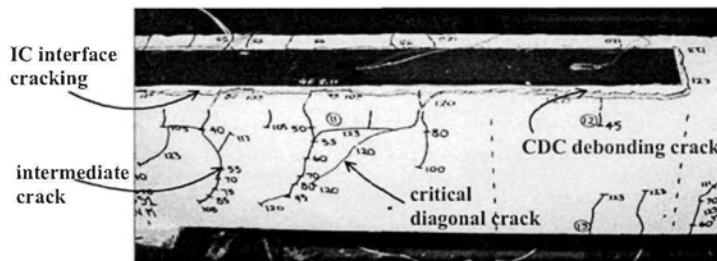


Figure 1.18 Critical diagonal crack debonding amongst flexural/shear cracks

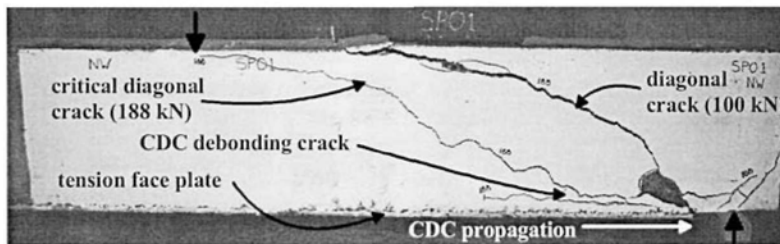


Figure 1.19 Sudden occurrence of critical diagonal crack

1.3.3 Plate end (PE) debonding

Plate end (PE) debonding is considered the easiest form of debonding to visualise as illustrated in Fig.1.20. As curvature is applied to the beam, the plate tries to remain straight which causes debonding cracks to start at the plate ends and propagate inwards, this is referred to as plate end debonding. Unlike IC and CDC debonding where the debonding cracks start within the plated region and propagate outwards towards the plate ends, for PE debonding the debonding cracks initiate at the plate ends and propagate inwards.

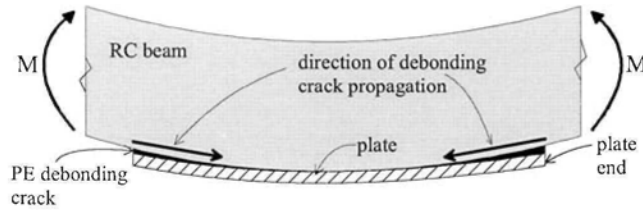


Figure 1.20 Plate end (PE) debonding mechanism

An example of plate end debonding is shown in Fig.1.21 for a beam with a side plate. The debonding crack first gradually propagated from the plate end inwards as the load was increased, and then rapidly, causing the strains in the plate to reduce upon which debonding was assumed to have occurred. In summary, plate end (PE) debonding is a gradual form of failure and is induced by curvatures in the beam.

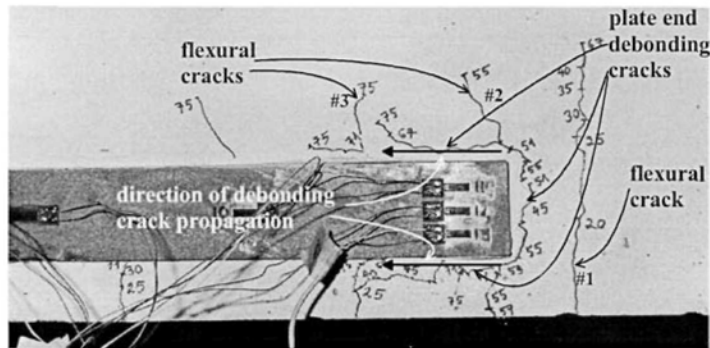


Figure 1.21 Plate end (PE) debonding in a side plated beam

1.3.4 Interface shear stress ($V\Delta y/Ib$) debonding

The interface shear stress between the plate and the RC beam can be derived from elementary structural mechanics using the well known $V\Delta y/Ib$ or equations that depend on the vertical shear force V at a section of a beam. The first author has tested hundreds of plated beams and none would appear to have failed by this mechanism of failure. However, there is a possibility that the interface shear stress $V\Delta y/Ib$ might cause debonding when thick plates are used, such as might occur if plating is used at serviceability to reduce deflections. Furthermore, the $V\Delta y/Ib$ shear stress may be more likely to cause debonding in plated prestressed beams as the prestress will inhibit the formation of the intermediate and critical diagonal cracks and hence delay

both IC and CDC debonding. Hence, it is good practice to check the V_Ay/Ib shear stress and if necessary restrict it to less than the tensile strength of the concrete.

Figure 1.22 shows IC debonding of a tension face plate in a constant moment region and Fig.1.23 shows PE debonding also in a constant moment region where obviously in both cases the vertical shear force V is zero. Hence it can be seen that as the V_Ay/Ib shear stress depends on the vertical shear force V , restricting the V_Ay/Ib shear stress will not prevent either IC or PE debonding. Furthermore, as CDC debonding is due to a rigid body shear displacement as shown in Fig.1.19, limiting the V_Ay/Ib shear stress cannot be used to design against CDC debonding. In summary, the V_Ay/Ib shear stress should not be used to design against IC, CDC and PE debonding. The V_Ay/Ib shear stress should be considered as the fourth major mode of debonding and restricted to less than the tensile strength of the concrete.

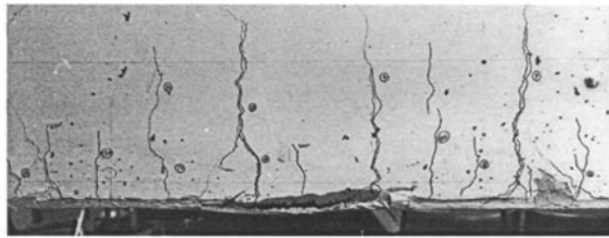


Figure 1.22 IC debonding of a tension face plate in a constant moment region

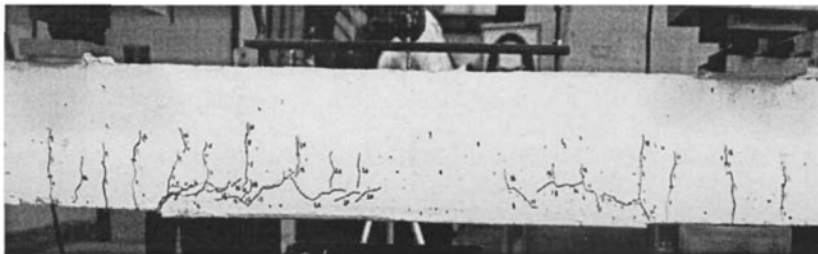


Figure 1.23 PE debonding of a tension face plate in a constant moment region

1.3.5 Desired form of flexural failure

Figures 1.24 and 1.25 show examples of side and tension face plated beams in which concrete crushing occurred prior to debonding of the plates. Small amounts of IC interface cracking can be seen along the edges of the plates but this was not sufficient to reduce the stresses in the plates so that the beams achieved their theoretical flexural capacities based on the material properties. This may be considered as the desired form of failure as most reinforced concrete beams and slabs are designed to fail due to concrete crushing whether they are under-reinforced or over-reinforced.

The desired concrete crushing failures shown in Figs. 1.24 and 1.25 can only be achieved if IC, CDC and PE debonding can be prevented from occurring before the design load to cause concrete crushing. However, this may not always be possible; in which case, it may be necessary to design for either IC or CDC debonding to occur at the design load so that concrete crushing will not occur. Rarely will PE debonding

control the design capacity as this mode of failure can be easily prevented by terminating the plate at a point of contraflexure or at least in a low moment region.

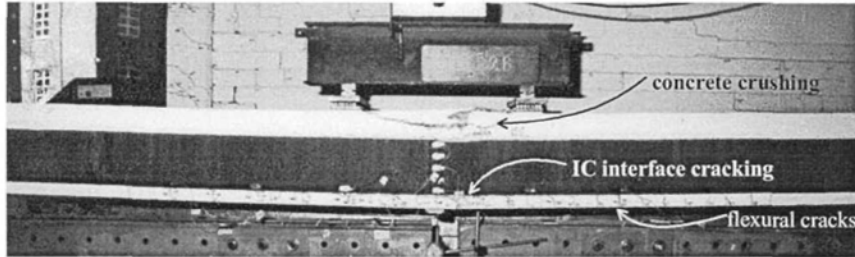


Figure 1.24 Flexural failure of a side plated beam

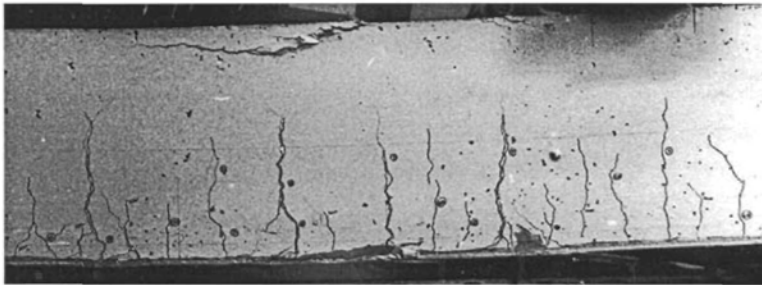


Figure 1.25 Flexural failure of a tension face plated beam

It may be worth noting that even if it is possible to design a plated beam or slab so that the concrete crushes prior to debonding, numerous tests by the authors have shown that there is a very good chance that the plates will still debond after the maximum flexural capacity has been reached. Hence, debonding may still affect the ductility of the section and the ability to redistribute moment within a continuous beam. However, this restricted ductility can be designed for and is an illustration of the advanced analysis procedures that have to be applied in designing plated structures, particularly if ductility is required to redistribute moments, to resist seismic loads or to absorb dynamic loads.

1.3.6 Summary of common debonding mechanisms

The three common major debonding mechanisms, that is intermediate crack (IC), critical diagonal crack (CDC) and plate end (PE) debonding, apply to all forms of plating and for all types of plate material. Longitudinal tension face plates as in Fig.1.26 are probably the most common form of plating and are susceptible to IC, CDC and PE debonding in both the positive and negative moment regions as shown. Exactly the same mechanisms apply to side plated beams as shown in Fig.1.27.

Plates can be bonded to the compression face as in the upper plate in Fig.1.28, or tension face plates can be extended into the compression faces, as in the lower plate, to try to inhibit debonding. However, these compression face plates are also susceptible to CDC and PE debonding as shown, but obviously not to IC debonding as

the intermediate crack which is a requirement for IC debonding will not occur in the compression zone.

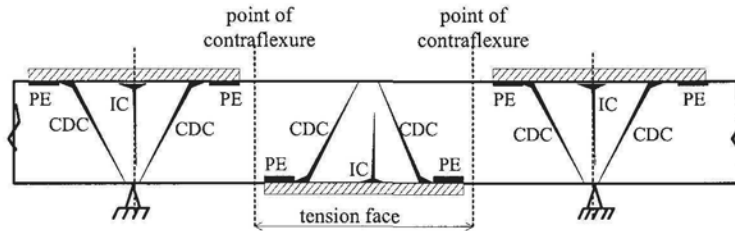


Figure 1.26 Longitudinal tension face plates

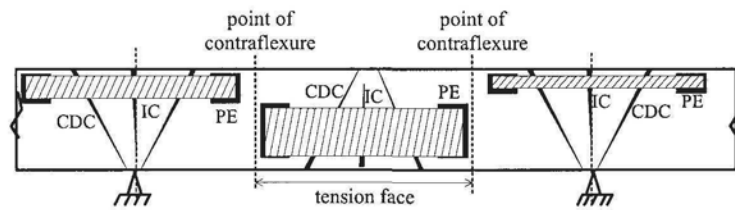


Figure 1.27 Longitudinal side plates

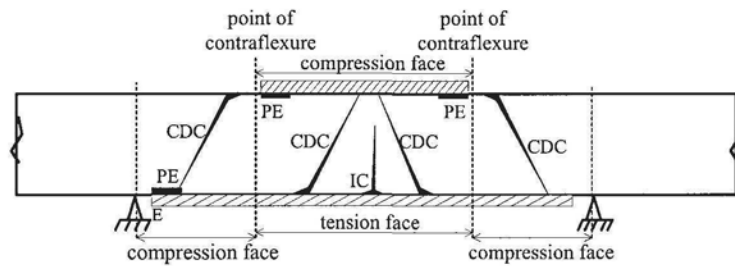


Figure 1.28 Longitudinal compression face plates

It may be worth noting that transverse plates such as A and B in Fig.1.29, although not the subject of this book, are also susceptible to IC debonding as shown.

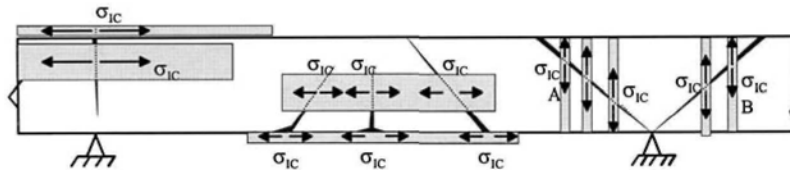


Figure 1.29 IC debonding in transverse plates

1.4 Failure of bolted plates

In Fig.1.30, thick FRP plates have been bolted to the sides of an RC beam. The behaviour of this beam is similar to the behaviour of commonly used composite steel and concrete beams. It can be seen that the concrete has crushed and the beam has attained its desired theoretical ultimate strength.

The bolts or bolt shear connectors in Fig.1.30 are analogous to mechanical stud shear connectors in composite steel and concrete beams and require slip to transmit the shear forces. Compared with an adhesive bond which is brittle, bolt shear connectors are ductile and, unlike adhesively bonded plates, can easily accommodate any critical diagonal crack. Hence this system can be used in regions of a continuous beam where CDC debonding or ductility requirements prevent the plates from being adhesively bonded.

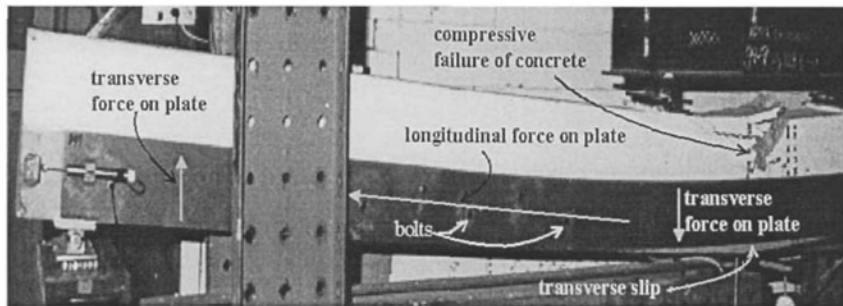


Figure 1.30 Flexural failure of a bolted plated beam

As with stud shear connectors in composite steel and concrete beams, bolt shear connectors can fail by fracturing due to excessive slip as shown in Fig.1.31(a), but this can be easily prevented by designing for full shear connection. Placing the side plate partly in the compression region can increase the ductility of the beam but the plate is then susceptible to buckling as shown in Fig.1.31(b). Comprehensive design rules (Smith, Bradford and Oehlers 1999a, 1999b, 2000, 2001) are available for quantifying the plate buckling load and for distributing the bolts so that buckling does not occur. However, a simple solution is to prevent plate buckling by restricting the plates to the tension zones as in Figs.1.30 and 1.31(a).

1.5 Plate material and geometry

The type of plate material used may often be governed by durability requirements as well as the intended form of bonding.

1.5.1 Adhesively bonded plates

A comparison of the mechanical properties of materials that are frequently bonded to concrete structures is shown in Fig.1.32. The strength, stiffness and ductility of adhesively bonded plated sections depends on all the properties shown in Fig.1.32; it depends on the material stiffness E , the FRP fracture stress f_{FRP} or the metal yield

stress f_y , the FRP strain capacity ϵ_{FRP} as well as the extent of the metal yield plateau that is the metal ductility.

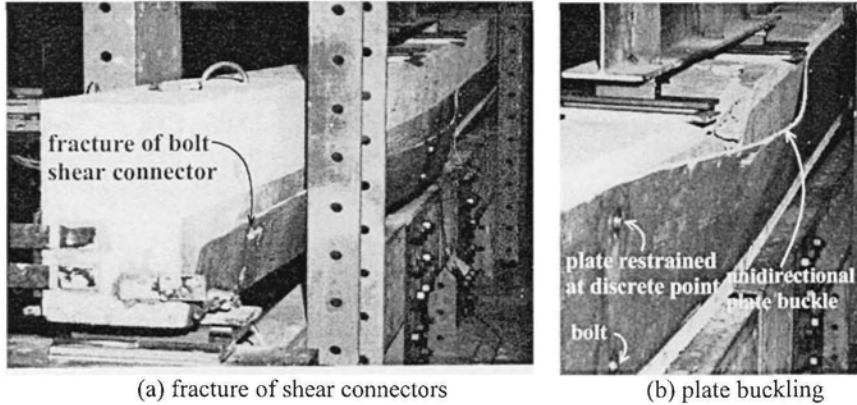


Figure 1.31 Premature failure of bolted plated beams

Steel can be considered as stiff and ductile having a relatively high Young's modulus (E_s) and, hence, high material stiffness followed by a large yield plateau which signifies a high material ductility. Aluminium tends to be less stiff (E_{al}) than steel and is also ductile. In contrast to metal plates, fibre reinforced polymer plates are totally brittle, that is without a ductile plateau, and fracture at a strain ϵ_{CFRP} and ϵ_{GFRP} that depends on the fibres being used. The stiffness of fibre reinforced polymer (FRP) plates E_{CFRP} and E_{GFRP} depends primarily on the type and concentration of the fibre. For example, carbon fibre reinforced polymer (CFRP) plates can be made with sufficient fibres so that the plate is stiffer than steel as shown and reducing the density of the fibre will obviously reduce the Young's modulus. Glass fibre reinforced polymer (GFRP) plates tend to fracture at a higher strain than carbon fibre plates but are less stiff and both generally fracture at strains well below the fracture strain of steel but at much higher stresses.

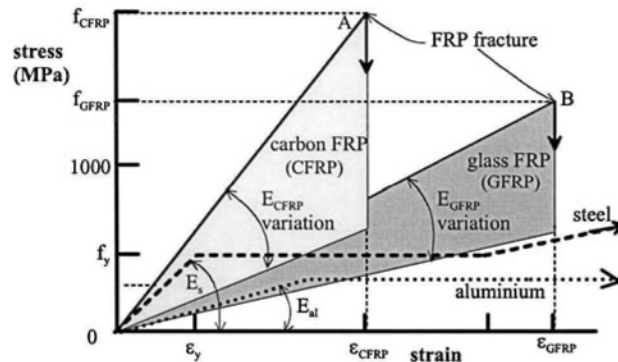


Figure 1.32 Adhesively bonded plate materials

Whilst the plate material remains linear elastic, the dependence of the plate debonding stress σ_{IC} is given by the following empirically derived rule (Teng et al 2002).

$$\sigma_{IC} \propto \sqrt{\frac{E_p \sqrt{f_c}}{t_p}} \quad 1.1$$

where E_p = Young's modulus of the plate, f_c = compressive cylinder strength of the concrete and t_p = plate thickness. It can be seen in Eq.1.1 that the concrete term has a minimal effect on the debonding stress as, for example, doubling the concrete strength will only increase the debonding stress by 19%. Rearranging Eq.1.1 gives the following debonding strain ε_{IC} .

$$\varepsilon_{IC} \propto \sqrt{\frac{\sqrt{f_c}}{E_p t_p}} \quad 1.2$$

FRP plates are commonly chosen to maximise the debonding stress in order to maximise the increase in the flexural capacity. Hence from Eq.1.1 thin stiff plates are suitable, and from Fig.1.32 carbon FRP would be the best choice. As an example, pultruded carbon FRP plates are usually supplied in thicknesses $t_p \approx 1.2$ mm with a Young's modulus $E_p > 150$ GPa which gives debonding stresses σ_{IC} of about 450 MPa, which can be compared with the ultimate fracture stress $f_{CFRP} > 1500$ MPa. It can be seen that the debonding stress is little more than that of high yield steel and well below the ultimate tensile strength of the FRP. However, if ductility is a requirement, then Eq.1.2 suggests that thin plates with a low Young's modulus would be the preferred option such as that provided by glass FRP as shown in Fig.1.32. Several layers of FRP plates can be used, however from Eqs. 1.1 and 1.2 both the strains and stresses at debonding reduce making the system mechanically even less efficient, although generally the force in the plate increases as the thickness increases. This could be an option for reducing deflections at serviceability where the working stresses are lower than at ultimate which will allow thicker plates. Pultruded plates tend to have unidirectional fibres whilst those plates manufactured from FRP sheets using the wet lay-up process tend to be bi-directional.

Metal plates can be designed using Eq.1.1 to remain linear elastic prior to debonding; this may be a suitable approach for plating at serviceability stresses as it would allow thick plates. However at the ultimate limit, metal plates have one advantage over FRP plates in that they can be designed to yield prior to debonding which can ensure a reasonable amount of ductility if required. Typically, steel plates of thickness $t_p < 4$ mm will yield before debonding although plated beam tests show that debonding will eventually occur but at relatively high strains.

1.5.2 Bolted plates

The criteria for choosing plates for bolting are totally different from those for adhesive bonding. Debonding is now no longer an issue so thick plates can be used. Thick plates are also required so that they do not buckle if placed in the compression zone as in Fig.1.31(b) and in order to transmit the bearing force from the bolts. Typical examples of materials used in bolted plates are shown in Fig.1.33.

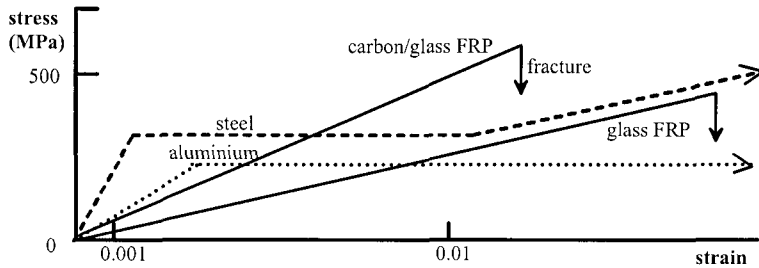


Figure 1.33 Bolted plate materials

As thick plates can be used and are in fact beneficial, plates can be made not only from metals but also from glass fibre which is less expensive than carbon fibre or from a combination of carbon and glass; these plates range from 5 mm to 15 mm thick. The FRP fibres have to be in at least two directions to resist the splitting forces from the bolts. The ultimate fracture strength of these FRP plates is of the same order as steel so that a much larger proportion of the ultimate strength can be used in design as compared to adhesively bonded FRP plates where the debonding stress is usually much lower than the fracture stress.

1.6 Commentary of design guides for longitudinal plating

1.6.1 Scope of comparison

Numerous papers have been published on adhesive bonding external plates and most manufacturers give or refer to guidelines. However, this comparison is restricted to the approaches listed in Table 1.1 which consist of the Australian research brought together and documented in this book as a design guide, as well as the Hong Kong research and design guide also issued as a book, and the British, European and American guidelines, as it is felt that these are fairly comprehensive and reasonably independent.

Table 1.1 FRP plating guidelines

Australian	Oehlers and Seracino (2004) Design of FRP and steel plated RC structures
British	Canakya et al Concrete Society Technical Report No. 55 (2000) Design guidance for strengthening structures using fibre composite materials
European	Triantafillou et al fib bulletin 14 (2001) Externally bonded FRP reinforcement for RC structures
Hong Kong	Teng, Chen, Smith and Lam FRP Strengthened RC structures (2002)
USA	Rizkalla et al ACI 440.2R-02 (2002) Guide for the design and construction of externally bonded FRP systems for strengthening concrete structures

In the following comparison and discussion of the guidelines in Table 1.1, it may be worth bearing in mind that these guidelines were issued as early as the year 2000 and during this intervening period there has been very rapid improvements in the understanding of plated structures and in the development of design rules. Hence, when these guidelines were first issued, they were the state-of-the-art and provided design guidelines for a new and very complex subject which was, and still is, evolving rapidly. To help in a systematic comparison of these guidelines, the Australian design approach will be described first as it covers all forms of plating, after which the comparison will be restricted to adhesively bonded FRP tension face plated structures as all the guidelines apply to this form of plating.

1.6.2 Australian approach

The scope of the Australian approach is summarised in Fig.1.34. The designer first requires the distribution of the envelopes of applied vertical shear and bending moment. These are shown schematically in Fig.1.34(a). They are a reminder that the stress resultants can vary at a design point particularly if designing for moving loads, as in a bridge, where there may not be a convenient position of zero moment. The design approach then consists of the follow steps:

- Choose the type of plate material at a given hogging or sagging region by considering durability, ductility, moment redistribution requirements and ease of application. Combinations of plate materials can be considered for example steel plates may be required in the hogging regions for ductility whilst carbon FRP plates can be used in the sagging regions.
- Decide on the plate position, such as side or tension face plates, for convenience or for mechanical considerations such as strength or ductility. For example, it may not be convenient to plate the tension faces of the hogging regions in which case the underside of the flanges or the sides of the webs could be plated.
- Choose a plate thickness and hence plate stress and plate strain, as governed by *IC debonding*, at positions of maximum moment. In some cases, it may be ineffective to adhesively bond FRP plates to the tension faces, as the plates may debond before the tension reinforcing bars yield. In which case, it may be more appropriate to plate regions closer to the neutral axis such as the underside of the flanges in the hogging regions so that the reinforcing bars yield before the plates debond. The plate thickness will also depend on the limit state, as for example at serviceability lower stresses occur so that thicker plates can be used.
- Determine the cross-sectional area of plate for flexural requirements of strength or serviceability.
- Assume the plate extends to the points of contraflexure or where the moment is low, that is the shear span is fully plated. Determine the *CDC resistance and the position of the critical diagonal crack*. Where the CDC resistance is too low, either try to add plates to increase the resistance or if this is not sufficient change to *bolting plates* in this region.
- If the CDC resistance of the fully plated region is sufficient, determine the extent of plating which is governed by the *position of the CDC and by PE debonding*.

It can be seen in the design steps listed above that IC debonding is the dominant debonding mechanism as it controls the type, size and position of the plate. However, CDC debonding may prevent the use of adhesively bonded plates in some shear spans, in which case bolted plates can be substituted. CDC debonding also

controls the extent of plating as the plate has to extend beyond the critical diagonal crack. PE debonding also governs the extent of plating but rarely, if ever, prevents plating as it can be designed against by simply terminating the plate at a point of contraflexure or where the curvature is low.

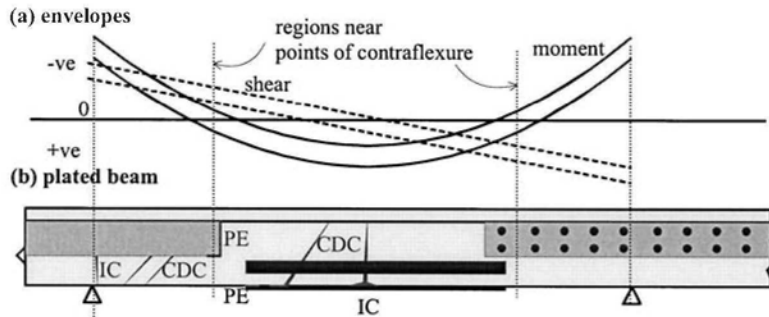


Figure 1.34 Australian approach

1.6.3 Adhesively bonded FRP tension face plated structures

As all of the design guidelines in Table 1.1 cover plating using FRP tension face plates as shown in Fig.1.35, this form of plating will be used to compare the different guidelines. The design rules cover both the hogging (-ve) and sagging (+ve) regions of the beam. For convenience, we will consider the sagging region in Fig.1.35 which is represented as a simply supported beam in Fig.1.36.

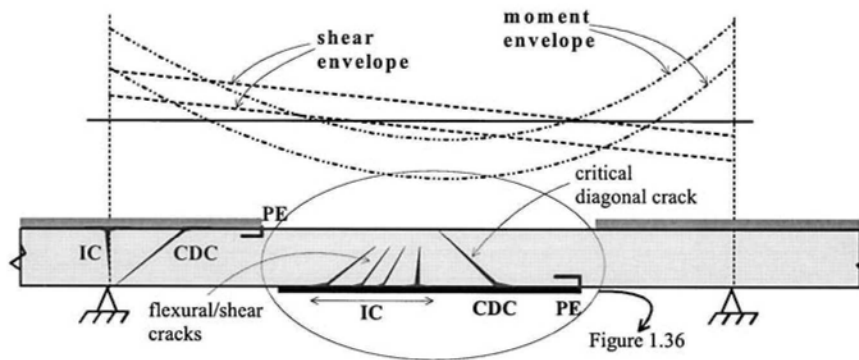


Figure 1.35 Tension face plates

The different debonding failure mechanisms, which have already been described in Section 1.3, are shown again in Fig.1.36. The 5 mechanisms encircled in Fig.1.36 were extracted from the five guidelines in Table 1.1. The names used for each mechanism, as listed in the boxes in Fig.1.36, may differ between the guidelines but there appears to be an almost unanimous agreement on the mechanisms of debonding which is a very important first stage in the development of design rules. The USA guidelines do not describe the failure modes directly but do refer to three conference papers which clearly describe failure Mechanisms 1-4; this has been referred to as *referenced* in the boxes in Fig.1.36. Similarly, the British guideline also

refers to a conference paper for Mechanism 4. Much of the agreement shown in Fig.1.36 would appear to ensue from an excellent conference paper by Blaschko et al (1998). The European approach makes the distinction between the cracked region of a beam and the uncracked region as shown in Fig.1.36 and it is a requirement that the plate is anchored in the uncracked region. This leads to the three IC debonding failure regions: at the anchorage zone (Mechanism 1); at the position of maximum moment (Mechanism 2); and at flexural/shear cracks (Mechanism 3).

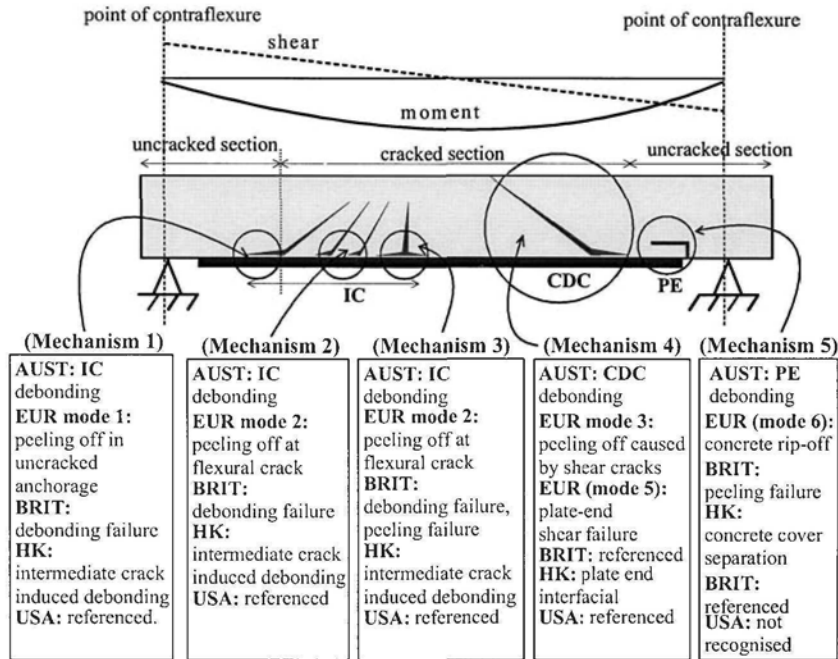


Figure 1.36 Comparison of debonding failure mechanisms

For Mechanism 1 in Fig.1.36, there is a general agreement in calculating the axial force in the plate allowing for the bond length. There is also general agreement for Mechanisms 2 and 3, although in the latter there is a slight confusion with the British approach which first refers to it as *debonding failure* but then suggests using the equation for *peeling failure* in this region. For Mechanism 5, there is also general agreement. However, the European approach describes the failure, identified as mode 6 in the box, but does not give design rules. This is probably because plate end debonding is very unlikely to control design when using FRP plates as they are usually very thin and also because of the necessity for terminating the plate in an uncracked region which by definition will be at or close to a point of contraflexure.

Finally, there is further general agreement for Mechanism 4 where design rules originating from the concrete shear capacity V_c are proposed. However, there is slight confusion with the European approach which gives it two labels and describes *plate-end shear failure* (identified as mode 5) using Fig.1.37. This figure shows a simply supported beam with plates terminating almost at the supports and with a horizontal debonding crack on the right hand side and a diagonal crack on the left

hand side. The authors are familiar with plate end debonding as in Fig.1.23 which looks familiar to the debonding crack on the right side of Fig.1.37, but this only occurs when the plate is terminated in a region of high curvature which does not exist at the supports.

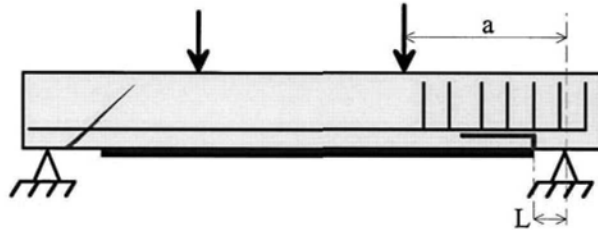


Figure 1.37 fib 14 diagram for 'FRP plate-end shear failure'

Combining the two cracks in Fig.1.37, resembles the CDC debonding failure in Fig.1.19 and which is also shown in Fig.1.38 for a plated beam without stirrups and in Fig.1.39 for a plated beam with stirrups. Whether or not this is the *plate-end shear failure* described in the European guideline, these failed beams show that it may be difficult to find an uncracked region of a beam within which to anchor the plate end as required in the European guideline simply because shear cracks can occur near points of contraflexure.

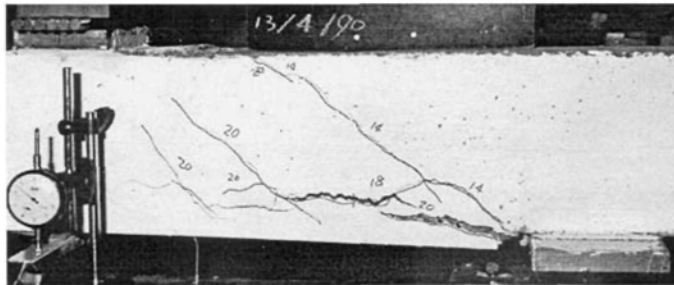


Figure 1.38 'plate-end shear failure' of beam without stirrups (CDC debonding)

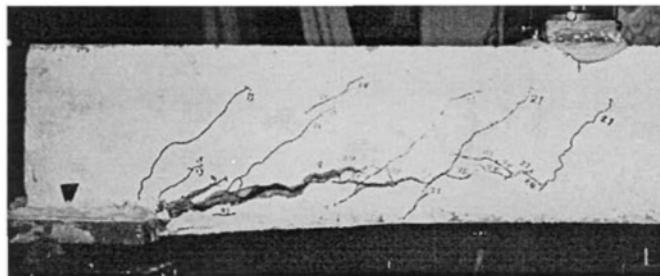


Figure 1.39 'plate-end shear failure' of beam with stirrups (CDC debonding)

1.7 Conclusions

It has been shown that there is a very wide variety of forms of plating available to designers in order to develop a retrofitting solution for their problems. Plates of any material or of any shape and size can be adhesively bonded or bolted to any surface of the reinforced concrete structure. The designer can choose or design a plating system for durability, flexural strength, stiffness or ductility, and shear strength. It has also been shown, that there is a general consensus on the debonding mechanisms.

Design rules are now available for all the different forms and for all the debonding mechanisms described in this chapter. Chapter 2 describes IC debonding, which is the dominant mode of debonding as it controls the choice of plate material, size, shape and position. A comparison is also made of the different guidelines for the IC debonding resistance as well as the emerging design philosophies based on the European and Australian approaches. Having chosen the plate size, the analyses for the flexural strength and ductility are described in Chapter 3, where it is shown that the ability or requirement for moment redistribution can have a major effect on the choice and effectiveness of the plating system.

Having now designed for IC debonding, the beam must be checked for CDC debonding. This is first done in Chapter 4 for tension face plates in order to compare the different guidelines directly, and then in Chapter 5 for other forms of plating in which the Australian approach is used as the other approaches are not applicable. Having now designed for CDC debonding and determined the extent of plating required to encompass the critical diagonal crack, the plate is extended further in Chapter 6, if need be, to ensure that PE debonding does not occur. At this stage, all the design rules have been described and implemented, and Chapter 7 is used to illustrate the full extent of the analyses and in particular how combining different forms of plating can often achieve the best results. The European and Australian design philosophies are implemented. However, most of the analysis techniques used in following the design philosophies apply the Australian approach only because this covers all forms of plating.

1.8 References

- ACI 440.2R-02 (2002). Emerging Technology Series. *Guide for the Design and Construction of Externally Bonded FRP Systems for Strengthening Concrete Structures*. Reported by ACI Committee 440. American Concrete Institute, Farmington Hills, Michigan, USA.
- Blaschko, M., Nierdermeier, R., and Zilch, K. (1998). "Bond failure modes of flexural members strengthened with FRP". *Proceedings of Second International Conference on Composites in Infrastructures*, Saadatmanesh, H. and Ehsani, M. R., eds., Tucson, Arizona, 315-327.
- Concrete Society Technical Report No. 55 (2000). *Design guidance for strengthening concrete structures using fibre composite materials*. The Concrete Society. Century House, Telford Avenue, Crowthorne, Berkshire, UK.
- fib bulletin 14 (2001). *Externally bonded FRP reinforcement for RC structures. Design and use of externally bonded fibre reinforced polymer reinforcement (FRP EBR) for reinforced concrete structures*. Task Group 9.3 FRP reinforcement for concrete structures. Lausanne, Switzerland.
- Oehlers, D. J. and Bradford, M. A. (1995). "Composite Steel and Concrete Structural Members: Fundamental Behaviour". *Pergamon Press*, Oxford.
- Oehlers, D.J. and Bradford, M.A. (1999). "Elementary behaviour of Composite Steel and Concrete Structural Members". *Butterworth Heinemann*, Oxford, September.
- Oehlers, D.J. and Seracino, R. (2004). "Design of FRP and steel plated RC structures: retrofitting of beams and slabs for strength, stiffness and ductility". Elsevier.

- Smith, S.T., Bradford, M.A. and Oehlers, D.J. (1999) "Local buckling of side-plated reinforced concrete beams. Part 1: Theoretical study". *ASCE Structural division, Journal of Structural Engineering*, June, 622-634.
- Smith, S.T., Bradford, M.A. and Oehlers, D.J. (1999). "Local buckling side-plated reinforced concrete beams. Part 2: Experimental study". *ASCE Structural division, Journal of Structural Engineering*, June, 635-643.
- Smith, S.T., Bradford M.A. and Oehlers, D.J. (2000). "Unilateral buckling of elastically restrained rectangular mild steel plates". *Journal of Computational Mechanics*, Vol.26, No.4, 317-324.
- Smith, S.T., Bradford, M.A., and Oehlers, D.J. (2001). "Buckling tests on steel plates restrained at discrete points in the retrofit of reinforced concrete beams", *Proc. ICE, Structs. & Bldgs*, 146(2), 115-127, May.
- Teng, J.G., Chen, J.F., Smith, S.T., and Lam, L. (2002). "FRP Strengthened RC Structures". *John Wiley and Sons*. Ltd. Chichester, England.

Chapter 2: Intermediate Crack (IC) Debonding

2.1 Introduction

The intermediate crack debonding mechanism has been described in Section 1.3.1. It was shown that a crack that intercepts a plate must induce some debonding in the vicinity of the crack to relieve the strain concentrations. This was referred to as IC interface cracking and is of little consequence unless it propagates sufficiently to cause substantial separation of the plate from the concrete which then reduces the strains in the plate. At this stage it is referred to as IC debonding.

Intermediate crack (IC) debonding can be considered the dominant mode of debonding as it affects both the flexural strength and ductility of the beam and, as will be shown in Chapters 4 and 5, it affects indirectly the CDC debonding resistance. The fact that it is referred to as the dominant mode of failure does not necessarily mean that it is the most common mode of failure as analyses of published test data suggest that CDC debonding occurs more often. As IC debonding is a plate strain related debonding mechanism, it generally initiates at the position of maximum moment, as in Fig. 2.1, where the flexural crack intercepts the plate and where the strains in the plate are at their maximum.

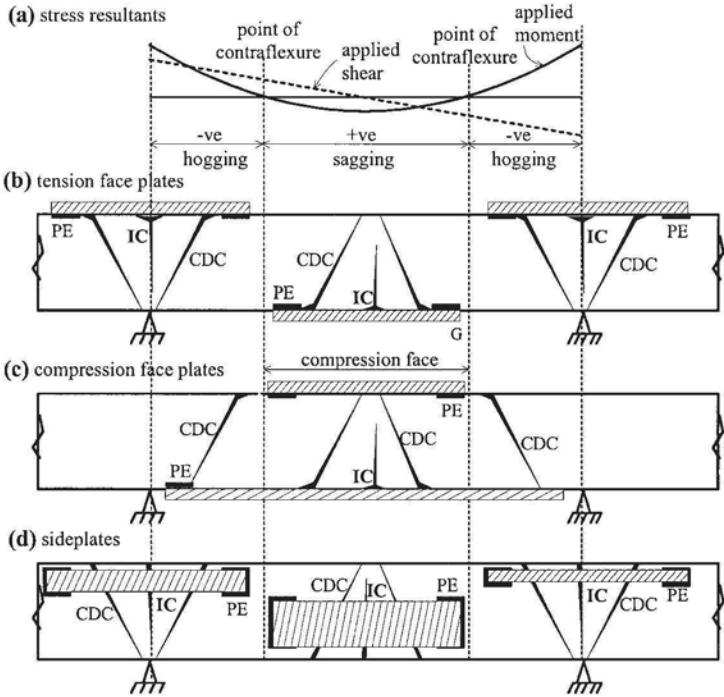


Figure 2.1 Occurrence of IC debonding

Before the flexural strength, flexural stiffness or flexural ductility can be assessed, the strain and stress at IC debonding needs to be determined for plates in

any of the positions shown in Fig. 2.1, which is the subject of this chapter. Examples of IC debonding are first described in this chapter, which is then followed by a description of the IC debonding mechanism in pull tests and in beam tests. From a comparison of the IC debonding resistances, there would appear to be emerging two distinct design philosophies both of which are correct but which are based on significantly differing premises.

2.2 Examples of IC debonding

2.2.1 Adhesively bonded longitudinal plates predominantly in flexure

2.2.1.1 Tension face plates

The IC interface cracks initiate within the region of maximum moment as shown in the tension face plated beam in Fig. 2.2, and then the individual IC interface cracks gradually propagate, from their associated flexural and flexural/shear intermediate cracks, towards the plate ends as can also be seen in Fig. 1.15. Eventually these cracks join up or merge as shown in Fig. 2.3 where only the ends of the plate are attached or anchored.

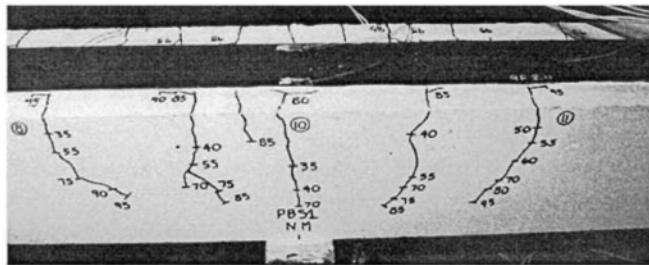


Figure 2.2 IC interface cracking

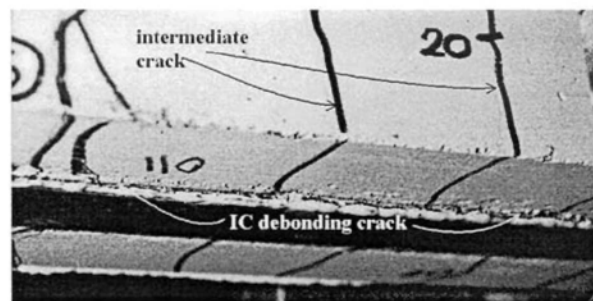


Figure 2.3 IC debonding

At the stage of IC interface cracking shown in Fig. 2.3, where only the plate ends are attached, the plate is acting like an external prestressing rod with uniform strain between the end anchorages so that standard beam theory cannot be applied. This behaviour may be sufficient to cause the strains in the plate to reduce, even though the ends of the plate are still anchored, in which case IC debonding has

occurred. Alternatively, soon after the IC interface cracks merge the debonding cracks spread rapidly to the plate ends causing IC debonding as shown in Fig. 1.1. Tests have shown that the spread of IC interface cracking prior to IC debonding can vary from as little as 10% of the plate length to about 40%, so that the extent of the spread of IC interface cracking is not a reliable guide to eventual IC debonding.

Unlike interface shear stress ($V\Delta y/lb$) debonding described in Section 1.3.4, IC debonding is not directly related to the vertical shear force V as it can occur in a constant moment region as shown in Fig. 2.4. The behaviour of IC debonding is more akin to the partial-interaction behaviour of embedded reinforcing bars between flexural cracks or the partial-interaction behaviour of stud shear connectors in composite steel and concrete beams.

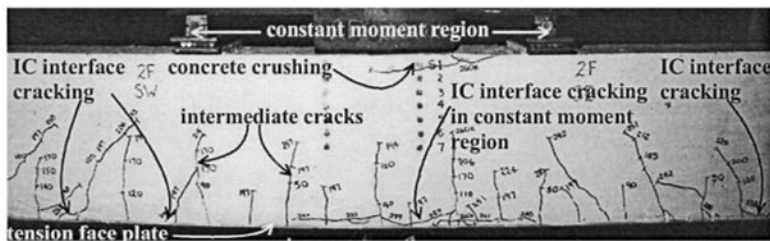


Figure 2.4 IC interface cracking in a constant moment region

2.2.1.2 Side plates

Figure 2.5 shows the hogging (-ve) region of a two span continuous beam in which longitudinal side plates have been adhesively bonded to the tension region of the side of the beam. The side plates have been deliberately extended past the points of contraflexure into what may be termed flexurally uncracked regions. Under the hogging region plate, the ends of the side plates for the sagging regions can be seen, which have also been extended past the point of contraflexure into the uncracked regions. It can be seen that IC debonding and its associated IC interface cracking also occurs in side plated beams. As would be expected, the intermediate cracks mainly consist of inclined flexural/shear cracks that are concentrated in the region of maximum moment. It can also be seen that where these intermediate cracks intercept the longitudinal side plate they induce IC interface cracks at the top and bottom edges of the longitudinal plate that propagate away from the position of maximum moment towards the plate ends. The IC interface cracks on the right hand side have reached the point of contraflexure after which the strains in the strain gauges, which can be seen at the mid-depth of the plate, reduced significantly indicating IC debonding was complete even though the anchorage zones were still attached.

Figure 2.6 shows IC debonding in a steel side plate in which the plate ends were still anchored, which is the same behaviour as the tension face plate in Fig. 2.3. In contrast, Fig. 2.7 shows how IC debonding has caused the end anchorages to debond in all of the longitudinal plates in the two span continuous beam with carbon FRP side plates that were attached to the tension zones.

It is the experience of the authors that the vast majority of plates in adhesively bonded plated beams will debond at some stage of their loading cycle. This is because IC debonding is not solely dependent on the strain in the plate but also depends on the width of the intermediate crack that has to be accommodated by the plate. Hence, even when the applied load is reducing causing the strains in the plate also to reduce,

the plate will still usually debond at some stage of the loading cycle because of the widening of the intermediate cracks. It is, therefore, necessary to design for ductility for which design procedures are available.

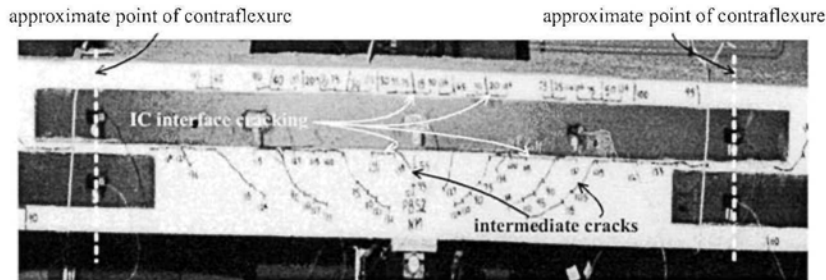


Figure 2.5 IC interface cracking and IC debonding of steel plates

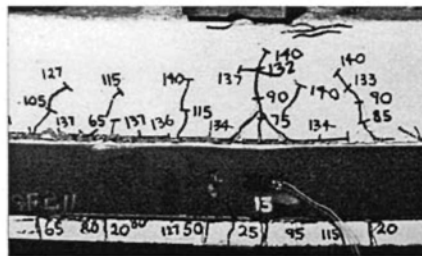


Figure 2.6 IC debonding with plate ends still anchored



Figure 2.7 IC debonding throughout longitudinal carbon FRP side plates

2.2.2 Adhesively-bonded and bolted longitudinal plates predominantly in flexure

Unlike adhesively-bonded plates, bolted plates can exhibit a large amount of ductility as shown in Fig. 2.8. Figure 2.8 is an example of a tension face plate that has been both adhesively-bonded and bolted. Bolts form a ductile connection that requires significant slip in the order of millimeters to transfer the interface shear forces. In contrast, an adhesive bond is a stiff brittle joint that requires slips of the order of micrometers prior to IC interface cracking and only tenths of millimeters after IC interface cracking to resist shear. Hence, the adhesively-bonded and bolted plate in Fig. 2.8 first acts purely as an adhesively bonded plate where it can be seen that the intermediate cracks induce IC interface cracking.

Eventually the IC interface cracks in Fig. 2.8 merge and allow the plate to substantially slip relative to the RC beam. This then allows the bolts to slip to resist the longitudinal shear, as can just be seen in Fig. 2.9(a) by the distance between the bolt head and its original position to the left. This form of plate retrofitting, that is

both adhesively-bonded and bolted was found to be extremely ductile as can be seen in Fig. 2.9(b) where the strains in the plate were sufficient to cause it to fracture.

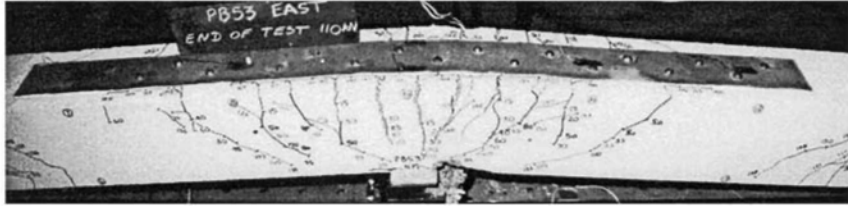


Figure 2.8 Adhesively-bonded and bolted plated beam at failure

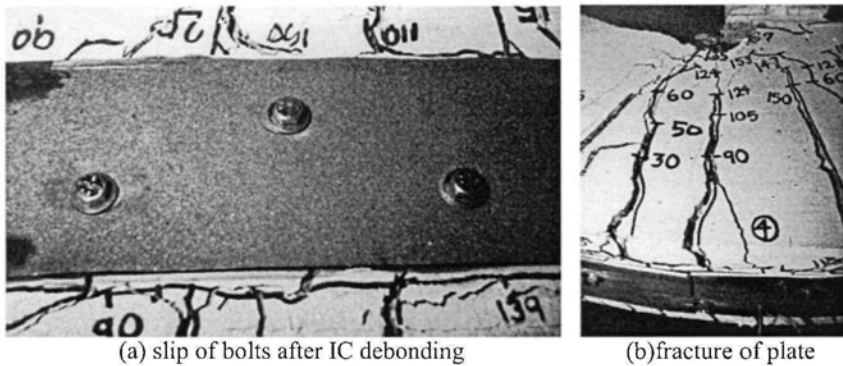


Figure 2.9 Ductility of a bolted plated beam

As a matter of interest, these tests showed that adhesively-bonded and bolted plated beams behave better than either adhesively plated beams or bolted plated beams. This is probably because after IC debonding the bolts not only resist longitudinal shear but by holding the plate/concrete interface together allow longitudinal shear to be transferred by aggregate interlock. Hence bolting plates or bolting and adhesively-bonding plates are an ideal choice if ductility is required. However, bolting does not affect IC debonding unless the bolts are deliberately pretensioned to impose interface compression; it is felt that this should not be relied upon. It is suggested that bolted and adhesively-bonded plates should be designed as separate bolted and adhesively-bonded structures.

2.2.3 IC debonding resistance contribution to vertical shear

Another example of IC interface cracking which may lead to IC debonding is shown in Fig. 1.16 where it can be seen that the intermediate diagonal cracks have induced IC interface cracking. In this example, IC debonding has not yet occurred. However, Fig. 1.16 does illustrate how the IC debonding resistance indirectly increases the shear resistance of the beam V_c . This is because the longitudinal plate spans the diagonal crack. Should this diagonal crack then try to open up or slip to resist the vertical shear, then the IC debonding resistance of the plate will prevent this shear displacement and help increase the shear capacity, in much the same way as longitudinal reinforcing bars or prestressing increases the concrete shear capacity of a beam or slab V_c .

A further example of the importance of the IC debonding resistance and why it is the dominant debonding mechanism is shown in Fig. 2.10 where external FRP stirrups that span a diagonal crack have detached due to IC debonding as also illustrated in Fig. 1.29; these external stirrups can also rupture if thin enough as when produced by the wet lay up process. Furthermore, if FRP stirrups can be wrapped or anchored in the flange of a T-section then failure can also be by rupture.

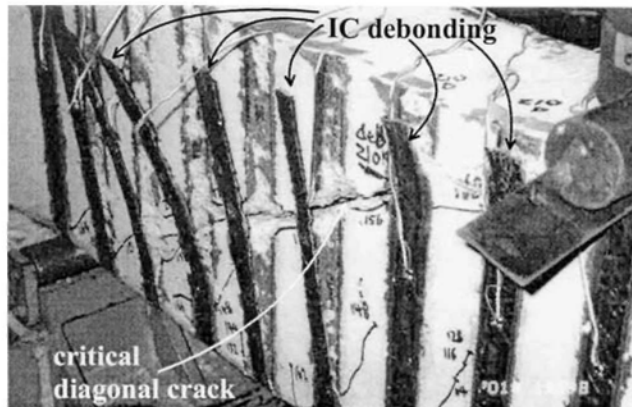


Figure 2.10 IC debonding in vertical FRP stirrups (Jin-Guang Teng)

2.3 IC debonding behaviour

2.3.1 IC debonding in pull-push tests

2.3.1.1 Pull-push tests

The resistance to IC debonding is often determined directly from simple single-lap pull-push tests of a plate-to-concrete joint such as that shown in Fig. 2.11(a). The plate is adhesively bonded to the concrete prism, the concrete is restrained and the plate pulled along its axis until failure occurs either by plate fracture or debonding. Typically, a wedge of concrete is pulled away at the loaded end of the concrete prism as can be seen in Figs. 2.11(b) and (c) and debonding occurs adjacent to the adhesive-concrete interface within the concrete adherend as can be seen in Figs. 2.12 and 1.8(a).

The pull-push specimen in Fig. 2.11(a) is a convenient and inexpensive way of estimating the IC debonding resistance in beams in much the same way as push tests are often used to estimate the shear resistance of new types of shear connectors in composite steel and concrete beams. The pull-push specimen may be considered to represent a beam such as that in Fig. 1.1 but with only a single flexural crack over the support. It is recognised that pull-push tests do not fully represent the behaviour in beams as they do not allow for the curvature in the beam, which may affect the interface normal stress distribution, nor do they allow for the interaction of interface shear stress distributions between closely spaced intermediate cracks. However, pull-push tests are a very convenient and inexpensive way of at least determining the parameters that affect IC debonding. Furthermore, it will be shown later, in Section 2.4.4, that the IC debonding resistances derived from pull-push tests give a lower bound to those derived from plated beams and slabs and, hence, can be used as a safe design option.

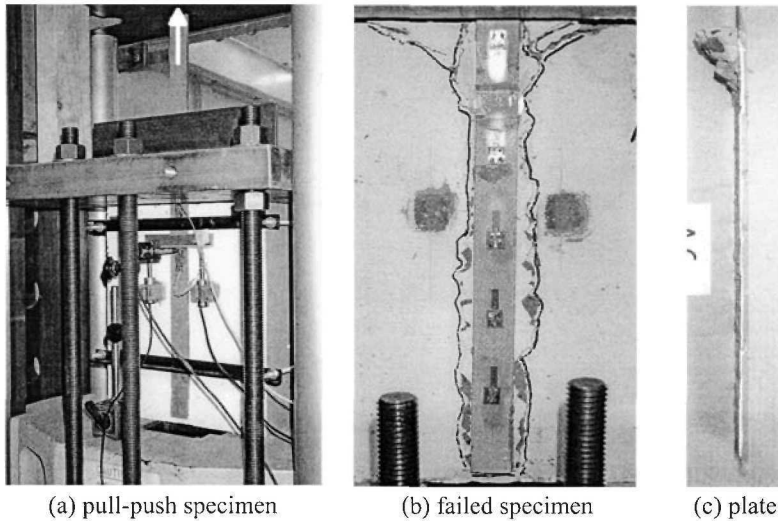


Figure 2.11 IC debonding pull-push specimens

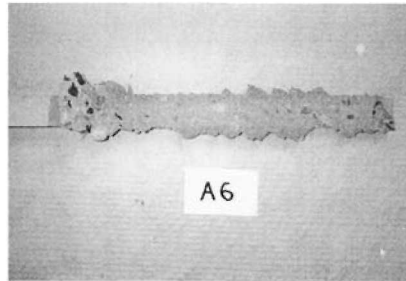


Figure 2.12 IC debonding within concrete

2.3.1.2 Global interface behaviour

The global distribution of the interface shear stress τ_{int} along the length of an adhesively-bonded plate in a pull-push test is shown in Figs. 2.13.

Figure 2.13 is the experimental interface shear stress τ_{int} distribution along the length of a 1.2 mm thick CFRP plate with an average adhesive layer thickness of 2 mm as the axial load in the plate is increased. The origin of the graph is at the loaded end (top) of the concrete prism in Fig. 2.11(b) which represents the position of an intermediate crack. Up to an applied load of 9.8 kN, the plate-to-concrete joint is uncracked and the shape of the shear stress distribution is that given by classical linear elastic theory. As the load is further increased to 42.8 kN, a softening branch develops from the loaded end of the plate indicating the propagation of IC interface micro-cracks which are typically not visible by the naked eye. At this load, the extent of IC interface micro-cracking is approximately 100 mm which is determined by the location of the peak shear stress as it moves towards the end (bottom) of the plate. As the load is increased to the peak load of 51.5 kN, a region of IC interface macro-

cracking develops from the loaded end of the plate and the elastic-softening region of the distribution moves towards the end of the plate. The extent of IC interface macro-cracking, identified by the length of plate from the loaded-end (or intermediate crack) and the start of the softening branch which is approximately 120 mm in Fig. 2.13, is the IC interface debonding crack that is visible as in Fig. 2.2. Under displacement control, a portion of the post-peak response can be observed prior to complete debonding as can be seen by the shear stress distribution at a load of 47.1 kN where the IC interface debonding crack has propagated approximately 150 mm from the loaded-end of the concrete prism.

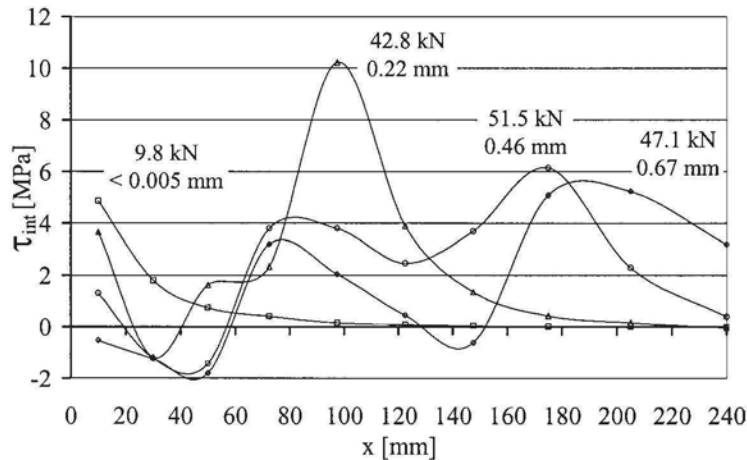


Figure 2.13 Distribution of interface shear stress τ_{int} with applied load and δ_{IC}

The variation in the shear stress distribution observed in Fig. 2.13 within the region of IC interface macro-cracking is a result of local bending of the plate due to the roughness along the IC interface crack. The negative shear stresses within the first 50 mm of the bonded joint after IC interface macro-cracking is an aberration due to the distortion of the strain in the vicinity of the concrete wedge attached to the plate such as at the top of the plate in Fig. 2.11(c).

Also given in Fig. 2.13 is the value of end slip δ_{IC} between the concrete and plate at the loaded end (top) of the concrete prism for the interface shear stress distributions shown. As the top of the concrete prism is equivalent to the position of an intermediate crack (IC), this slip has been referred to as δ_{IC} . It can be seen that very small changes in δ_{IC} cause very large changes in the distribution of τ_{int} .

2.3.1.3 Local and fundamental partial-interaction interface behaviour

(a) Shear-stress/slip

Of special significance is the variation of the interface shear stress τ_{int} with the interface slip δ_{int} at a specific position x along the plate as shown in Fig. 2.14. This variation is very important as it controls the propagation of the IC interface crack and ultimately the IC debonding mechanism and resistance. The τ_{int}/δ_{int} relationship is equivalent to a material property, such as the stress/strain relationship of a material, and if known could theoretically be input into numerical simulations of plated beams to determine IC debonding resistances. The τ_{int}/δ_{int} relationship is the fundamental property that controls IC debonding.

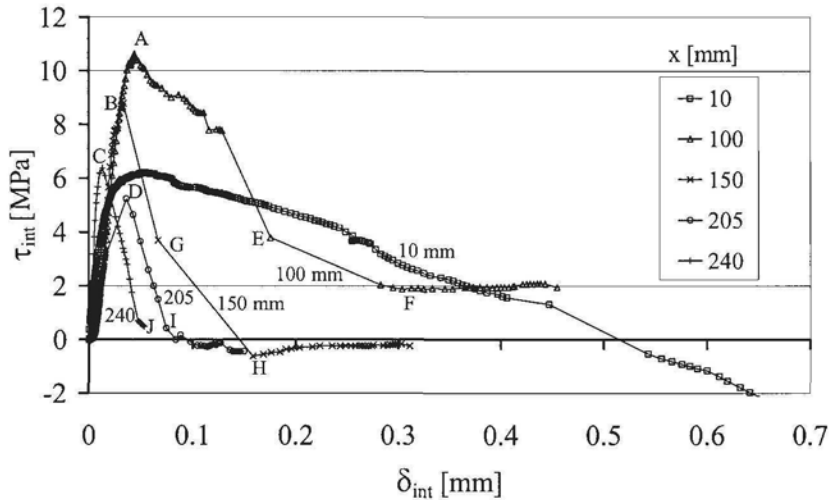


Figure 2.14 Variation of interface shear stress τ_{int} with interface slip δ_{int}

The best analytical solutions of the IC debonding mechanism in pull-push tests have used bilinear local τ_{int}/δ_{int} models such as those shown in Fig. 2.15. Bilinear models consist of an initial linearly ascending branch up to a peak interface shear stress τ_f followed by a linearly descending branch representing interface softening, or micro-cracking, until the interface shear stress reaches zero at which time macro-cracking, or IC interface debonding, is assumed to occur at a slip of δ_f . The absence of any residual shear strength after debonding in the bilinear models imply that friction and aggregate interlock over the debonded length is ignored.

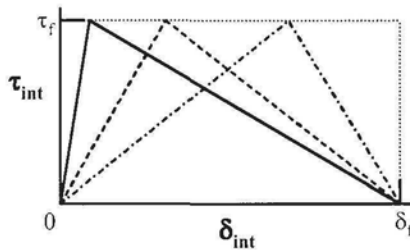


Figure 2.15 Idealised local shear stress slip relationship

Although the local τ_{int}/δ_{int} distributions shown in Fig. 2.14 can be idealised as bi-linear, it is clear that the distribution varies considerably along the length of the bonded joint. With the exception of the local τ_{int}/δ_{int} distribution 10 mm from the loaded-end of the concrete prism, which is affected by the concrete wedge attached to the plate as discussed in the previous section, two trends in the variation can be observed. One is that the peak shear stress, such as A, B, C and D in Fig. 2.14, prior to softening reduces further from the loaded-end, or as interface cracking propagates. Note that the maximum peak interface shear stress occurs locally at a distance of

about 100 mm (line $x = 100$ mm in Fig. 2.14) which corresponds to the location of the peak stress when a load of 42.8 kN in Fig. 2.13 was applied to the plate; this is the initiation of macro-cracking as described in Fig. 2.13. The second trend is the transition from a bilinear descending or interface softening branch, A-E-F and B-G-A in Fig. 2.14, near the loaded-end of the plate to a linear descending branch, D-I and C-J, towards the end of the plate. The softening response stiffness, the rate of reduction in shear in Fig. 2.14 after the peak shear, is less near the loaded-end of the plate which can be attributed to aggregate interlock and friction along the debonding crack as the interface slip increases. The frictional component is of course a function of the normal stress distribution across the bonded joint which in pull-push tests is highest near the loaded-end of the plate. Once softening begins near the end of the plate for longer bonded lengths the IC interface crack propagates rapidly and hence, there is no stiffening of the softening branch. However, as expected, one similarity between the local τ_{int}/δ_{int} distribution is the slope of the initial ascending branch as the interface is linear elastic within this region.

Factors that affect the local τ_{int}/δ_{int} distribution in pull-push tests include the material properties of the adherends E_p and E_c , the concrete strength, and geometric properties t_p and b_p/b_c . The influence of these factors on the IC debonding resistance is discussed in Section 2.4. Another factor that as of yet has not been adequately considered is the stiffness of the adhesive layer $E_a t_a$.

The τ_{int}/δ_{int} relationships for both the IC interface cracking of an adhesively bonded plate and that for an embedded reinforcing bar are compared in Fig. 2.16. It can be seen that embedded reinforcing bars have a ductility that is an order of magnitude greater than that of the plate, that is the slip capacity is much greater and the bond strength over this slip is fairly constant. Hence, the design principles applied to the anchorage of reinforcing bars cannot be applied to the anchorage of adhesively bonded plates. Because the bond/slip characteristics of embedded reinforcing bars is characteristically ductile, it is a standard design procedure to assume the bond strength is constant over the anchor zone in calculating the anchorage length required. This same principle cannot be applied to adhesively bonded plates as the bond characteristics are brittle.

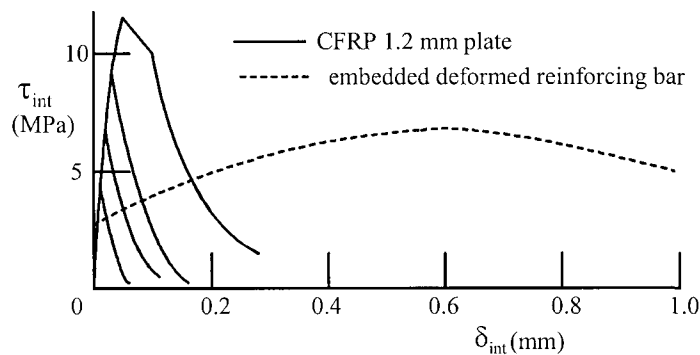


Figure 2.16 Comparison of plate and reinforcing bar τ_{int}/δ_{int} relationship

(b) Plate-axial-stress/slip

Finally, the variation of the plate stress at the intermediate crack $\sigma_{p,IC}$ with the slip at the same position δ_{IC} is shown in Fig. 2.17. This local behaviour at the intermediate

crack is a function of the global variation of τ_{int}/δ_{int} between intermediate cracks, that is the local variation σ_{IC}/δ_{IC} at an intermediate crack represents the behaviour between cracks. The $\sigma_{p,IC}/\delta_{IC}$ relationship for adhesively plated structures is equivalent to the load/slip relationship of shear connectors in composite steel and concrete beams. Stud shear connectors in composite steel and concrete beams can fail prematurely due to excessive slip and this is the situation with plated beams. This analogy helps to illustrate the similarity between these two systems and the fact that it is a partial interaction problem, that is there is a step change in the strain profile between the plate and the RC beam due to the slip, which was first solved for linear elastic composite beams by Newmark (1951).

The variation of plate stress with end slip is easily obtained from pull-push tests and can be used to identify the initiation of micro-cracking and macro-cracking as indicated in Fig. 2.17 by the abrupt changes in the response of the bonded joint. It has been shown (Yuan et al 2003) how these points on the $\sigma_{p,IC}/\delta_{IC}$ response can be used to define the bilinear local τ_{int}/δ_{int} model discussed in the previous section. Furthermore, experimental and parametric studies have shown that by increasing the bond length the ductility of the bonded joint can be increased and increasing the stiffness of the plate per unit width ($E_p t_p$) increases σ_{IC} at IC debonding at the expense of a reduced ductility.

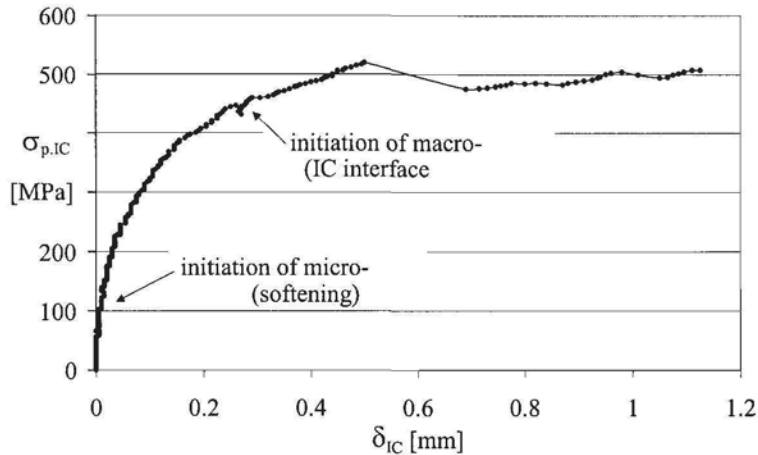


Figure 2.17 Variation of plate stress $\sigma_{p,IC}$ with end slip δ_{IC}

2.3.2 IC debonding in beams

2.3.2.1 IC interface crack propagation

The two span continuous beam in Fig. 2.18 is plated over its hogging region. The plates are terminated well past the points of contraflexure and close to the applied loads so that it can safely be said that the plates are anchored in an uncracked region.

IC debonding of a steel tension face plate is shown in Fig. 2.19. These beams were specifically designed so that IC debonding would precede PE debonding as well as precede CDC debonding and, hence, the absence of any critical diagonal cracks in the beam. The point of contraflexure can be estimated to lie approximately midway along the flexurally uncracked region E-D and so it can be seen that the plate was terminated well into the compression face and, hence, anchored in an uncracked

region. As designed for, PE debonding which propagates from the plate ends inwards, did not occur so that the only mechanism of debonding which occurred in this beam was IC debonding.

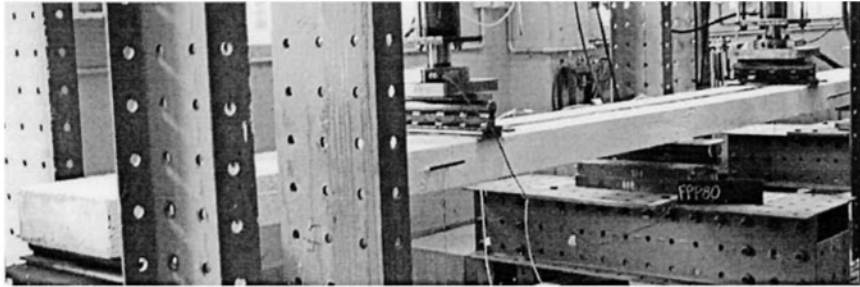


Figure 2.18 Two span continuous beam plated in hogging region

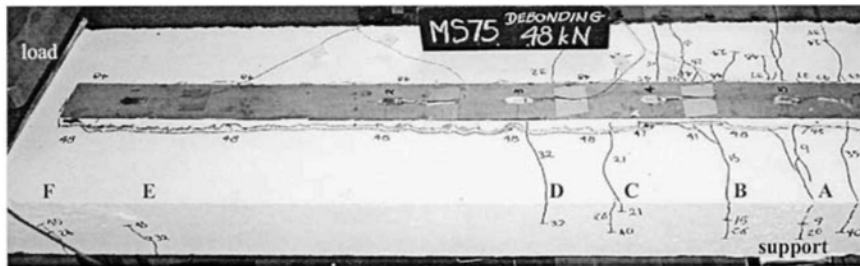


Figure 2.19 IC debonding failure of a steel tension face plated beam

The sequence of cracking is illustrated in Figs. 2.20 and 2.21 for a CFRP plate of the same length and width as the steel plate in Figs. 2.18 and 2.19. A flexural crack first formed over the support at a load that is marked 9 in Fig. 2.20(a) and from this intermediate crack, interface cracks propagated in both directions toward the plate ends. Further flexural cracks then occurred as the load was increased from 24 kN to 35 kN in Fig. 2.20(b) and from each emanated an IC interface crack which propagated towards the nearest plate end, that is away from the internal support. Hence in general, except for the flexural crack at the position of maximum moment where the IC interface crack propagated in both directions, the IC interface crack propagates in one direction towards a region of lower moment. At the load of 35 kN, the IC interface cracks are still concentrated close to the position of maximum moment. A further increase in load from 35 kN to 45 kN in Fig. 2.21 caused IC debonding as the IC interface crack propagated more rapidly to the point of contraflexure, and then at 45 kN it continued very rapidly towards the plate end in the anchorage zone although the plate end still remained attached.

Figure 2.19 illustrates the difference between IC debonding in a beam and IC debonding in a pull-push test as in Fig. 2.11(b). In Fig. 2.19, the force in the plate is transmitted from the concrete in the *uncracked* zone E-D which is equivalent to the pull-push specimen in Fig. 2.11(b), plus the force in the concrete between what is sometimes termed the concrete teeth D-C, C-B and B-A. Hence in this example, there are 4 zones in the shear span, bordered by the intermediate cracks, through which

shear forces can transmit the axial forces in the plate. These four zones pull the plate but may not necessarily achieve their maximum force at the same time which adds to the complexity of the problem. These concrete teeth are equivalent to the shear connectors in composite steel and concrete beams and their individual $\sigma_{p,IC}/\delta_{IC}$ behaviours (as described for pull-push tests in Section 2.3.1.3 and in Fig. 2.17) control the axial force in the plate. It is an irony of this mechanism that intermediate cracking may actually help to increase the force in the plate above that achieved from pull-push tests. It must be emphasised that this is a simplistic description of the shear force mechanism which it is felt is much more complex as it is also affected by the curvature in the beam.

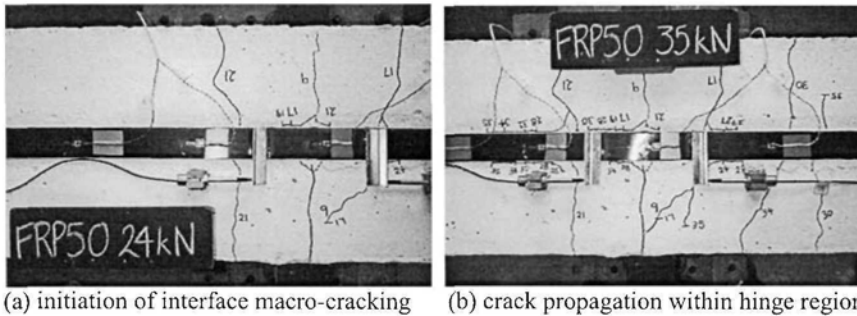


Figure 2.20 IC interface cracking

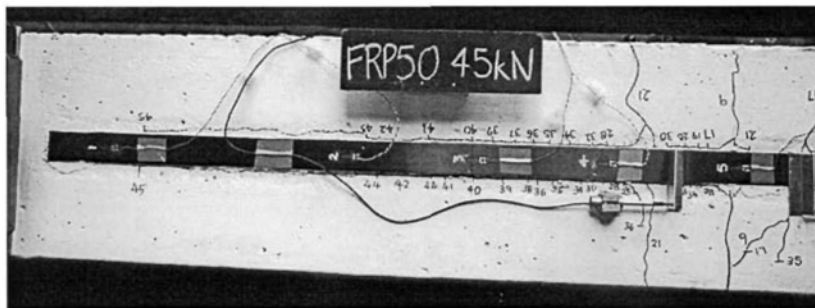


Figure 2.21 IC debonding crack propagation to uncracked anchorage zone

2.3.2.2 IC interface crack propagation simulations

Much research is still required to develop practical models that can adequately quantify the IC debonding stress of plates bonded within cracked regions of beams or slabs. However, several researchers (Monti et al 2003, Niu and Wu 2003) have developed fully non-linear finite element models to determine the influence of intermediate cracks on the interface shear stress distribution and IC debonding stress.

Except for the effect of curvature, it is generally accepted that pull-push tests are a good approximation of the behaviour in flexural members where IC debonding is controlled by a single dominant intermediate crack as may be the case in cantilever slabs, or where intermediate cracks are spaced far apart as in lightly reinforced members or strengthened plain concrete members. However, the IC debonding stress

obtained from pull-push tests is a lower bound to the IC debonding stress in flexural members where intermediate cracks are spaced closer than two times the effective length of the plate. The effective length of an adhesively bonded plate is commonly defined as the bond length under linear elastic deformation over which the interface shear stresses resist a minimum of 97% of the applied load for a joint with an infinite bond length. For example, for the pull-push test results shown in Fig. 2.13, the effective length at the linear elastic load limit of 9.8 kN is approximately 100 mm. When intermediate cracks are spaced closer than twice the effective length there is an interaction of the interface shear stress distribution between cracks. Within an uncracked block between intermediate cracks the interface shear stresses are in opposite directions and the resultant distribution may be simply obtained by superposition. The end result is that a larger force in the plate is required to propagate the IC interface debonding crack. In other words, the propagation of the debonding crack in one direction is hindered by the interface shear stresses acting in the opposing direction from the adjacent crack which must first be overcome before propagation continues towards the plate ends, eventually leading to complete IC debonding.

2.4 Comparison of IC debonding rules

2.4.1 Effective length or anchorage length concept

The axial force to cause debonding in a pull-push test, such as that shown in Fig. 2.11, depends on the length of plate bonded to the concrete. The typical variation obtained from pull-push tests in Fig. 2.22(a) is illustrated in Fig. 2.22(b). As the bonded length of the plate l_b is increased, the force in the plate to cause debonding P_{IC} also increases as shown. However, beyond a certain length L_e , the force to cause debonding remains constant at $(P_{IC})_{max}$; of course $(P_{IC})_{max}$ is limited by the force to fracture an FRP plate or yield a metal plate. As discussed in Section 2.3.1.1, this maximum resistance $(P_{IC})_{max}$ is because the IC interface crack bond behaviour is predominantly brittle as illustrated in Fig. 2.15. The minimum anchorage length of plate required to achieve the maximum axial force in the plate $(P_{IC})_{max}$ is often referred to as the effective length L_e . This anchorage length is typically 50 to 100 times the plate thickness t_p . As an example, for a 1.2 mm thick pultruded CFRP plate L_e may only be about 100 mm which is very short whereas for 7 mm steel plates it may be in the order of about half a meter.

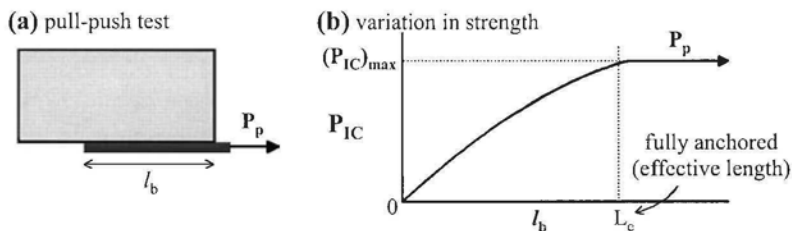


Figure 2.22 Effective length (anchorage length)

2.4.2 Effective width concept

Tests have also shown that the width of a plate b_p as a proportion of the width of the concrete element b_c , that is the parameter b_p/b_c as illustrated in the symmetrically

plated beam in Fig. 2.23(a), can also affect the debonding strength. This is a result of the interaction of the stress field in the disturbed region surrounding individual plates when they are placed close together, as shown in the top plates in Fig. 2.23(b). Placing the plate close to the edge of a concrete element, as in the bottom plate in Fig. 2.23(b), will also have the same effect by reducing the width of the debonding plane.

It is not always clear what width of the concrete element should be used in the parameter b_p/b_c when the plate is placed eccentric to the overall width of the concrete element as shown in Fig. 2.23(c). It is suggested that the principles used in national standards in determining the effective width of a beam allowing for shear lag or the principles used in determining the effective width of the concrete element resisting the anchorage forces in a post-tensioned beam can be used (Oehlers and Bradford 1999). Examples of these effective widths are shown in Fig. 2.23(c) in terms of the half effective widths $b_c/2$ where the smaller of the half widths $(b_c/2)_1$ and $(b_c/2)_2$ should be used in determining b_c . A similar approach can be used for interacting plates as in Fig. 2.23(d) where the mid-distance between plates is used as one boundary.

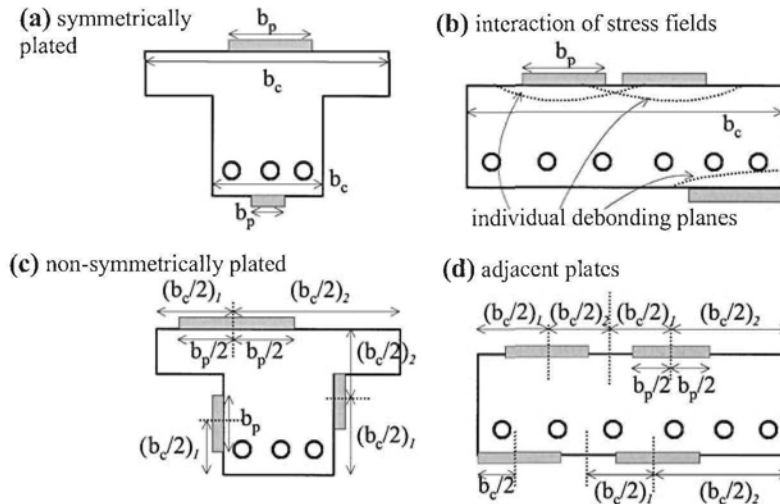


Figure 2.23 Effective widths

2.4.3 IC debonding resistances

Teng et al (2001) have published a comprehensive and excellent analysis of the IC debonding resistances of FRP and steel plated tests as well as a comparison of published debonding equations. They recommended the following form of equation for the IC debonding resistance for fully anchored plates based on fracture mechanics and experimental data.

$$\sigma_{IC} = \alpha \beta_p \beta_L \sqrt{\frac{E_p \sqrt{f_c}}{t_p}} \quad \text{N and mm} \quad 2.1$$

The parameter β_p allows for the width of the plate relative to the width of the concrete element as explained in Section 2.4.2 and is given by the following expression.

$$\beta_p = \sqrt{\frac{2 - b_p/b_c}{1 + b_p/b_c}} \quad 2.2$$

Although a limit was not placed on the parameter b_p/b_c , it is recommended that $b_p/b_c \geq 0.33$ as recommended in the European guidelines (Table 1.1).

The full anchorage length or effective length of a plate in a pull-push test or in an uncracked zone is given by

$$L_e = \sqrt{\frac{E_p t_p}{\sqrt{f_c}}} \quad \text{N and mm} \quad 2.3$$

Tests have shown that when the bonded length l_b is less than L_e in Fig. 2.22, the strength varies according to the following function as shown in Fig. 2.22(b).

$$\beta_L = \begin{cases} 1 & \text{if } l_b \geq L_e \\ \sin[\pi L/2L_e] & \text{if } l_b < L_e \end{cases} \quad 2.4$$

However, it is suggested that where possible all plates should be designed as fully anchored ($l_b > L_e$) and hence $\beta_L = 1.0$, if not then for a safe design and to simplify the analysis, the variation could be considered linear between $l_b = 0$ to $l_b = L_e$.

The α coefficient in Eq.2.1 was calibrated using a large number of tests that included steel plates, FRP plates, pull-push tests, slab tests and beam tests and the results are summarised in Table 2.1. Within these tests the plate thickness t_p varied from 0.11 mm to 3 mm, the Young's modulus E_p from 29 GPa to 230 GPa, and the concrete cylinder compressive strength f_c from 20 MPa to 48 MPa. The mean value of the α coefficient is given in row 1 and the 95% characteristic value in row 2.

Table 2.1 IC debonding coefficient α

α	pull tests			slabs	beams	slabs & beams	
	(1)	(2)	(3)	(4)	(5)	(6)	(7)
		FRP	Steel	Steel & FRP	-	-	-
(1) mean		0.448	0.401	0.427	0.720	1.100	0.887
(2) 95%		0.322	0.324	0.315	0.478	0.544	0.379

The α coefficient of 0.427 corresponding to the mean strength in Table 2.1 for all the pull-push tests in column 4 is less than that in slabs and beams of 0.887 in column 7. This suggests that the IC debonding mechanism in flexural members, described in Section 2.3.2, in which the *concrete teeth* created by the intermediate cracks, and which act as shear connectors can significantly increase the axial force in the plate (in this case allow the axial stress to be doubled). Possibly of more significance is that doubling the α coefficient in Eq.2.1 will allow the plate thickness to be quadrupled. However, the scatter of results, as represented by the 95% characteristic values in row 2 of Table. 2.1, is very large suggesting much more research is required to identify and quantify the parameters that control IC debonding.

2.4.4 Comparison of IC debonding resistances

A comparison of recommendations for IC debonding resistances is given in Table 2.2. To help in the comparison, the properties of the FRP plate used in Table 2.2 were assumed to be: $E_p = 160$ GPa; $f_c = 30$ MPa, $t_p = 1.2$ mm unless shown otherwise; and $b_p/b_c = 0.5$. In the first four rows in Table 2.2, the Chen and Teng results are based on the Hong Kong approach, Neubauer and Rostasy from the European approach, and both the Concrete Society and the German Institution of Construction from the British approach, as listed in Table 1.1. The remaining rows from 5 to 9 are the results from plated beam tests from The University of Adelaide. Rows 5 and 6 are the results from FRP plated tests with 1.2 mm plates which were increased to 2.4 mm thick in row 7. The results of 3 mm thick steel plated beam tests are included in rows 8 and 9 for comparison. The strains at debonding are listed in columns 1 for the 95% characteristic value and in row 2 for the mean value where given. Where columns 1 and 2 are combined, these are recommendations or test results. The stresses at debonding are listed in rows 3 and 4 and where combined are also the recommended or test results.

Table 2.2 FRP IC debonding resistances

Source	ϵ_{IC} 95% (1)	ϵ_{IC} mean (2)	σ_{IC} [MPa] 95% (3)	σ_{IC} [MPa] mean (4)
1) Chen and Teng	0.0027	0.0053	427	854
2) Neubauer and Rostasy	0.0026			
3) Concrete Society	0.0060 - 0.0080		960 - 1,280	
4) German Inst. of construction	0.0065 - 0.0085		1,040 - 1,360	
5) Adelaide FRP beam tests 1999	0.0046 - 0.0052		782 - 884	
6) Adelaide FRP beam tests 2002	0.0025 - 0.0027		425 - 459	
7) Adelaide FRP beam tests 2002 (2.4 mm)	0.0015		255	
8) Adelaide Steel beam tests 1999 (3 mm)	0.0201 - 0.0213			
9) Adelaide Steel beam tests 20002 (3 mm)	0.0045			

The effective length of the 1.2 mm FRP plates in Table 2.2 was derived as 187 mm from Chen and Teng's model and 189 mm from Neubauer and Rostasy which shows a good agreement. By convention, the characteristic debonding strains in column 1 are the strains which would be used in design with an appropriate strength reduction factor. In column 1, Chen and Teng's characteristic debonding strain of 0.0027 is in close agreement with Neubauer and Rostasy's 0.0026, is significantly less than the test results in row 5 and is about the same as the test results in row 6. Chen and Teng's mean value of 0.0053 is in agreement with the test results in row 5. Chen and Teng's mean and characteristic results, Neubauer and Rostasy's characteristic result, and the tests results in rows 5 and 6 are well below the range of recommendations by the Concrete Society and the German Institution of Construction in rows 3 and 4 which should therefore be used with extreme caution. In row 7, the plate thickness was doubled and as would be expected the debonding strains reduced.

In row 8 in Table 2.2, the steel plated beams first yielded and then debonded at strains that were an order of magnitude greater than in the FRP tests in rows 5 and 6. This illustrates how, unlike FRP plates which are elastic/brittle, metal plates can be designed to yield prior to debonding and also how debonding still occurs after yielding as explained previously in Section 2.2.1.2. Also included in row 9 are the results of more recent tests in which the steel plates also yielded prior to debonding

but then debonded at much lower strains than those in row 8. The variations between test results illustrate the complexity of the problem. For example, another parameter in addition to intermediate crack spacing and curvature that may affect the IC debonding behaviour is adhesive stiffness $E_{a,t}$ which is not considered by existing models as discussed in Section 2.3.1.3.

In Table 2.3, are listed the plate thicknesses in columns 3 and 4 at which the IC debonding resistance of a fully anchored metal plate is equal to its yield capacity. Hence, plate thicknesses below these values will yield prior to debonding. A mild steel plate, of $E_s = 200$ GPa and $f_y = 300$ MPa, and two aluminium plates, with $E_{al} = 63$ GPa and with different yield capacities of 125 MPa and 215 MPa, as listed in rows 1 to 3 and are used in this comparison. The results based on the characteristic debonding resistances are given in column 3. For steel plates the maximum thickness is about 3 mm. As the aluminium has a Young's modulus about one-third that of steel, it is more likely to debond as shown in Eq.2.1. Hence, for high yield capacity aluminium only very thin plates of about 2 mm can be used but thicker plates of 5 mm can be used if the aluminium has a low yield strength. It is worth comparing the plate thicknesses in column 3 that are based on the characteristic resistances with those in column 4 which are based on the mean resistances. It can be seen that if the mean values could be used, then the plate sizes could be quadrupled.

Table 2.3 IC debonding of metal plates

Metal	E [GPa] (1)	Ultimate			Serviceability	
		f_y [MPa] (2)	$t_{p,95\%}$ [mm] (3)	$t_{p,mean}$ [mm] (4)	f_t [MPa] (5)	$t_{p,95\%}$ [mm] (6)
1) Steel	200	300	3.0	12.1	150	12
2) Aluminium	63	125	5.6	22.0	63	22
3) Aluminium	63	215	1.9	7.5	107	8

Not only are adhesively bonded plates used to increase the strength of a structure, but they are often used to improve their serviceability behaviour such as to reduce deflections or vibrations. For convenience, it has been assumed that the serviceability stresses listed in column 5 are half the yield stresses in column 2 in Table 2.3. The maximum plate thicknesses for these serviceability stresses are listed in column 6. These can be compared with those for the ultimate strength limits in column 3. As the plate stresses have been halved, the plate thicknesses have quadrupled. This illustrates how thick metal plates can be used at serviceability. However, the thicknesses given in column 6 should be viewed with caution as it is doubtful whether Teng's model (Eq.2.1) was calibrated with plates of these thicknesses.

2.5 IC debonding design philosophies

From the design guidelines listed in Table 1.1, there would appear to be two distinct design philosophies that are emerging. The Australian and Hong Kong approaches restrict IC interface cracks to a region around the position of maximum moment and this will be referred to as the *hinge approach*. Alternatively, in the European approach, the plate ends are anchored in an uncracked region where the IC interface

cracks are allowed to propagate and this will be referred to as the *anchorage* approach.

2.5.1 Anchorage design philosophy

The anchorage design philosophy developed in Europe (Table 1.1), which is only applicable to tension face plates, is illustrated in Fig. 2.24. In order to design for IC debonding at the positions of maximum moment, the tension face plates in both the hogging and sagging regions have to be terminated in uncracked regions indicated by the hatched areas. This suggests that the plates should be extended at least up to the points of contraflexure as shown. The axial force in the plate is, therefore, the sum of the forces imposed by each concrete tooth, formed by the intermediate cracks as shown, over half a region (that is half the hogging or half the sagging region) that is $\sum P_{IC_tooth}$. Plus the anchorage force in the uncracked region which is assumed to be the pull-push test strength P_{pull_test} . Hence the axial force in the plate P_p is given by

$$P_p = \sum P_{IC_tooth} + P_{pull_test} \quad 2.5$$

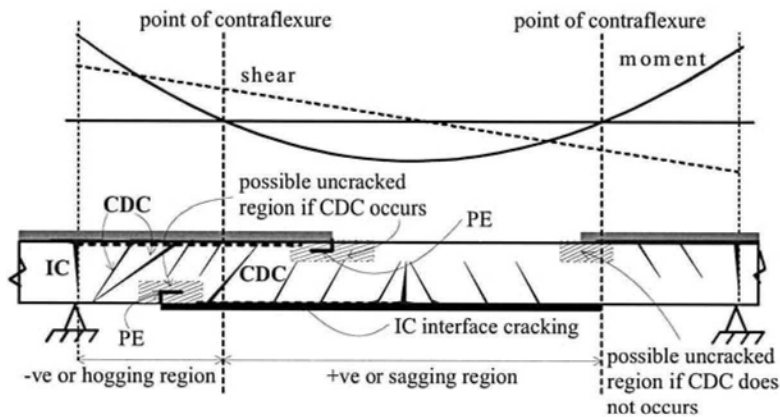


Figure 2.24 Anchorage design philosophy

One design difficulty that might occur on occasions is identifying an uncracked region with which to anchor the plates. For example, the anchorage design approach requires that the sagging region plate in Fig. 2.24 is extended towards the points of contraflexure. Hence, the plate ends are being extended into regions where the vertical shear force is increasing. There is, therefore, the possibility that the plates are being extended in regions where critical diagonal cracks will occur. If we are dealing with a beam with stirrups, then there may be a chance that the sagging region plates cannot be anchored in a region void of shear cracks. In contrast, if we are dealing with a slab, then there is a good chance that the plate can be anchored in a region void of critical diagonal cracks, as slabs are usually designed for only the concrete component of the vertical shear capacity V_c , that is they are usually designed without stirrups so that critical diagonal cracks do not occur. The hogging region plates in Fig. 2.24 are less of a problem, as the plates are being extended into regions where the vertical shear force is reducing. Hence, it should be possible to find an uncracked region.

Having designed for IC debonding in Fig. 2.24, CDC debonding still has to be checked in each region. Although, because of the distribution of vertical shear, the plate is more likely to fail by CDC debonding in the hogging region than in the sagging region. PE debonding still has to be checked but this is unlikely to be a problem as the plates having to be anchored in an uncracked region will probably be terminated near the points of contraflexure where the curvature is low. However, it should be remembered that PE debonding can occur in plates terminated in compression faces but they are less likely to debond than tension face plates.

In summary, it can be seen that the anchorage approach allows high stresses in the plate. This is because the axial force in the plate is contributed by both the ΣP_{IC_tooth} and P_{pull_test} components. Hence relatively small but highly stressed cross-sections of plate are required, however, the plate has to be extended over the whole hogging or sagging region. It is very important to recognise the fact that the anchorage design approach prevents IC debonding from interacting with PE debonding. The authors do not know of any research that has studied this interaction and feel that the best solution is to prevent this interaction as this approach does.

2.5.2 Hinge design philosophy

The hinge design philosophy proposed by the Hong Kong (Table 1.1) and Australian (Table 1.1) approaches is summarised in Fig. 2.25. In this approach, the axial force in the hogging and sagging region plates at the positions of maximum moment are restricted to the IC debonding resistance in pull-push tests.

$$P_p = P_{pull-test} \quad 2.6$$

As shown in Eq.2.5, the force required to debond a fully plated beam is $\Sigma P_{IC_tooth} + P_{pull-test}$, hence, restricting the plate force to $P_{pull-test}$ will limit the IC interface cracks to the region near the position of maximum moment where a plastic hinge may occur indicated by the hatched areas in Fig. 2.25. As the plates in the hogging and sagging regions in Fig. 2.25 do not have to be anchored in uncracked regions, the extent of these plates is determined by CDC and PE debonding and, hence, the plates can be terminated short of the points of contraflexure.

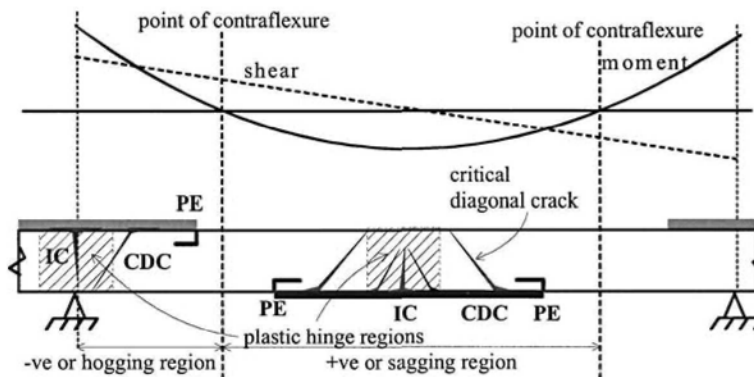


Figure 2.25 Hinge design philosophy

In the hinge approach, the plate is only allowed to carry a smaller force than in the anchorage approach so that a larger cross-section of plate is required for the same increase in strength. However, a shorter plate than in the anchorage approach can be used. As the anchorage approach allows higher strains in the plate than in the hinge approach, the anchorage approach will allow greater curvatures and hence may be more suitable where ductility is required. The hinge approach has the advantage that the IC debonding resistance can be determined directly from pull-push tests. As with the anchorage approach, it is very important to realise that the hinge approach prevents any interaction between IC and PE debonding as it restricts IC interface cracking to within the hinge region.

Both design philosophies are correct; they just approach the problem in different ways. An analogy can be made with earthquake design where the structure can be made very strong to directly resist the earthquake forces, or the structure can deliberately be made ductile to absorb the earthquake energy as it becomes non-linear. Both design philosophies are correct and the engineer can choose the appropriate one. However, the design philosophies should only be combined with care. For example, restricting the axial force in the plate to $P_{\text{pull_test}}$ and anchoring the ends in uncracked regions is very safe. However, designing for the maximum theoretical force $\Sigma P_{\text{IC_tooth}} + P_{\text{pull_test}}$ and then terminating the plate short of an uncracked region is very unsafe. In comparison, the anchorage approach requires small cross-sections of highly stressed plates over long lengths, whereas the hinge approach requires large cross-sections of low stressed plates over short lengths.

2.6 Conclusions

If nothing more, this chapter has illustrated the complexities of IC debonding. It has been shown how IC debonding can be considered as a partial interaction problem as the progression of the IC interface crack allows slip between the plate and the concrete. However, and more importantly, there is also partial interaction because of the creation of plated concrete teeth between the intermediate cracks which act in a similar fashion to shear connectors in partial interaction composite steel and concrete beams. It should be recognised that this unique and highly original approach is proposed by both Niedermeier and Matthy in the European guideline (Table 1.1).

It has also been shown why IC debonding cannot be dealt with using the V_{Ay}/I_b approach, how bonded plates cannot be treated as reinforcing bars, and how bolting adhesively bonded plates can produce a highly ductile section. The very advanced work on the IC debonding resistance of Neubauer and Rostasy in the European guideline (Table 1.1) and that of Chen and Teng in the Hong Kong approach (Table 1.1) has given designers a comprehensive and safe tool to use in IC debonding design. In particular, the work of Chen and Teng in showing the difference in the IC debonding resistances in pull-push tests and beam tests should be recognised as it independently confirms the work of Niedermeier and Matthy.

Because of the work of Niedermeier and Matthy, Neubauer and Rostasy, and Chen and Teng, there would appear to be two emerging design philosophies. The *anchorage approach* extracts as much as possible from the plate by allowing for partial interaction but requires the entire hogging or sagging region to be fully plated. Hence, this approach leads to the minimum cross-sectional area of a highly stressed plate but over the longest length. In contrast, the *hinge approach* restricts the IC interface cracking to a small hinge area by limiting the strains in the plate. Hence, this

approach leads to a larger cross-sectional area of plate than in the anchorage approach, that is less stressed and required over a shorter length. Both approaches are correct and it is up to the designer to choose the most appropriate one. The anchorage approach does allow higher strains and hence higher ductility and the hinge approach allows the IC debonding resistance to be determined directly from pull-push tests. In both design philosophies, metal plates can be designed to yield prior to IC debonding to allow increases in ductility.

This chapter has not only qualitatively described the fundamental behaviour of IC debonding, but also provided quantitative design rules for determining the IC debonding resistance at the positions of maximum moment in the hogging and sagging regions in Fig. 2.1. In chapter 3, this will be used to quantify the flexural capacities, flexural stiffnesses and flexural ductilities.

2.7 References

- Monti, G., Renzelli, M. and Luciani, P. (2003) "FRP adhesion in uncracked and cracked concrete zones." *Proceedings of the 6th International Symposium on FRP Reinforcement for Concrete Structures (FRPRCS-6)*, World Scientific Publishing Company, Edited by: K.H. Tan, Singapore, 8-10 July, pp 183-192.
- Newmark, N.M., Siess C.P. and Viest I.M. (1951). "Tests and analysis of composite beams with incomplete interaction." *Proceedings Society for Experimental Stress Analysis*, 9, No.1, pp.75-92.
- Niu, H.D. and Wu, Z.S. (2003) "Debonding and failure mechanisms of FRP-strengthened R/C beams influenced by flexural cracks." Submitted to *Journal of Composites for Construction, ASCE*.
- Oehlers, D.J. and Bradford, M.A. (1999). *Elementary behaviour of Composite Steel and Concrete Structural Members*. Butterworth Heinemann, Oxford, September.
- Teng, J.G., Chen, J.F., Smith, S.T., and Lam, L. (2002). *FRP Strengthened RC Structures*. John Wiley and Sons. Ltd. Chichester, England.
- Yuan, H., Teng, J.G., Seracino, R., Wu, Z.S. and Yao, J. (2003) "Full-range behavior of FRP-to-concrete bonded joints: A closed-form analytical solution." Submitted to *Engineering Structures*.

Chapter 3: Flexural Strength and Ductility

3.1 Introduction

The strains at which IC debonding occurs have been quantified in Chapter 2. These IC debonding strains are now used in this chapter to determine the flexural capacities and flexural ductilities at sections of maximum moment, such as those shown in Fig. 2.1, and also the ability of the beam to redistribute moment between hogging and sagging regions for any form of plated beam with any type of plate material.

Adhesively bonded plated structures will probably debond at some stage of their load cycle; for example, debonding can occur prior to the tension reinforcing bars yielding, whilst the concrete is still elastic or while the flexural strength is reducing in the falling branch. Hence, the problem of ductility is very important in plated structures. The elementary concepts of ductility are first described and may cover basic ideas already familiar to the reader. This is followed by a section on moment redistribution, because it will be shown that often the choice of the plating material and technique is governed by the ability to redistribute moment. In fact, it will be shown through worked examples in Chapter 7 that, in some cases, if moment redistribution is not allowed or cannot be allowed then the increase in strength due to plating may be minimal and the structure not worth plating.

Having allowed for moment redistribution, the designer now knows the required moment capacities at the positions of maximum moment to resist the applied load and in particular the type of plate material or bonding technique that can be used. The derivation of the flexural capacities of plated structures is now covered and the chapter is concluded with worked examples.

3.2 Ductility

The ductility of a structure is as important as its strength. Often in basic design, the design procedure directly addresses the flexural strength and indirectly addresses the flexural ductility by providing provisos such as requiring the section to be *under-reinforced* or placing limits on the neutral axis depth. This approach is fine when dealing with RC structures with steel reinforcing bars that have a high strain capacity and are fully anchored, but is not sufficient when dealing with brittle materials such as FRP or brittle failure mechanisms such as plate debonding.

There are many forms of ductility that affect the behaviour of a structure. The basic concepts of material ductility as represented by the stress/strain relationship are first covered. From the stress/strain relationships, can be derived the moment/curvature relationship for a given section which represents the sectional ductility which is then covered. The integration of the curvature along the beam can be used to derive the beam ductility which is finally covered.

3.2.1 Material ductility

The concept of material ductility has already been discussed in Section 1.5.1. The material ductility of steel, as illustrated in Fig. 1.32, can be considered as stiff, as it has a high Young's modulus E , and ductile because of the large yield plateau where strain hardening occurs at about ten times the yield strain and fracture after strain

hardening at a strain of about one hundred times the yield strain. For all intents and purposes, the strain capacity of most steels is usually considered in design as infinite as the concrete crushes in an RC beam well before the steel fractures and, hence, rarely is the fracture strain incorporated into the design procedure. Aluminium is also a ductile material, however it is also flexible as it has a Young's modulus about one-third of that of steel, and it has a large strain capacity. The FRP materials represented in Fig. 1.32 have a range of stiffnesses depending on the density of the fibre. The carbon FRP in Fig. 1.32 can be made as stiff as steel, however it is a totally brittle material as there is no ductile plateau and, furthermore, the strain at fracture is relatively small. The glass FRP is generally flexible with a low Young's modulus, brittle and with a higher strain capacity than carbon FRP but less than that in metals.

In conclusion, steel can be classified as a stiff ductile material with a high strain capacity. Aluminium is flexible and ductile with a high strain capacity. Carbon FRP can be stiff or flexible, depending on the density of the fibre, also brittle and has relatively low strain capacity. And finally glass FRP is flexible, brittle, with a moderate strain capacity. The stiffness, the ductility and the strain capacity can affect the sectional ductility.

3.2.2 Sectional ductility

3.2.2.1 Moment/curvature

The sectional ductility is usually represented by the moment/curvature relationship (M/χ). In Fig. 3.1 are typical examples of the sectional M/χ relationships derived from numerical simulations, for an unplated RC beam at A, for the same RC beam with a 3 mm thick by 80 mm wide adhesively bonded steel plate at B, for adhesively bonded carbon FRP plates of various thicknesses and widths, for FRP plated beams in which fracture of the FRP controlled the strength such as at E, and for FRP plated beams in which plate debonding controlled the strength such as those in the region C.

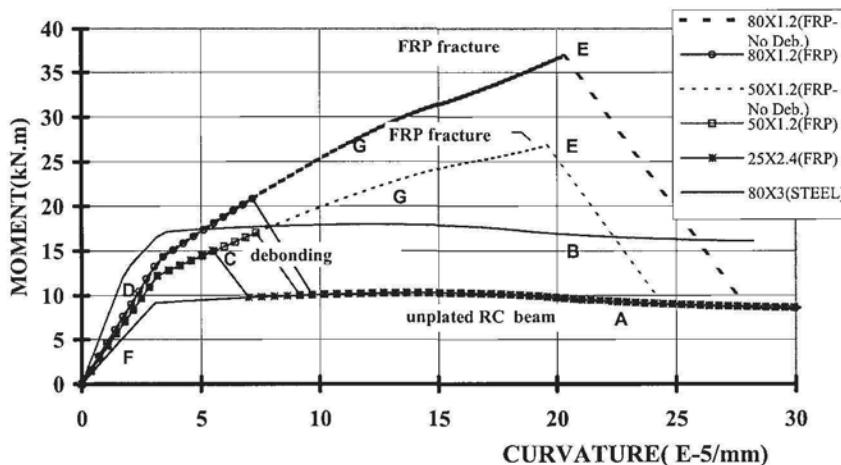


Figure 3.1 Moment/curvature relationships

The unplated RC beam shown as line A in Fig. 3.1 exhibits the classical M/χ relationship with an initial linear part at F, the slope of which is the flexural rigidity of the beam EI . After the tension reinforcing bars have yielded in the region D, there is a

near horizontal ductile plateau at A, the extent of which is limited by the concrete crushing. The effect of adding a 3 mm steel plate which was designed to yield before debonding is shown as line B. As the steel plate was assumed not to debond in this simulation, the characteristics or shape of the M/χ relationship are the same as that of the unplated beam at A, except that the initial flexural rigidity EI in region D has now two changes in slope, when the plate yields and when the reinforcing bars yields; this is of course ignoring the initial softening when concrete first cracks. However, it should be remembered that even when metal plates are designed so that the IC debonding strain is greater than the yield strain, that is they are designed to yield before debonding, tests have shown that debonding may still occur before the concrete crushes, as indicated by the debonding strains at rows 8 and 9 in Table 2.2 which are much greater than the yield strain of steel. When debonding does occur, the M/χ relationship simply reverts back to that of the unplated beam.

In contrast to the steel plated beam at B in Fig. 3.1, an FRP plated beam does not have a horizontal plateau. Instead, the moment keeps increasing, after the tension reinforcement has yielded, but at a more gradual rate as at G. This is because the FRP plate, being an elastic material that does not yield, keeps attracting more force until either the force in the plate causes IC debonding, such as at region C, or the plates fracture in region E, after which the behaviour of the beam reverts to that of the unplated structure at A. Generally for FRP plates and in particular pultruded plates, the plate debonds well before the plate fractures as shown in the simulation in Fig. 3.1 and which is also indicated by the IC debonding strains in Table 2.2 that are much smaller than typical fracture strains of 0.01 or greater. Both the short inclined region after the reinforcing bars yield around D and prior to debonding at C, and the fact that the plated hinge keeps attracting moment, inhibit the ability of FRP plated joints to redistribute moment.

3.2.2.2 Maximum curvatures

Of importance are the curvatures at the maximum moments in Fig. 3.1 as they directly affect the ability of a beam to redistribute moment. These curvatures can be derived from a commonly used standard sectional analysis as illustrated in Fig. 3.2 for a side plated beam. The maximum curvature χ_{\max} at the maximum moment capacity M_{cap} depends on one of the following criteria: the concrete crushing strain ϵ_c ; the plate IC debonding strain ϵ_{db} ; or the plate fracture strain ϵ_{fract} .

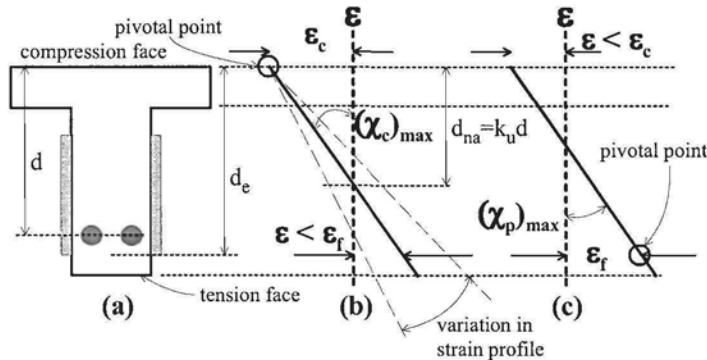


Figure 3.2 Pivotal points in strain profiles

The derivation of the maximum curvature when concrete crushing at a strain ϵ_c is assumed to control the analysis is illustrated in Fig. 3.2(b); this represents the standard analysis used for RC beams with steel reinforcing bars. As the concrete is assumed to crush first, the strain at the top compressive surface at failure is known and, therefore, fixed at the concrete crushing strain ϵ_c which is usually around 0.003 or 0.004 depending on the national standard being used. This point on the strain profile will be referred to as the pivotal point and is identified by the circle in Fig. 3.2(b). It is referred to as the pivotal point as the linear strain profile can then be swung around this pivotal point like a pendulum as shown, until a strain profile is reached which from the ensuing stress profile the forces in the cross-section sum to zero; this procedure will be explained in detail in Section 3.4. From the strain profile at longitudinal equilibrium, can be derived the maximum curvature when concrete crushing controls the design $(\chi_c)_{\max}$. Also from the strain profile at equilibrium can be derived the maximum strain in the plate, which in the example in Fig. 3.2(a) will occur at the bottom edge of the plate at distance d_p from the compression face. The strain capacity of this plate is the lesser of either the IC debonding strain ϵ_{db} or the plate fracture strain ϵ_{fract} which is shown as ϵ_f in Fig. 3.2(b). If the maximum strain in the plate is less than ϵ_f , as shown in Fig. 3.2(b), then the initial assumption that concrete crushing controls the analysis is correct and $(\chi_c)_{\max}$ is the maximum curvature.

If the initial assumption of ϵ_c controlling the design was found to be incorrect in the preceding paragraph, a further analysis has to be done where the pivotal point is moved to the level of the maximum strain in the plate as shown in Fig. 3.2(c). In this case, the pivotal strain ϵ_f is the lesser of ϵ_{db} or ϵ_{fract} and the strain profile is pivoted about this new point until longitudinal equilibrium is achieved whence $(\chi_p)_{\max}$ and also the moment capacity at plate debonding M_{cap} . It is also worth noting at this stage that the minimum secant flexural rigidity that the section can attain is also given $(EI)_{\min} = M_{\text{cap}}/\chi_{\max}$ as it will be shown later in Section 3.3.2 that this controls the amount of moment redistribution that can occur.

3.2.2.3 Moment/strains

It is often very difficult to directly measure the moment/curvature relationship in RC beams due to concrete cracking and crushing. However, a good indication of the M/χ relationship of a plated beam is the moment/plate-strain (M/ϵ_p) relationships, as the curvature would be expected to be in proportion to the plate strain as indicated in Fig. 3.2. The following moment/plate-strain relationships were derived from tests on two span continuous beams in which the RC beams and test set up were identical so that the only variation was the plate and bonding technique.

The moment/plate-strain relationship for a beam with an adhesively bonded 3 mm thick and 100 mm wide steel tension face plate is shown in Fig. 3.3. In this test, all the plates yielded at an early stage of loading and before the maximum moment capacity was reached. This was to be expected as the plates were mild steel as compared to the high yield tension reinforcing bars; furthermore, being tension face plates and, therefore, further from the neutral axis than the tension reinforcing bars, they were always subjected to higher strains. The hogging region plate failed prematurely due to CDC debonding, after the plate had yielded but before the tension reinforcing bars had yielded; compared with the sagging region plates which failed through IC debonding, it can be seen that CDC debonding is extremely brittle and should be avoided at all cost. The sagging region plates remained adhered to the beam well after yielding of the tension reinforcing bars and attained very high strains at

virtually a constant moment before eventually debonding occurred at strains of about 0.02, which is an order of magnitude greater than the crushing strain of concrete or the yield strain of the reinforcing bars. Even though IC debonding did occur, it is suggested that this plated section is ductile.

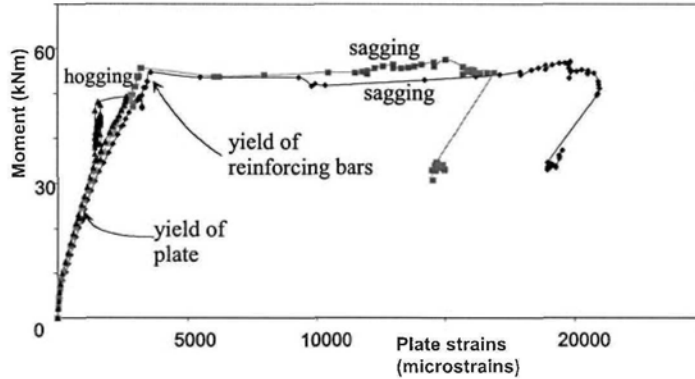


Figure 3.3 M/ϵ_p relationship of an adhesively bonded steel tension face plated beam

The moment/plate-strain relationship for a carbon FRP tension face plated beam is shown in Fig. 3.4; the plate thickness was 1.2 mm and the plate width 50 mm. The plates remained adhered to the beam after the tension reinforcing bars had yielded and eventually failed through IC debonding at a strain of about 0.005. This is a relatively large debonding strain for FRP plates as it is close to Chen and Teng's mean value of 0.0053 in row 1 of Table 2.2 and well above the characteristic values of Chen and Teng's and Neubauer and Rostasy's in rows 1 and 2 of about 0.0026. Even though these tension face plates were further from the neutral axis than the tension reinforcing bars, these debonding strains were sufficiently large to allow the tension reinforcing bars to yield. It may be worth noting that if these plates had debonded at the characteristic value of 0.0026 in Table 2.2, then it can be seen from Fig. 3.4 that the reinforcing bars would not have yielded prior to debonding so that this would have been a very inefficient form of rehabilitation or strengthening. It can be seen in Fig. 3.4 that after the tension reinforcing bars had yielded, the moment capacity still increased gradually because the plates, being elastic, kept attracting load as explained in Section 3.2.1.2. From a comparison of the steel plate results in Fig. 3.3 in which debonding occurred at plate strains of about 0.02, with the FRP plate results in Fig. 3.4 in which debonding occurred at plate strains of about 0.005, it is suggested that FRP plated sections can be considered as on the brittle side but with some ductility.

In Fig. 3.5 are the results from a test in which the steel plates were both bolted and adhesively bonded. The same 3 mm thick steel plates, as were used in the adhesively bonded plate in Fig. 3.3, were used in this test; the hogging region of the tested beam is shown in Fig. 2.8. The thin 3 mm thick steel plates are probably not ideally suited to bolting as, because of their thinness, there is only a small area of plate bearing against the bolt. Hence, the main advantage in bolting this adhesively bonded plate is probably the additional passive clamping action across the plate/beam interface that the bolts provide, that allows more shear to be transferred by aggregate interlock once IC debonding has occurred, as described in Section 2.2.2. However, as

can be seen in Fig. 3.5 when compared with Fig. 3.3, the adhesively bonded and bolted plates performed well. Plate strains of about 0.04 were achieved compared with those of 0.02 in the adhesively bonded steel plate which suggests a very ductile behaviour. The increase in strength between the bolted plates in Fig. 3.3 and the adhesively-bonded and bolted plates in Fig. 3.5 was not due to the addition of bolts but because the bolted plates had a slightly higher yield capacity than the adhesively bonded plates.

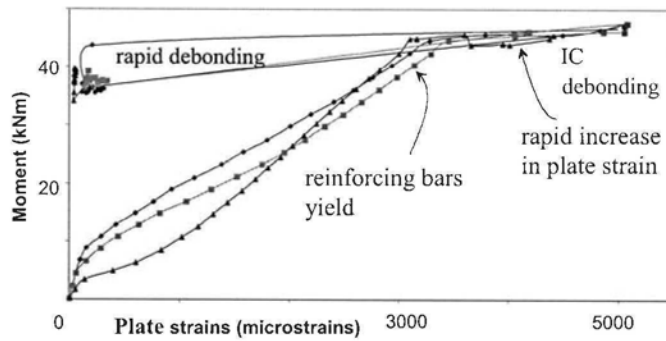


Figure 3.4 M/ϵ_p relationship of an adhesively bonded FRP tension face plated beam

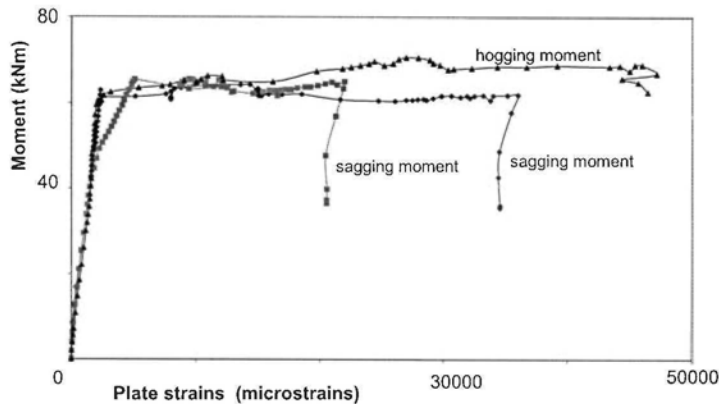


Figure 3.5 M/ϵ_p relationship of a bolted and adhesively bonded steel tension face plated beam

In summary, the adhesively bonded and bolted steel plated sections showed very good sectional ductility reaching strains of 0.04, the adhesively bonded steel plated section showed good ductility with strains of 0.02 and importantly, the adhesively bonded FRP plated section showed some ductility at strains of 0.005.

3.2.3 Beam ductility

There are numerous ways of measuring the beam ductility. In this section, we will be looking at the non-linear deflection as it is a good indication of the ability of the beam

to absorb energy. Furthermore, the ability of a *joint* in a beam to maintain a moment as the beam deflects and loads up other *joints* is also an indication of the ability to redistribute moment in a statically indeterminate beam. The term *joint* will be used loosely to represent any position of maximum hogging or sagging moment where ductility or a reduction in flexural rigidity is required to redistribute moment; a *plastic hinge* being a special case of a joint.

3.2.3.1 Moment/deflection

The moment/deflection (M/δ) plots for tension face plated beams are given in Fig. 3.6 for a beam with adhesively bonded steel plates, in Fig. 3.7 for a beam with adhesively bonded FRP plates and in Fig. 3.8 for a beam with steel plates that were both bolted and adhesively bonded; these are the same beams as in Section 3.2.2.3 where the M/ϵ_p behaviours were described.

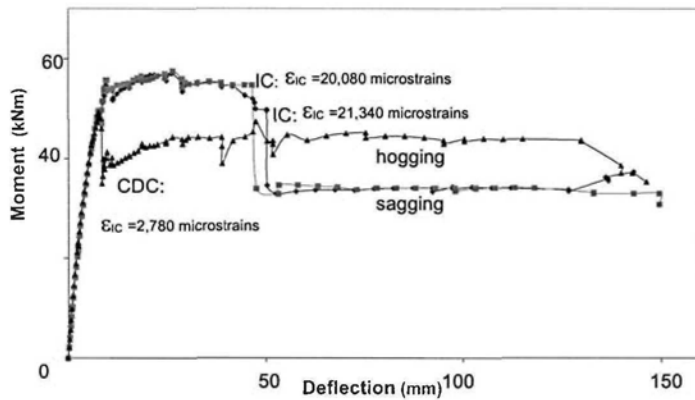


Figure 3.6 M/δ relationship of an adhesively bonded steel tension face plated beam

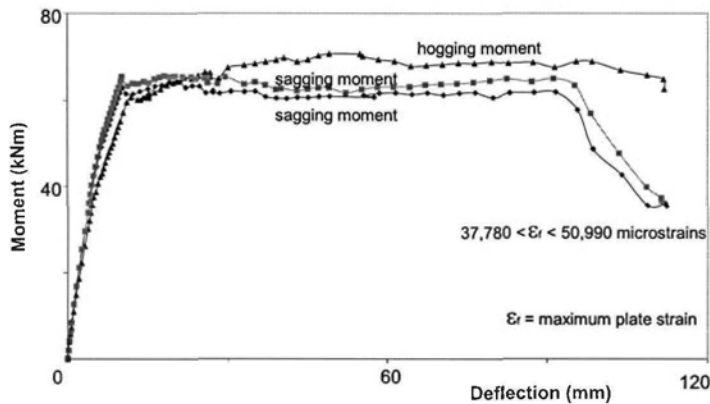


Figure 3.7 M/δ relationship of a bolted and adhesively bonded steel tension face plated beam

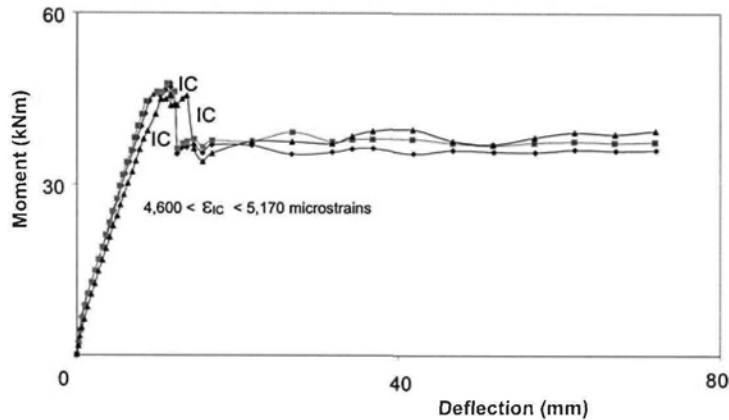


Figure 3.8 M/δ relationship of an adhesively bonded FRP tension face plated beam

Apart from the hogging region plate in Fig. 3.6 in which CDC debonding occurred, the adhesively bonded steel plated sections in the sagging regions in Fig. 3.6 had substantial ductile plateaus that extended through a deflection of about 38 mm whilst maintaining their moment capacities, after which the behaviour reverted back to that of the unplated section. The adhesively bonded and bolted steel plated beam in Fig. 3.7 had an excellent ductile plateau and was able to maintain its moment capacity over a deflection of 85 mm. The results from the adhesively bonded FRP plated beam is shown in Fig. 3.8, where it can be seen that there is hardly any ductile plateau. The same RC beam with FRP side plates is shown in Fig. 3.9. In this case, a softened but still increasing moment M/δ response after yield of the tension reinforcing bars at point A is observed over a deflection of about 8 mm.

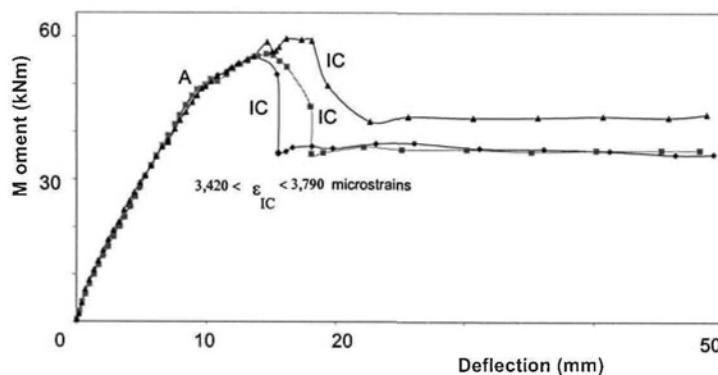


Figure 3.9 M/δ relationship of an adhesively bonded FRP side plated beam

3.2.3.2 Moment redistribution concept

In order to illustrate the phenomenon of moment redistribution, that is the ability of statically indeterminate beams to redistribute moment, let us consider the *encastre* or

built in beam of length L in Fig. 3.10(c), which can also be considered to represent an internal span of a continuous beam. For convenience, let us assume that the same longitudinal reinforcing bars are in the top and bottom of the beam. Hence, the hogging and sagging regions have the same moment/curvature relationships as shown in Fig. 3.10(a), where the idealised perfectly elastic portion has a flexural rigidity of EI up to an ultimate moment capacity of M_u at a curvature χ_y , after which there is a perfectly plastic ductile plateau up to an ultimate curvature of χ_u at which failure occurs. Let us also assume that the beam is only subjected to a uniformly distributed load w kN/m, as shown in Fig. 3.10(c), so that whilst elastic, that is whilst the flexural rigidity of the whole beam remains at EI , the moment at the supports M_{hog} is twice that at mid-span M_{sag} . Hence for this specific beam, there is no moment redistribution whilst the maximum hogging moment M_{hog} is equal to twice the maximum sagging moment M_{sag} . However, when $M_{hog} \neq 2M_{sag}$, then moment redistribution is assumed to be occurring. We will, therefore, define moment redistribution as occurring when the distribution of moment within a beam is not given by elastic analyses that assume EI is constant within the beam. We will use this simple definition for convenience, as designers generally assume in their elementary analyses that EI is constant within a beam in determining the initial distribution of moment which can then be redistributed.

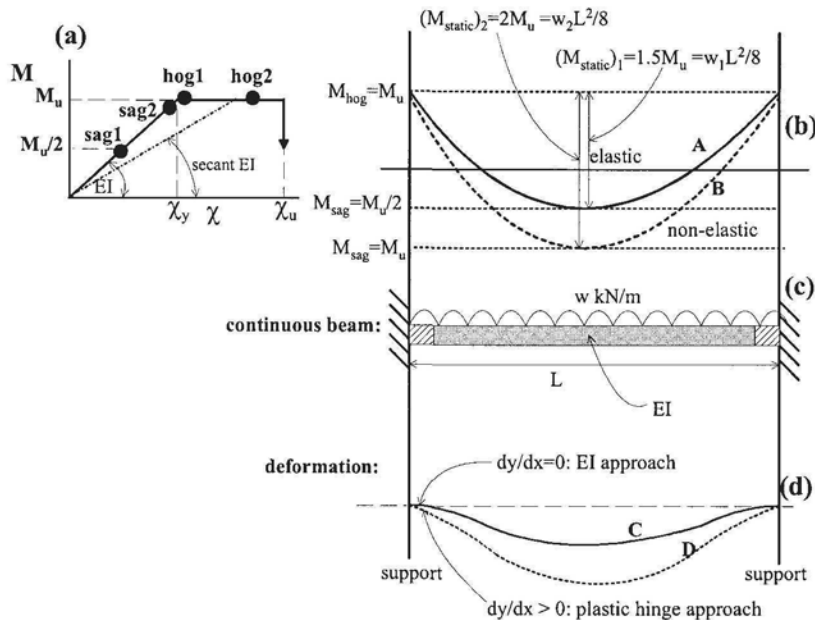


Figure 3.10 Moment redistribution concept

As the uniformly distributed load w is gradually applied to the beam in Fig. 3.10(c), the beam is initially elastic so that $M_{hog} = 2M_{sag}$ so that there is no moment redistribution. When the support moment first reaches its moment capacity M_u as shown as the point *hog1* in Fig. 3.10(a), then the mid-span moment is at $M_u/2$ which is shown as *sag1*. At this stage, the total or static moment is $(M_{static})_1 = 1.5M_u = w_1 L^2/8$

as shown in Fig. 3.10(b) and labeled *elastic*, and the distribution of moment is given by line A. Up to this point, the beam remains linear elastic. As the load is further increased, the beam deflects further increasing M_{sag} above $M_u/2$ in Fig. 3.10(b) but the moment at the support remains at M_u . The only way the increased deflection or deformation due to the increased load can be accommodated is for the curvature at the supports to increase from *hog1* to *hog2* in Fig. 3.10(a) and the hogging curvature will keep increasing until the sagging curvature *sag1* reaches *sag2* in Fig. 3.10(a), that is the mid-span moment has reached its capacity M_u whilst the behaviour of the hogging region is no longer elastic. The total or static moment has now reached $(M_{\text{static}})_2 = 2M_u = w_2L^2/8$ in Fig. 3.10(b), which is the maximum static moment and, hence, the maximum load w_2 that can be applied as all the joints have reached their moment capacities and a collapse mechanism has formed. The distribution of moment within the beam is now given by line B which has been labeled *non-elastic*.

It can be seen, in the example in Fig. 3.10, that it is the hogging joints that are required to maintain the moment whilst their curvature is increasing. Hence in this example, it is the hogging joints that have to redistribute moment and it is their ductility that governs the amount of moment redistribution that can occur. If for example, it was necessary for *hog2* in Fig. 3.10(a) to exceed the curvature capacity of the section χ_u , to achieve the static moment $(M_{\text{static}})_2$ in Fig. 3.10(b), as may occur when there is a large amount of tension reinforcement or debonding occurs in the hogging section, then *sag2* in Fig. 3.10(a) cannot achieve M_u and the continuous beam fails before its theoretical plastic capacity can be achieved. It can be seen in this example that the sagging moment joint has only to reach its moment capacity, that is its curvature has only to reach χ_y , hence its ductility, that is its capacity to extend along the plateau in Fig. 3.10(a), is of no consequence. Unless of course the beam is required to absorb energy such as under seismic loads, in which case it may be a requirement that *sag2* also extends into the plastic zone to allow the beam to deflect further and absorb energy but with no increase in load.

Figure 3.10 is concerned with redistribution of moment from the hogging region to the sagging region. However, moment redistribution can occur either way. Consider, for example the beam in Fig. 3.11(b). Let us assume that the design loads induced the elastic distribution of moment line B in Fig. 3.11(a); in which case, the maximum hogging moment is two-thirds the static moment as shown and the maximum sagging moment one-third. The continuous beam can be designed for a smaller hogging moment capacity and a corresponding larger sagging moment capacity as shown by line C which has the same static moment capacity M_{static} as line B. In this case when the beam is gradually loaded, as initially $M_{\text{hog}} = 2M_{\text{sag}}$ but the capacity $(M_{\text{hog}})_u < 2(M_{\text{sag}})_u$, the support moment capacity is reached first and we have the situation described in Fig. 3.10 where ductility is required in the hogging region. If instead, it is decided to make the hogging regions stronger as shown by line A, then as the beam is gradually loaded, the moment capacity at mid-span is reached first. In which case, the sagging region has to be ductile as moment is being redistributed from the sagging region to the hogging region.

3.2.3.3 Moment redistribution capacity

To determine whether a beam is ductile enough to redistribute moment is an extremely complex problem and there is much good ongoing research to try to find a comprehensive and simple solution. The problem is to find out how the beam can deform to accommodate the non-elastic distribution of moment line B in Fig. 3.10(b) and then to determine whether the deformation capacity of the beam can

accommodate this required deformation. There would appear to be two approaches: we can either assume that there is a discontinuity of the slope at the supports as shown in line D in Fig. 3.10(d) and this will be referred to as the *hinge approach*; or it can be assumed that there is no discontinuity, such as at line C, and this will be referred to as the *flexural rigidity approach*. In many ways, these approaches can be combined and they are illustrated in Fig. 3.12.

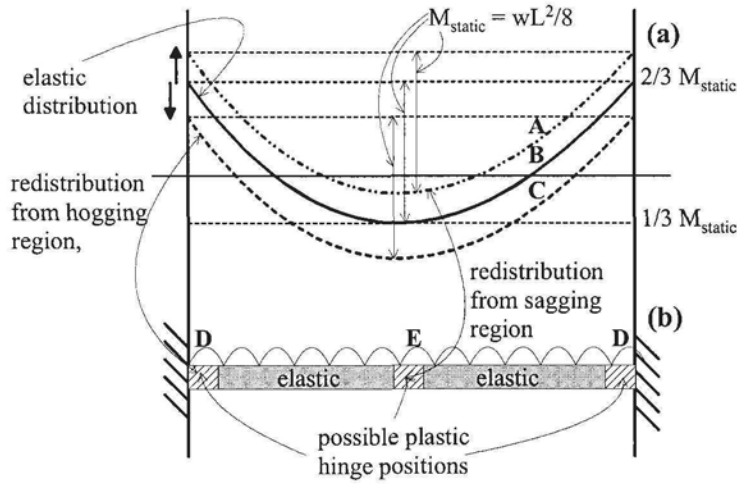


Figure 3.11 Moment redistribution

(a) Hinge approach

In the hinge approach, it is assumed that most of the beam of length L remains linear elastic at a flexural rigidity EI as shown in Fig. 3.12(c), and that there are small hinge regions at the joints of length L_{hinge} where moment redistribution requires ductility as explained in Fig. 3.10. The hinge length $L_{hinge} \ll L$, being the order of magnitude of the depth of the beam. It is assumed that the hinge, often referred to as the *plastic hinge*, accommodates the discontinuity of slope at the supports in line D in Fig. 3.12(f). This discontinuity is caused by the non-elastic moment distribution, line B in Fig. 3.12(a), where there are support moments M_u and an applied load w_2 kN/m that induces a static moment $(M_{static})_2$. The discontinuity of slope can be determined from the analyses depicted in Figs. 3.12(d) and (e). In Fig. 3.12(d), the redundant support moments are removed so we are dealing with a statically determinate simply supported beam with a uniformly distributed load w_2 of flexural rigidity EI ; the slope at the supports $(dy/dx)_{static}$ can be derived by integration of the curvature along the length of the beam. The simply supported beam is now subject to only the end moments M_u as in Fig. 3.12(e). Also from integration of the curvature, can be derived the slope at the supports $(dy/dx)_{support}$. Hence the discontinuity of the slope in line D in Fig. 3.12(f) is equal to the difference between $(dy/dx)_{static}$ and $(dy/dx)_{support}$ and which is accommodated by the plastic hinge. As the length of the hinge is very small, it is often assumed that the curvature within the hinge is constant so that the rotation capacity of the hinge is simply $\chi_u L_{hinge}$ where χ_u is the curvature capacity of the section as illustrated in Fig. 3.10(a). It can be shown for the very simple case of an encastre beam with a uniform load that for design

$$\frac{L}{2EI} \left[\frac{2}{3} M_{static} - M_u \right] \leq \chi_u L_{hinge} \tag{3.1}$$

where the left hand side of Eq. 3.1 is the discontinuity in the slope in line D in Fig. 3.12(f) and the right hand side is the rotation capacity of the hinge. The main problem in this approach is in deciding what to use for the length of the hinge.

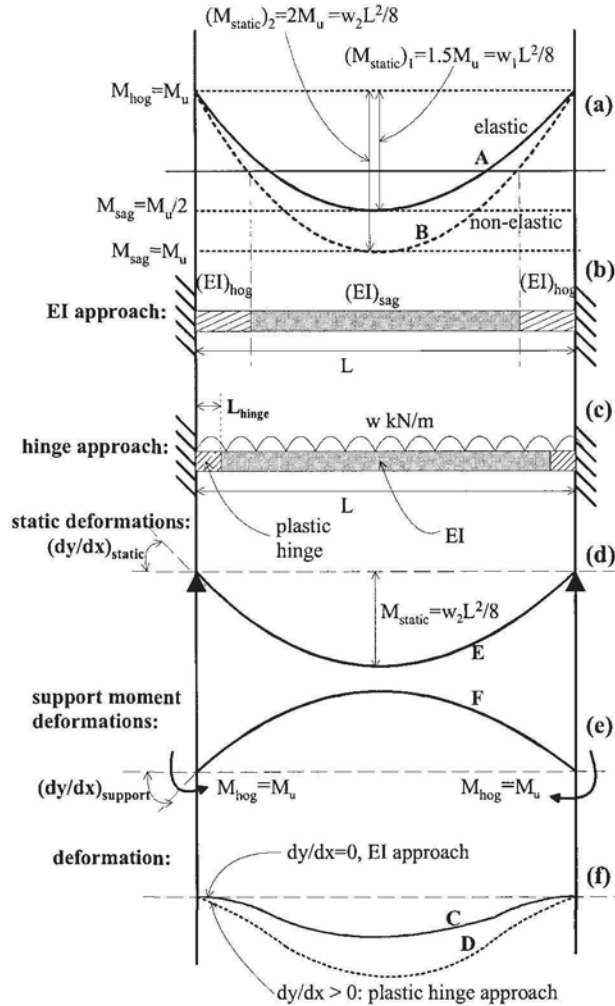


Figure 3.12 Compatibility in moment redistribution

(b) Flexural rigidity approach

In contrast to the *plastic hinge* approach, the *flexural rigidity* approach (Oehlers et al 2003(a) and (b)) assumes that the slope at the supports is zero as shown in line C in Fig. 3.12(f). This can only be accommodated by allowing variations in the flexural

rigidity along the length of the beam as shown in Fig. 3.12(b), where $(EI)_{\text{hog}}$ represents the flexural rigidity of the hogging region and $(EI)_{\text{sag}}$ that of the sagging region. It is not the magnitudes of these flexural rigidities that controls redistribution but their relative values or proportions, that is $(EI)_{\text{hog}}/(EI)_{\text{sag}}$. For example when $(EI)_{\text{hog}} = (EI)_{\text{sag}}$, that is $(EI)_{\text{hog}}/(EI)_{\text{sag}} = 1$, then, in this example, the elastic distribution of moment is achieved so that $M_{\text{hog}} = 2M_{\text{sag}}$ so that there is no moment redistribution. Even if we were to double both flexural rigidities, $(EI)_{\text{hog}}/(EI)_{\text{sag}}$ remains at unity and, therefore, M_{hog} remains at $2M_{\text{sag}}$ so there is still no moment redistribution. However, if the secant $(EI)_{\text{hog}}$ is taken, it reduces as χ increases along the plateau in Fig. 3.10(a), then $(EI)_{\text{hog}}/(EI)_{\text{sag}}$ also reduces and as M_{hog} is constant whilst M_{sag} is increasing $M_{\text{hog}} < 2M_{\text{sag}}$, that is moment redistribution is occurring. The minimum flexural rigidity of M_{hog} depends on the sectional curvature capacity χ_u in Fig. 3.10(a).

Another way of visualising the flexural rigidity approach is that as the flexural rigidity at the supports $(EI)_{\text{hog}}$ in Fig. 3.12(b) reduces relative to $(EI)_{\text{sag}}$, the support attracts less moment. For example, when $(EI)_{\text{hog}} \rightarrow 0$, the continuous beam in Fig. 3.12(b) reverts to a simply supported beam, so that all of the hogging moment has been redistributed to the sagging region. On occasions in the remainder of this book, we will refer to the regions where the flexural rigidity is reducing, such the hogging region in Fig. 3.12(b), as the *plastic hinge* even though we are dealing with the *flexural rigidity* approach. This is just to emphasise that it is this region that exhibits ductility in order to achieve moment redistribution. It may be worth noting at this stage that for the *flexural rigidity* approach, the length of the *hinge* is the length of the hogging region bound by the points of contraflexure as shown in Fig. 3.12(b); the reason for this is explained later in Section 3.3.2 and 3.3.3.

(c) Test example of moment redistribution

A typical test result of moment redistribution from two span continuous beams such as that shown in Fig. 2.18 is given in Fig. 3.13. The beams were plated over their hogging region as shown in Fig. 2.18 with a 50 mm wide 1.2 mm thick carbon FRP plate, and designed and loaded to achieve their moment capacity in the hogging regions first so that moment redistribution occurred from the hogging region to the unplated sagging region. The loading arrangement was such that in an elastic analysis in which EI was assumed constant, the hogging moment would be 75% of the static moment as shown by the horizontal line in Fig. 3.13. Hence, if the beam remained elastic the hogging moment should remain at 75% of the static load. It can be seen that up to applied loads of 15 kN the beam does behave elastically (the line from the origin should be ignored as the graph should start at the first load point), after which the hogging moment reduced in proportion to the static moment indicating that moment redistribution occurred in this FRP plated beam.

3.3 Moment redistribution capacities

3.3.1 Neutral axis depth approach

Most national codes use the neutral axis factor $k_u = d_{na}/d$ in Fig. 3.2, where d is the effective depth of the beam and d_{na} the depth to the neutral axis both measured from the compression face, to ensure sufficient sectional ductility at a *joint* for moment redistribution in unplated reinforced concrete beams. As defined previously, the term *joint* will be used to represent any position or region of maximum hogging or sagging moment where a *hinge* may have to occur to redistribute moment such as the hatched

regions D and E in Fig. 3.11 as well as the hatched regions in Figs. 3.12(b) and (c). A *hinge* will be defined loosely as a region where the curvature has to follow the plateau in Fig. 3.10(a) such as at *hog2*. Hence, the term *hinge* will be used where a plastic hinge is required such as in the hatched regions in the hinge approach in Fig. 3.12(c) or where the flexural rigidity has to reduce as in the hatched region in the EI approach in Fig. 3.12(b).

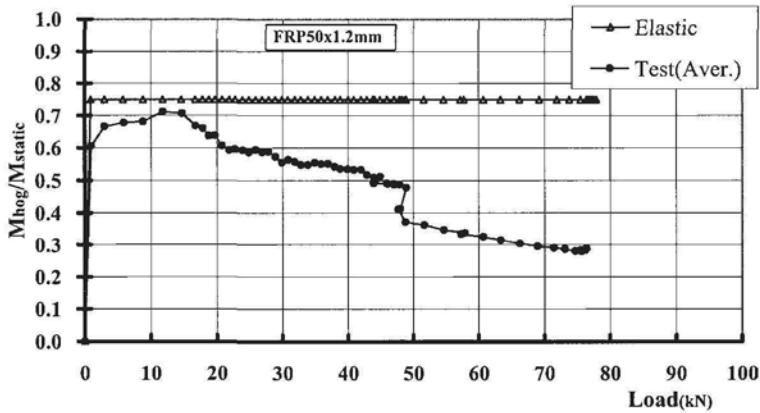


Figure 3.13 Moment redistribution in a two span continuous beam test

The range of moment redistributions allowed in national codes is illustrated in Fig. 3.14. Most codes allow up to 30% redistribution for k_u values that range from zero to 0.3, and zero redistribution for k_u values that range from 0.2 to 0.6. As an example of the application of k_u values, let us assume that the design load has been applied to a beam and from an elastic analysis, based on EI being constant along the length of the beam, the moment at one joint is $M_{elastic}$. The Australian code suggests that if $k_u < 0.2$ at that joint then that joint can form a hinge and redistribute 30% of its elastic moment $M_{elastic}$. Hence the joint can be designed for 70% of $M_{elastic}$, just as long as the other joints in the beam are increased in strength to allow the same total or static moment in the beam. The Australian code also suggests that if $k_u > 0.4$ at that joint then moment redistribution is not allowed to occur at that joint; which means that that joint cannot reach its moment capacity prior to the total design load being applied (that is it cannot form a hinge) but is allowed to just reach its moment capacity when the full design load is reached.

How the neutral axis depth factor k_u affects the ductility is illustrated in Fig. 3.15 for the values used in the Australian Code. It is assumed in this analysis that concrete crushing causes failure (that is the strength reduces after the concrete starts to fail) and that this occurs at a strain $\epsilon_c = 0.003$. Hence $\epsilon_c = 0.003$ is the pivotal point, as described in Fig. 3.2, of the analysis as shown in Fig. 3.15. As the pivotal point is fixed at $\epsilon_c = 0.003$, the k_u factor controls the strain in the tension face. For example, when $k_u = 0.2d$ in Fig. 3.15, then the tension face strain is $\epsilon_{0.2d} = 0.012$, as shown, and when $k_u = 0.4d$ then the tension face strain is $\epsilon_{0.4d} = 0.0045$ (this assumes that the effective depth d of the beam is close to the depth of the beam h as shown). The k_u factor does not control the curvature which is given by $\epsilon_c/k_u d$ as this depends on the effective depth of the section d . However, the k_u factor does control the rotation of the

plastic hinge θ_{hinge} as this is given by $\chi_u L_{\text{hinge}} = (\epsilon_c/k_u d) L_{\text{hinge}}$ and if $L_{\text{hinge}} \approx d$ then the rotation, that is the change in slope within the hinge, is given by $\theta_{\text{hinge}} \approx \epsilon_c/k_u$.

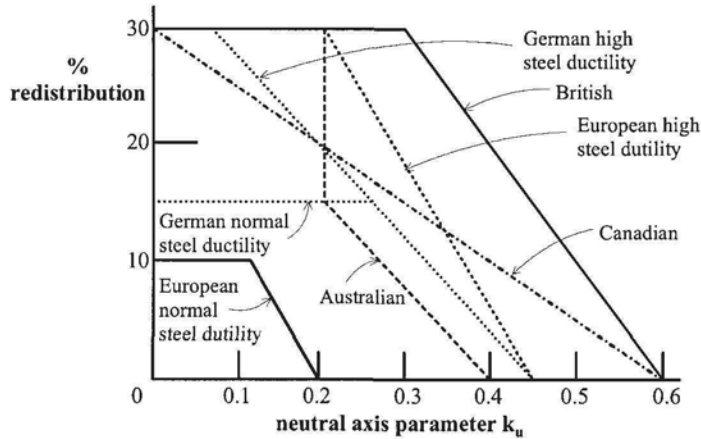


Figure 3.14 Moment redistribution code requirements

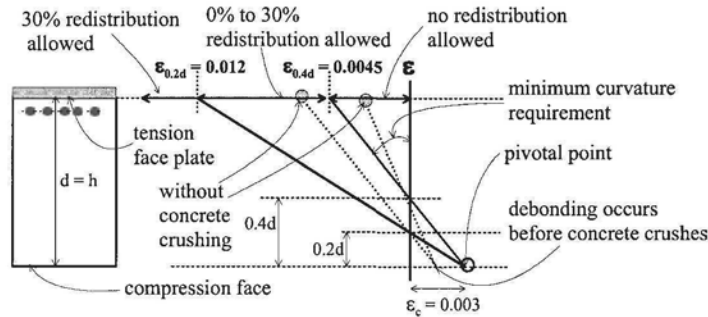


Figure 3.15 Plate strain requirements for moment redistribution

The Australian code requires that $k_u < 0.2d$ to allow 30% redistribution and, as shown in Fig. 3.15, this requires a tension face strain of 0.012 which means that if a plate were attached to the tension face then the IC debonding strain would have to be greater than 0.012. It can be seen in Table 2.2 that this strain of 0.012 is much greater than all the recommendations for FRP plates in rows 1 to 4. It is even much greater than the upper limit to the Concrete Society and German recommendations in rows 3 and 4. Even if the upper bound limit of the British recommendation of $k_u = 0.3$ for 30% redistribution, as shown in Fig. 3.14, is used, the strain required of $\epsilon_{0.3d} = 0.007$ is still only within the Concrete Society and German recommendations and well above those determined from beam tests, in rows 5 to 6 of Table 2.2, and above the mean values for pull tests in row 1. Hence it would appear that a 30% redistribution or more is very unlikely to be achieved in FRP plated structures. However, the steel debonding strains of 0.0201 – 0.0213, in row 8 of Table 2.2, are well above the

required strain of 0.012, which would suggest that some steel plated beam joints can redistribute 30% or more of their elastic moment.

At the other extremity of redistribution in Fig. 3.14, the Australian, German and European codes require that no redistribution is allowed when k_u is greater than about 0.4. As shown in Fig. 3.15, this neutral axis depth factor requires a strain on the tension face of $\varepsilon_{0.4d} = 0.0045$. This is still above the characteristic FRP values proposed by Chen and Teng, and Neubauer and Rostasy in rows 1 and 2 in Table 2.2 and only just achievable in the FRP plated beams in rows 5 and 6. Hence it would appear that redistribution should not be allowed for FRP plated beams as suggested in the European guidelines (2001) in Table 1.1. However, the steel plated specimens in rows 8 and 9 in Table 2.2 can achieve these strains and hence are capable of at least some moment redistribution; this is because steel or other metal plates can be designed to yield before IC debonding.

It could be argued and it is true that the plates will probably debond before the concrete crushes, and hence the pivotal point moves to the left as shown in Fig. 3.15. This shift of the pivotal point would change the strain profiles to the broken lines and would require smaller tension face strains to achieve the required k_u factors as shown. However as can be seen, from the difference in slope between the broken and solid lines, the required curvatures reduce and, hence, also their sectional ductility and, therefore, the ability of a joint to redistribute moment. Hence, it is suggested that the k_u factor should not be used to control moment redistribution in plated structures where concrete crushing does not control failure as the rotation of the plastic hinge is no longer proportional to ε_c/k_u . The British guidelines (2000) recommend using the k_u factor to control ductility in flexural calculations that are based on concrete crushing, which is fine for plated structures where IC debonding does not precede concrete crushing.

In conclusion, it is suggested that the k_u factor should not be used to control ductility in plated structures, that FRP plated joints should in general not be allowed to redistribute moment, and that metal plated joints have the ability to redistribute as the plate can be designed to yield before debonding.

3.3.2 Flexural rigidity approach

Tests on two span continuous plated beams (Oehlers et al 2003(a) and (b)), such as in Fig. 2.18, have shown that the *flexural rigidity* approach described in Section 3.2.3.3 can be used to predict the amount of moment redistribution that plated structures can withstand. Of the different approaches described in Section 3.2.3.3, the *flexural rigidity* approach probably works best because plated structures tend to debond before the concrete crushes.

To illustrate the analysis, let us consider the propped cantilever in Fig. 3.16(a), which is an analysis of the two span beam in Fig. 2.18. It will be assumed that metal plates are used in the hogging region and the sagging region remains unplated. The M/χ relationship for the hogging region is shown as the hogging joint in Fig. 3.17; the elastic part is that of the cracked plated section of flexural rigidity EI_{hcr} which can be derived from transformed sections and by assuming that the tensile strength of the concrete is zero. The ultimate strength of this plated section M_{hu} is the strength when both the metal plate and the tension reinforcing bars have yielded. The length of the ductile plate from point B_h onwards is governed by either the concrete crushing at χ_c or the plate debonding at χ_{deb} and the curvatures and strains at which this occurs can be derived from the analyses illustrated in Fig. 3.2. The same approach can be applied

to determining the M/χ relationship for the sagging region which is shown as the sagging joint in Fig. 3.17 and which in this example is assumed to be unplated.

Let us first assume that the hinge occurs at the hogging joint in Fig. 3.16(a), that is the plated hogging section has to exhibit ductility whilst the sagging region only has to achieve its ultimate strength at point C_s in Fig. 3.17. Hence at debonding, the hogging joint has a flexural rigidity of EI_{hdeb} as shown in Fig. 3.17, and the sagging joint has a flexural rigidity EI_{scr} . The flexural rigidity approach is very simple. It assumes that the whole of the hogging region of length L_h in Fig. 3.16(b) and (c) has a flexural rigidity of $EI_h = EI_{hdeb}$ and the whole sagging region of length L_s has a flexural rigidity of EI_s . The reason that this approach works is that moment redistribution does not depend on the magnitude of the flexural rigidities but on their proportions as explained in Section 3.2.3.3. Hence, just as long as the relative stiffnesses between the two regions is correct, it does not matter what the actual stiffnesses are.

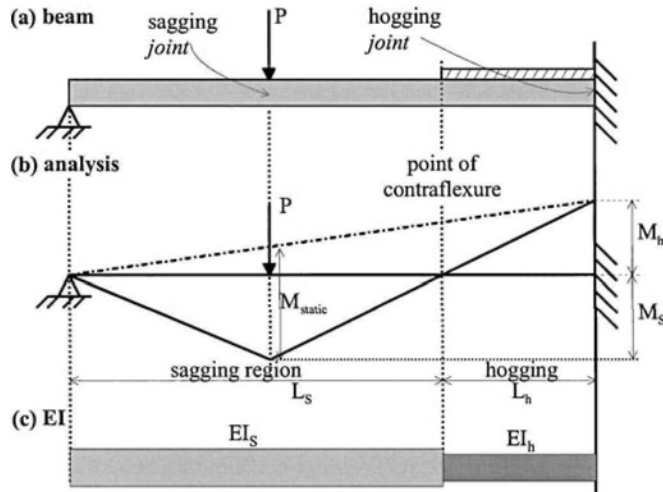


Figure 3.16 Flexural rigidity analysis

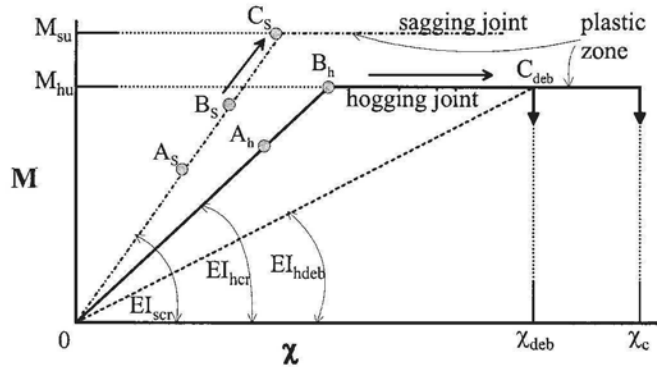


Figure 3.17 M/χ response with horizontal plateau

There are closed form solutions for simple load configurations and simple restraints. However, an elementary beam stiffness computer program is ideal for the analysis. Let us consider the beam in Fig. 3.16(a) and we wish to determine the applied load to cause debonding, the distribution of moment at failure, and hence determine whether the amount of moment redistribution that the indeterminate beam was designed for can be accommodated. As described in the previous paragraph, the flexural rigidity of the hogging region is $EI_h = EI_{hdeb}$ and that of the sagging region $EI_s = EI_{scr}$. The problem is that the point of contraflexure is not known, because it depends on the variation in EI along the length of the beam, so that the position of the point of contraflexure L_h has to be initially guessed. The beam is then loaded to determine whether the point of contraflexure coincides with the guessed value of L_h and iterated until it does. As this is an elastic analysis, the point of contraflexure is independent of the magnitude of the load so that any load can be applied just as long as the distribution is correct. Once the correct spread of the flexural rigidities has been found, that is L_h corresponds with the point of contraflexure, the analysis will give the proportion M_h/M_s in Fig. 3.16(b). This proportion can then be compared with the capacity proportion M_{hu}/M_{su} from Fig. 3.17, to ensure that debonding occurred before the sagging capacity was achieved as was assumed in this analysis.

An alternative approach is to first assume that both of the zones L_s and L_h in Fig. 3.16(b) and (c) are initially elastic, that is they have flexural rigidities EI_{scr} and EI_{hcr} , then repeat the iterative approach described in the previous paragraph to find M_h/M_s , and compare this with the capacities M_{hu}/M_{su} to determine which region reaches its capacity first. For example, let us assume that a load P in Fig. 3.16(b) is applied, and from the iterative analysis we derive that the moment in the sagging region is A_s and that in the hogging region is A_h as in Fig. 3.17. Increasing these moments in the same proportion would give B_s and B_h which shows that the hogging joint reaches its capacity first. Hence, by applying further load and going from B_s to C_s and from B_h to C_{deb} , it now needs to be determined whether the ultimate strength M_{su} at C_s or debonding at C_{deb} first occurs. The flexural rigidity in the hogging region gradually reduces between B_h and C_{deb} along the plastic zone. The simplest solution is to go straight to C_{deb} by using EI_{hdeb} in the hogging region whilst maintaining EI_{scr} in the sagging region as described in the previous analysis in the previous paragraph. From a comparison between M_h/M_s and M_{hu}/M_{su} can be determined whether debonding first occurs at C_{deb} or whether the sagging capacity M_{su} is first reached. If the sagging capacity is first reached, then both capacities M_{hu} and M_{su} are achieved prior to debonding. If the sagging capacity is not reached, then the moment in the sagging region at debonding in the hogging region will have been derived already from the analyses using EI_{scr} and EI_{hdeb} which is the moment that occurs on debonding.

The analysis of FRP plated sections will follow the same procedure as with metal plates. In this case, for the M/χ relationship for the FRP section in the hogging region, there will be softening after yielding of the tension reinforcement, which will be referred to as the plastic zone, with a reduced (non-zero) positive tangent stiffness, instead of a horizontal plateau as shown in Fig. 3.18. If the sagging joint is unplated or has a metal plate, it will have a horizontal plateau (plastic zone), as shown, so that the moment capacity does not increase; that is the analysis is stopped when point B_s is reached, so that the analysis procedure described in the previous paragraph can be applied. However, if the sagging region has an FRP plate, the capacity can gradually

increase as shown, in which case the softened branch (plastic zone) of the sagging joint will have to be followed. Ignoring the plastic zone will give a safe design. Alternatively, using EI_{sdeb} and EI_{hdeb} for the sagging and hogging regions will first determine which plate debonds first. The plate that does not debond will lie somewhere in the plastic zone such as at A_s in the sagging joint, so that this flexural rigidity of EI_{sit} can be varied to iterate towards the correct solution when $M_{hu}/M_s = M_h/M_s$.

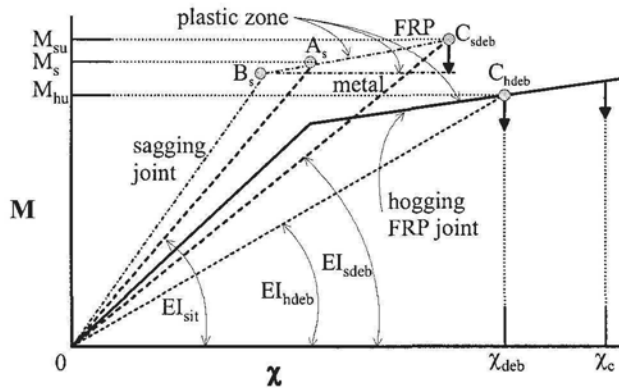


Figure 3.18 M/χ response with softening branch

3.3.3 Examples of moment redistribution capacities

In order to illustrate moment redistribution in plated beams, two span continuous beams were tested as shown in Fig. 2.18. Only the hogging regions were plated as shown in Fig. 3.19. The beams were deliberately designed so that the moment capacity would be reached first in the plated hogging region. Hence the ductility of this section, that is its ability to redistribute moment, could be measured. To ensure that the hinge formed in the hogging region and that there was ample scope for moment redistribution, there were only two 12 mm diameter tension reinforcing bars in the hogging region compared with four 16 mm tension reinforcing bars in the sagging regions so that the flexural capacity of the hogging region M_{hu} was much greater than that of the sagging region M_{su} . However, this difference in the longitudinal tension reinforcing bars also meant that there was a large difference in the flexural rigidities of the cracked sections EI_{cr} which by itself would affect moment redistribution as described in Section 3.3.2.

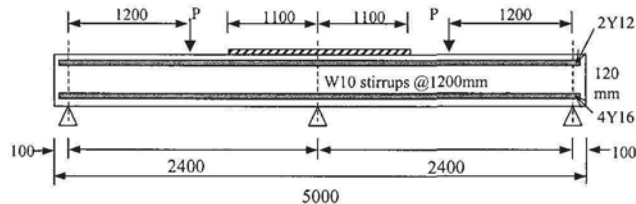


Figure 3.19 Moment redistribution test specimen

The test beam in Fig. 3.19 is symmetrical and hence acts as a propped cantilever as shown in Figs. 3.16 and 3.20. The broken line in Fig. 3.20 represents an elastic analysis in which EI is constant along a span. For the loading arrangement in Fig. 3.19, this gives a hogging moment $(M_h)_{el}$ that is 20% greater than the sagging moment $(M_s)_{el}$. Hence whilst the beam remains linear elastic and exhibits constant EI , it would be expected that $(M_h)_{el}/(M_s)_{el} = 1.2$. If in the tests $(M_h)_{test}/(M_s)_{test} < 1.2$ as represented by the unbroken line in Fig. 3.20 then this represents moment redistribution.

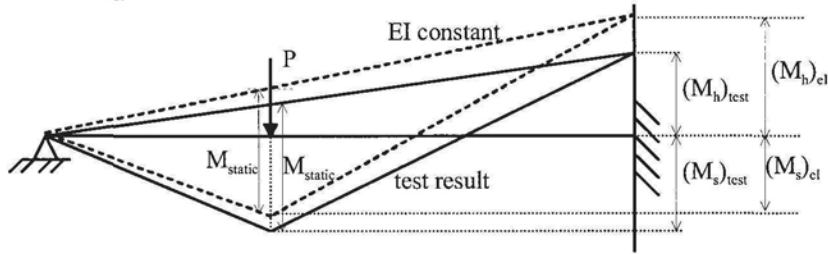


Figure 3.20 Distribution of static moment

The test results for a beam with a 2 mm thick mild steel plate is shown in Fig. 3.21. The ordinate gives the measured hogging moment in the test M_h as a proportion of the measured sagging moment M_s and the abscissa gives the measured static moment M_{static} , as shown in Fig. 3.20, as a proportion of the theoretical maximum static moment $(M_{static})_u$. The theoretical maximum static moment occurs when both the hogging and sagging joints reach their theoretical maximum sectional capacities M_{hu} and M_{su} in Figs. 3.17 and 3.18; this is the maximum static moment that can occur when there is sufficient ductility in the continuous beam to redistribute moment so that all the joints reach their ultimate capacity. The line marked *elastic (EI constant)* in Fig. 3.21 is the variation if EI is constant along the length of the beam which for this test is at 1.2. The line marked *EI approach* is based on a flexural rigidity analysis for moment redistribution as described in Section 3.3.2. The line marked *max moment redistribution prior to plate debond* signifies the amount of moment redistribution that can occur if the flexural capacities of both the plated hogging region and unplated sagging region are achieved which would be the aim in design. Finally, the line marked *max moment redistribution of unplated RC beam* represents the amount of redistribution that could occur after the plate has debonded and the beam is acting as totally unplated.

It can be seen in Fig. 3.21 that at the start of loading M_h/M_s is close to 120% which signifies that EI is constant along the length of the beam; the beam at these early stages of loading is uncracked under flexure, hence the flexural rigidities of the cross-sections are barely affected by the longitudinal reinforcement so that EI is constant. The divergence around the line $M_h/M_s = 1.2$ is simply the beam bedding down at very low loads. The hogging moment as a proportion of the sagging M_h/M_s then reduces gradually. Soon after the first flexural crack is visible the first IC interface crack can be seen when the hogging moment has reduced to about 90% of the sagging moment and the applied load is about 45% of the load that eventually caused IC debonding; the occurrence of the IC interface crack at such a small proportion of the load to cause IC debonding further reinforces the fact that IC interface cracking by itself is no problem and is also little indication of when IC debonding will occur. IC debonding then occurred at the maximum plate strain and

close to the value predicted by the flexural rigidity approach, where the hogging moment is now 66% of the sagging moment but short of the theoretical maximum redistribution at a hogging moment of 50% of the sagging moment. Hence, the beam has just failed prematurely, that is debonding of the hogging plate has occurred before the maximum capacity of the sagging region could be achieved. However, there has been a significant amount of moment redistribution as the hogging moment has reduced from 120% to 66% of the sagging moment and the continuous beam has achieved 79 % of its theoretical maximum capacity of $(M_{static})_u$.

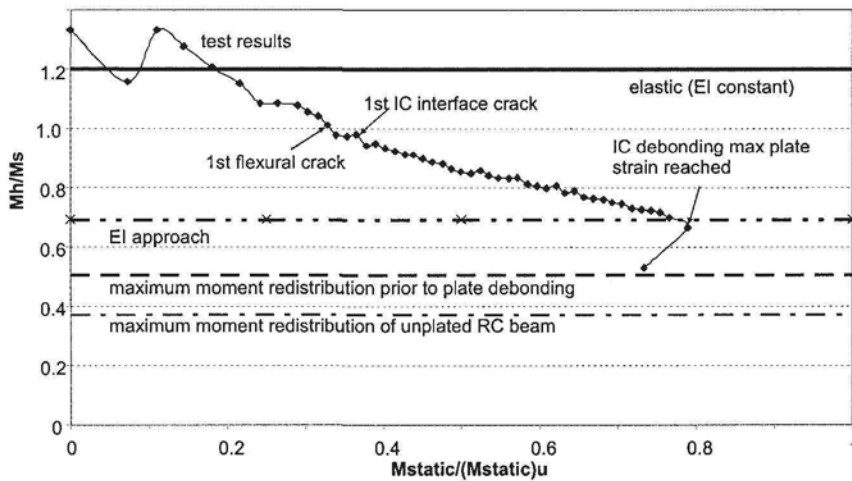


Figure 3.21 Moment redistribution in steel plated beam; $t_p = 2\text{mm}$

The test results from a carbon FRP plated beam with a 1.2 mm thick plate are shown in Fig. 3.22. The initial divergence from $M_h/M_s = 1.2$ at very low loads is simply due to bedding down of the beam. As with the steel plated beam in Fig. 3.21, M_h/M_s reduced gradually from a low load indicating moment redistribution started at an early stage. The first IC interface crack was also visible at an early load at about 35% of the load to cause IC debonding which further reinforces the point that the appearance of IC interface cracks is of little consequence. The maximum plate strain occurred at a redistribution close to that predicted by the flexural rigidity approach where the hogging moment was 72% of the sagging moment. After which, the plate strains reduced and debonding occurred at a hogging moment of 65% of the sagging moment and at an applied load of 58% of the theoretical maximum. The beam then reverted to the behaviour of an unplated beam. It is interesting to note that unlike the steel plated beam in Fig. 3.21, IC debonding occurred after the plate strains had reduced and not at the maximum plate strain.

The results from a series of tests with steel and carbon FRP plates are given in Table 3.1. In these tests, the steel plate thicknesses in column 1 were varied from 1 mm to 3 mm, and the FRP plates from very thin plates using the wet lay up procedure to quite thick plates for FRP at 2.4 mm. The maximum plate strains in column 3 just prior to debonding are in line with those already reported in Table 2.2; the steel plates having yielded prior to debonding and the FRP debonding strains are close to the characteristic values in Table 2.2.

The percentage moment redistribution in column 4 of Table 3.1 is derived from Eq. 3.2 with the moments in Fig. 3.20. It is the difference in the hogging moment between the theoretical elastic value based on EI being constant $(M_h)_{el}$ and the test result $(M_h)_{test}$ for the same static load as shown in Fig. 3.20.

$$\%MR1 = \frac{(M_h)_{el} - (M_h)_{test}}{(M_h)_{el}} \times 100 \quad 3.2$$

Hence, %MR1 in Table 3.1 is the percentage redistribution for a beam originally analysed using standard linear elastic theory where EI is assumed to be constant; as in standard design practice. It can be seen in column 4 that there has been a reasonable amount of moment redistribution; that for the steel plates varies from 22% to 48% and for the FRP plates from 28% to 35%. However, part of this moment redistribution is directly due to the difference in flexural rigidities of the hogging and sagging regions, EI_{hcr} and EI_{scr} in Fig. 3.17, because of the difference in their tension reinforcing bars as shown in Fig. 3.19. The hogging region has much less tension reinforcing bars than the sagging region. Hence the flexural rigidity of its cracked section EI_{hcr} in Fig. 3.17 would be expected to be much less than that of the sagging region EI_{scr} , and this difference by itself would account for a part of the moment redistribution, even if none of the joints reached and entered their plastic zones in Figs. 3.17 and 3.18 where the EI values would then start to reduce.

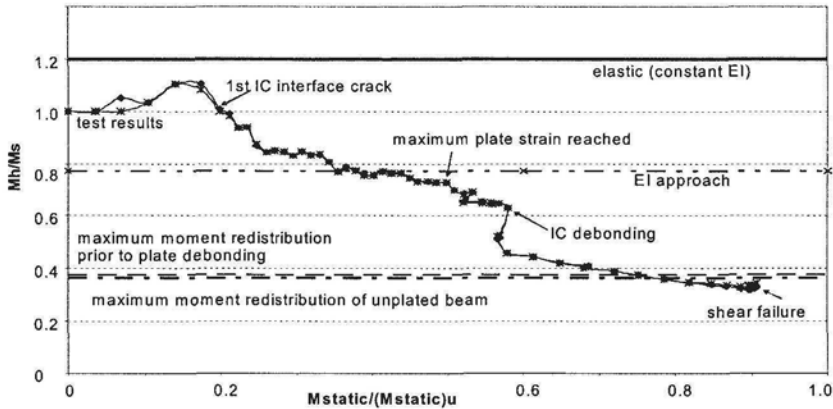


Figure 3.22 Moment redistribution in carbon FRP plated beam; $t_p = 1.2\text{mm}$

Let us determine how much of the moment redistribution in column 4 in Table 3.1 can be attributed to the difference between the elastic stiffnesses EI_{scr} and EI_{hcr} in Fig. 3.17 and how much is due to following the plastic zones. To do this, $(M_h)_{el}$ and $(M_s)_{el}$ in Fig. 3.20 needs to be derived from an analysis in which the stiffness of the beam is now EI_{scr} in the sagging region and EI_{hcr} in the hogging region, instead of being assumed constant at EI as in column 4 in Table 3.1. Hence the moment redistribution for the difference between EI_{scr} and EI_{hcr} is now accounted for in the analysis, so that any redistribution would now be due to following the plastic zones in Figs 3.17 and 3.18. Hence the percentage redistribution in column 5 in Table 3.1 is given by

$$\%MR2 = \frac{(M_h)_{EI\text{ cracked}} - (M_h)_{rest}}{(M_h)_{EI\text{ cracked}}} \times 100 \quad 3.3$$

For the steel plates in Table 3.1, the percentage redistribution due to following the plastic zones, which is given in column 5, is only slightly less than the total moment redistribution in column 4. In contrast for the FRP plated specimens, the moment redistribution due to following the plastic zones in column 5 is very small compared to the total redistribution in column 4. These results are to be expected as the sectional ductility of FRP plated sections, as shown by the plastic zones in Figs 3.1 and 3.4, is relatively small compared with the plastic zones of steel plated sections in Figs 3.1 and 3.3.

Table 3.1 Percentage moment redistribution

t_p (mm) (1)	plate material (2)	ϵ_{deb} (3)	%MR1 ($EI_{constant}$) (4)	%MR2 (EI_{crack}) (5)
3	steel	0.0044	22	16
2	steel	0.0059	33	28
1	steel	0.0149	48	43
2.4	CFRP	0.0020	30	5
1.2	CFRP	0.0029	29	4
1.2	CFRP	0.0025	28	7
wet lay up	CFRP	0.0041	35	6

In conclusion, FRP plated specimens can redistribute moment if this is a function of the elastic cross sectional stiffnesses but the plastic zone component of moment redistribution is negligible. On the other hand, metal plated specimens can redistribute due to both their initial cracked stiffness component as well as their plastic zone component.

3.3.4 Plating design considerations

To illustrate the concept of moment redistribution and in particular how it affects the choice and positioning of plates for rehabilitation, we will consider an internal bay of a continuous beam with uniformly distributed loads, which will be represented as an encastre beam. We will use the term *plastic hinge* to loosely refer to a region of a beam that requires ductility in order to redistribute moment, that is any region that has to follow the plastic zones as shown in Figs. 3.17 and 3.18. The plastic hinge will be shown as a circle in the diagram even though the region of the beam following the plastic zone or diverging from the elastic cracked section EI may be quite large. We will also use the word *rotate* to loosely to describe the act of moving along the plastic zone as this requires increases in the deflection but not necessarily a discontinuity in the slope as shown in Fig. 3.10(d). We will also assume that EI_{ser} and EI_{her} in Fig. 3.17 are roughly equal so that we can ignore moment redistribution due to their difference.

The basic design for moment redistribution will be first revised for an unplated beam, and then it will be presented in a form specifically for plated structures to illustrate how moment redistribution can affect the choice of the plating technique and can limit the increase in strength that can be achieved. As it was shown in the previous Section that carbon FRP plates can only achieve a small amount of moment

redistribution that is associated with the plastic zone, it will be assumed that FRP plated joints cannot redistribute moment whereas metal plated joints can.

3.3.4.1 Moment redistribution in unplated beams

(a) Plastic hinges at supports

Let us consider the beam in Fig. 3.23 which has been designed for a moment capacity of $(M_h)_u$ at the hogging joint and $(M_s)_u$ at the sagging joint. Hence, the curve marked A will be the distribution of moment at failure and the beam has been designed for the following static moment

$$M_{static} = (M_h)_u + (M_s)_u = \frac{w_{fail} L^2}{8} \tag{3.4}$$

where w_{fail} is the uniformly distributed load to cause failure. The elastic distribution of this static moment based on a constant EI value is shown as line B, where for this case of an internal bay with a uniformly distributed load

$$(M_h)_{el} = \frac{2}{3} M_{static} \quad \text{and} \quad (M_s)_{el} = \frac{1}{3} M_{static} \tag{3.5}$$

so that $(M_h)_{el} = 2(M_s)_{el}$. It can be seen in Fig. 3.23 that the designers have reduced the capacity of the hogging joint and increased that of the sagging joint from the elastic analysis. Therefore, the hogging region has to redistribute the moment, that is maintain its moment capacity and rotate until the sagging region reaches its moment capacity. The ability of the unplated hogging region to rotate depends on the neutral axis factor k_u as described in Section 3.3.1. It can be seen that the sagging region only needs to achieve its moment capacity and hence does not have to rotate and hence its neutral axis factor k_u is irrelevant.

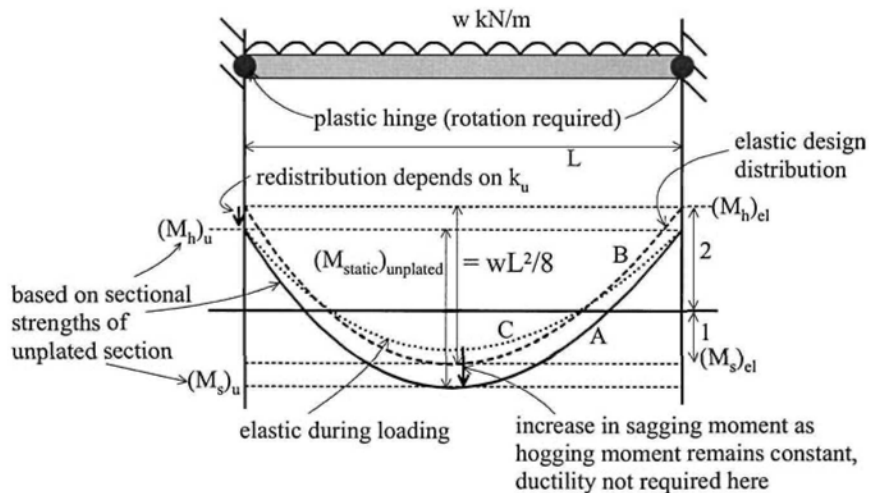


Figure 3.23 Moment redistribution in unplated beam - hogging hinges

Another way of viewing the moment redistribution in Fig. 3.23 is to consider the changes in the distribution of moment as the load is gradually increased from zero. Initially everything is elastic so that $M_h = 2M_s$. Therefore as the load is increased, the hogging joint will first reach its moment capacity as shown by the dotted line C. The hogging hinges shown now have to maintain their moment capacities and rotate until the sagging region reaches its moment capacity. Hence k_u of the hogging region determines the ability to redistribute moment in the case shown above. The thick arrow at the hogging joint in Fig. 3.23 indicates that the hogging moment is being reduced so that moment is being redistributed from the hogging region to the sagging region. Similarly for the sagging region, the thick arrow indicates that the moment is being increased.

(b) Plastic hinge in the sagging region

An example of redistribution from the sagging region to the hogging region is shown in Fig. 3.24. In this case, the designers have reduced the capacity of the sagging region and increased the capacity of the hogging region to maintain M_{static} . Hence on loading, the moment capacity of the sagging region will first be reached, as shown by the dotted line C, so that the plastic hinge at the sagging region needs to maintain its moment capacity whilst rotating to allow the moment capacities at the supports to be reached. Hence k_u at mid-span now determines the ability to rotate.

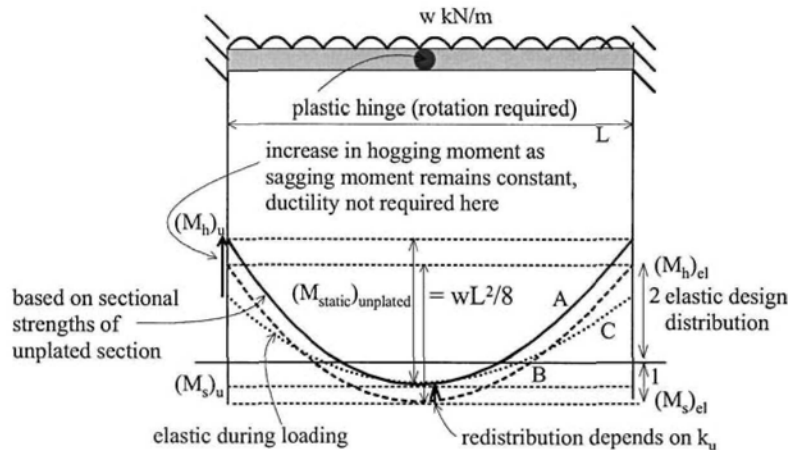


Figure 3.24 Moment redistribution in unplated beam – sagging hinge

As an example, if the mid-span was strengthened by plating so that $(M_s)_u$ in Fig. 3.24 is now the strength of the plated section, then metal plates would have to be used as FRP plated sections are too brittle to allow moment redistribution. However, FRP plates could have been used at the supports as moment redistribution is not required there. A similar argument applies to the hogging regions in Fig. 3.23. If the strength distribution line A was that of the plated beam, then metal plates would have had to be used at the supports to allow for moment redistribution, whereas, FRP plates could have been used at mid-span. It must be emphasised that the k_u factor for moment redistribution can only be applied directly to metal plated sections if it can be shown that concrete crushing controls the strength, that is at concrete crushing the strain in the plate is less than that required to cause debonding.

3.3.4.2 Moment redistribution in plated beams

Continuous beams plated with metal plates that are designed to yield before debonding and in which the concrete crushes prior to debonding can be designed directly as unplated beams, that is the moment redistribution can be based on the k_u factor. However, if the metal plates debond prior to the concrete crushing strain being achieved or if FRP plates are to be used, then moment redistribution may restrict the regions where plating can be used and control the type of plate used at a section.

(a) FRP plating sagging and hogging regions

It may be necessary to FRP plate both the hogging and sagging regions due to strength or serviceability requirements as shown in Fig.3.25. The use of FRP will preclude any moment redistribution so that the strengthened structure must have an elastic distribution of moment, which for this beam's restraints and loading configuration requires that the moment capacity of the hogging region is twice that of the sagging region as shown by the dotted line B. Hence, if it is necessary to increase the static moment capacity from that of the original unplated beam of $(M_{static})_{unplated}$ to $(M_{static})_{plated}$ as shown, then the amount of strengthening in each region is specifically defined as shown in Fig. 3.25. Theoretically this approach allows 'unlimited' strengthening or strengthening 'unlimited' by moment redistribution.

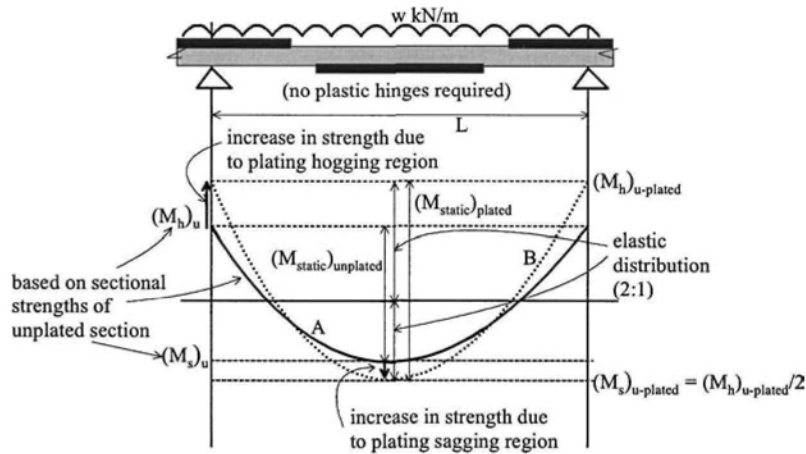


Figure 3.25 FRP plating all joints

(b) FRP plating hogging regions

As the hogging regions are to be plated with FRP in Fig. 3.26, plastic hinges are not allowed to form in the hogging regions and can only form in the sagging region as shown. Hence, it is necessary for the sagging region to remain unplated or plated with a metal plate that has been designed to allow the concrete to crush prior to debonding. The strength of the beam prior to plating is given by line A in Fig. 3.26; that is the distribution of moment at failure. The unplated beam can withstand a static moment of $(M_h)_u + (M_s)_u$ as shown and, hence, the uniformly distributed load at failure is given by Eq. 3.4. The problem is to determine how much the beam can be strengthened by only using FRP plates in the hogging regions; that is how much can the static moment $(M_h)_u + (M_s)_u$ be increased.

Let us first consider the option of not plating the sagging region but just using FRP plates in the hogging regions. Let us also assume that the ductility of the sagging region (as indicated by its neutral axis depth factor k_u as it is unplated) allows 30% moment redistribution, and as the hogging regions will have FRP plates, no redistribution is allowed there. The greatest increase in strength can be achieved by using the full moment redistribution capacity of the unplated sagging region. We are trying to find line C in Fig. 3.26, which is the distribution of moment of the plated structure at failure.

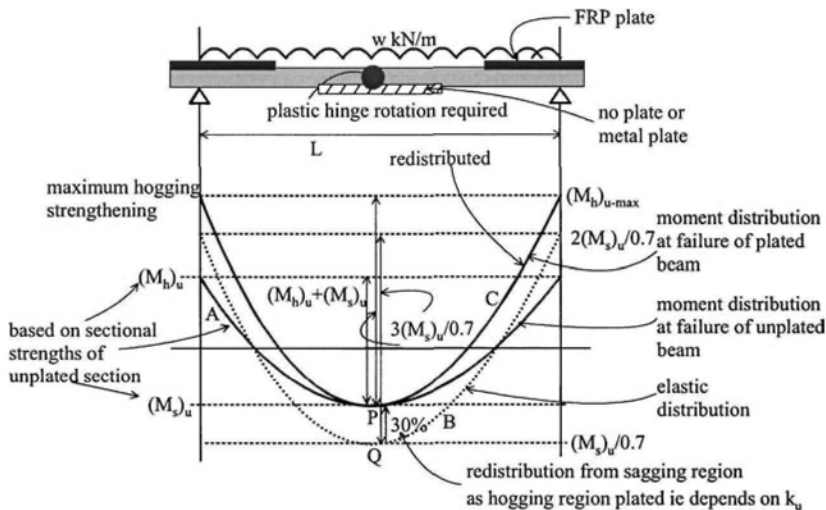


Figure 3.26 FRP plating hogging regions – 30% redistribution from sagging region

As the sagging region in Fig. 3.26 remains unplated, all we know is that line C, the strength of the plated beam, coincides with line A, the strength of the unplated beam, at point P at $(M_s)_u$ as shown. We do know that the sagging region can redistribute moment by 30%, which means that on applying the load to the elastic beam prior to moment redistribution, the moment at mid-span is greater than P and at point Q. The ductility of the sagging region allows part of this peak moment at Q to be redistributed to the hogging regions. As we know that 30% redistribution is allowed, the peak moment at Q is $(M_s)_u/0.7$, so that when 30% of this moment is redistributed then the moment becomes that at P of $(M_s)_u$. So we now have the magnitude of point Q of $(M_s)_u/0.7$. This is the moment prior to moment redistribution and, hence, it is just one point on the elastic distribution of moment on the beam; that is the distribution of moment based on EI being constant. As point Q, of magnitude $(M_s)_u/0.7$, is on the elastic distribution of moment, then the peak hogging moments must be twice this amount as shown, that is $2(M_s)_u/0.7$. Hence, the maximum elastic distribution of moment, line B, has been determined which has a static moment capacity of $3(M_s)_u/0.7$ as shown. This elastic distribution of moment can be redistributed by 30% of the sagging moment at Q to shift the whole curve upwards, as shown, to line C which is the redistributed moment at failure. From this redistributed moment can be derived the maximum possible hogging moment $(M_h)_{u-max} = 3(M_s)_u/0.7 - (M_s)_u$ which is the maximum hogging strength that can be attained when only the hogging regions are FRP plated. The increase in the static moment is given

by $3(M_s)_u/0.7 - [(M_s)_u + (M_h)_u]$ from which can be determined the increase in the applied load.

The rehabilitation procedure developed for plating is in many ways the inverse of a standard design procedure. Hence as a check to ensure our rehabilitation procedure is correct, we can apply the reverse design philosophy which is the standard design procedure. Line C in Fig. 3.26 is now the distribution of moment at failure of the plated structure which represents the strength of the structure and which we know the values of; we also know the value of the static moment for this distribution. Line B is the elastic distribution of line C; that is it has the same static moment and is distributed such that the maximum hogging moment is twice the maximum sagging moment. As we first apply and then gradually increase the load, such that the hogging moment is twice the sagging moment, the sagging moment capacity at point P is first reached. Hence, the sagging joint has to maintain this moment and keep rotating until the hogging moment capacities have been reached. If the capacity at point P is 30% (depending on the k_u value of the cross-section) less than that at point Q, then our retrofitting design procedure is correct.

If the sagging region, in Fig. 3.26, was plated with metal plates which were designed so that not only did the plates yield but that the concrete crushed before the plate debonded, then $(M_s)_u$ in Fig. 3.26 is simply that of the plated section and the above analysis can be used.

(c) FRP plating sagging regions

An example of FRP plating the sagging region is shown in Fig. 3.27. Exactly the same procedure as described in the previous Section on *FRP plating hogging regions* can be applied for this sagging region, except, of course, that the plastic hinges now occur in the hogging regions so that only the sagging regions can be FRP plated. It will be assumed that the hogging regions are unplated or that there are metal plates that allow the concrete to crush prior to debonding so that the ability to redistribute depends on the k_u factor which will be assumed allows 30% redistribution.

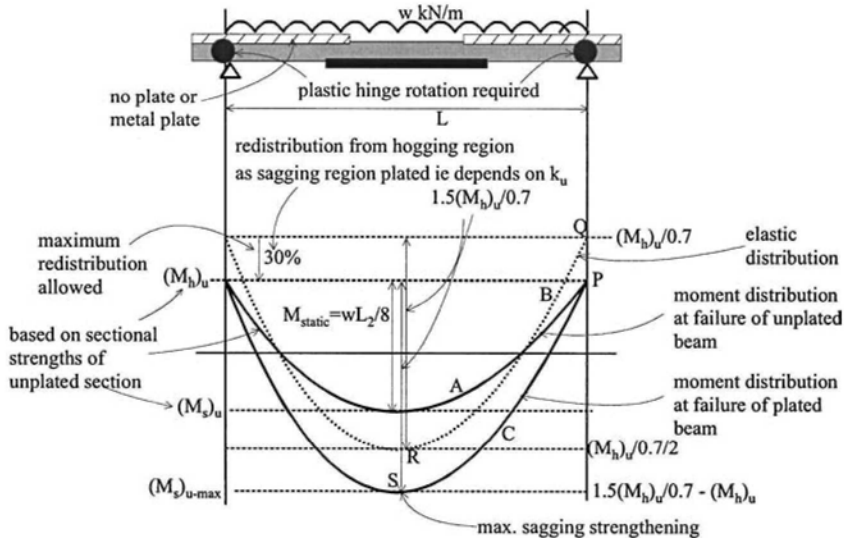


Figure 3.27 FRP plating sagging region – 30% redistribution from hogging regions

Line A in Fig. 3.27 depicts the strength of the beam without FRP plates; that is the distribution of moment at failure. Because the hogging regions can redistribute moment, one point on the elastic distribution prior to moment redistribution is given by point Q, such that a 30% reduction in Q, due to moment redistribution, gives point P. Having now fixed point Q, which is one point on the elastic distribution, point R is now fixed as it is half of the moment at Q, that is for this beam configuration. Hence, the whole elastic configuration of line B is now known. The moment distribution of line B can now be redistributed down by 30% of the hogging moment to give point S, which is the maximum strength that the plated sagging region can achieve based on moment redistribution.

Applying the converse of the rehabilitation approach to determine whether our analysis is correct. Line C in Fig. 3.27 is the strength of the plated structure. Line B is the elastic distribution. On applying the load gradually, the hogging capacity is reached first. Hence it is this joint that redistributed the moment and it is this joint that allows 30% redistribution. Hence if point P is 30% less than point Q then the original rehabilitation design is correct.

We have now reached the stage that for the beam in Fig. 3.27 we know, from moment redistribution considerations, that the most the sagging strength can be increased using FRP plates is $1.5(M_h)_u/0.7 - [(M_h)_u + (M_s)_u]$. Similarly, for the beam in Fig. 3.26, the maximum increase in the hogging region, that depends on moment redistribution, that can be achieved using FRP plates is $3(M_s)_u/0.7 - [(M_s)_u + (M_h)_u]$. The next step in the design procedure is to determine: whether these capacities can be achieved; if metal plates that have been used in other sections will allow the concrete to crush; and what is the maximum increase that can be obtained when moment redistribution is not required. This is the subject of the next section.

3.4 Sectional flexural strength and ductility capacity

The following analyses determine the flexural capacity of adhesively bonded plated sections in which failure is controlled by either concrete crushing, IC plate debonding or plate fracture. These analyses also derive the moment/curvature relationships, such as those in Figs. 3.17 and 3.18, that are required for the moment redistribution flexural rigidity approach in Section 3.3.2. These analyses also determine whether the IC debonding strain capacities in metal plated structures are sufficient to allow the concrete to crush and hence allow the k_u factor to be used for the plated section as discussed in Section 3.3.4.

The analyses are separated into propped structures, that is structures that are propped to remove the stresses within the structure prior to plating. This may be a useful technique for reducing deflections and crack widths at serviceability but the procedure can induce earlier debonding which can occur before the tension reinforcing bars have yielded. However, it is a useful starting point in the analysis as it is simpler than that for the ensuing section on unpropped construction. In unpropped construction, the beam or slab is plated whilst still carrying its self weight and some superimposed dead and live load. Hence the residual stresses in the RC section prior to debonding have to be taken into account. The residual stresses in the tension reinforcing bars are beneficial as they can ensure that the reinforcing bars yield before the plate debonds. This may be a major consideration when adhesively bonding FRP plates to the tension faces as FRP plates can debond at relatively low strains as shown

in Table 2.2. In fact, pre-loading beams prior to adhesive bonding can be very beneficial by ensuring yielding of the reinforcing bars prior to debonding.

3.4.1 Propped structure

The elementary flexural analysis of an unplated RC beam or slab is first revised. Then this standard approach is adapted to allow for the analysis of adhesively bonded metal and FRP plated structures where the plate is attached to a beam without any residual stresses, that is propped. The adhesively bonded approach is then adapted to allow for bolting.

3.4.1.1 Unplated section

A standard flexural analysis of an ordinary reinforced concrete beam is illustrated in Fig. 3.28. The beam cross-section is shown in Fig. 3.28(a) where the longitudinal reinforcement can be placed anywhere. Figures 3.28(b) to (d) depict the behaviour along the longitudinal axis of the beam at a specific section of the beam. Figure 3.28(b) is the distribution of longitudinal strain and will be referred to as the strain profile, Fig. 3.28(c) is the profile of the longitudinal stress, and that in Fig. 3.28(d) the longitudinal forces.

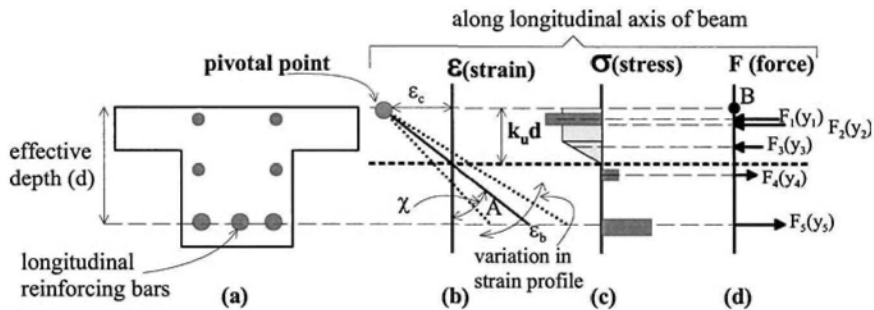


Figure 3.28 Standard flexural analysis of an RC beam

It is fairly standard practice to assume that the strain capacity of the longitudinal reinforcing bars is very large compared with the strain capacity of the concrete and, hence, does not cause failure; although this assumption can be easily checked. In which case, whether the longitudinal reinforcing bars have yielded or not, eventual failure of the beam is caused by the concrete crushing at a strain ϵ_c . This strain is given in national codes and is usually around 0.003 or 0.004. As concrete crushing at a strain ϵ_c causes failure, it is the one point on the strain profile that we know and it will be referred to as the pivotal point as shown in the strain profile in Fig. 3.28(b). The correct strain profile can be any strain profile that pivots about ϵ_c as shown in Fig. 3.28(b); that is the strain profile rotates about the pivotal point like a pendulum. An iterative procedure can be used to find the correct strain profile and spreadsheets are an ideal tool for doing these analyses.

A neutral axis depth $k_u d$ has to be guessed to fix the strain profile about the pivotal point, such as the profile A in Fig. 3.28(b). For the fixed strain profile A and from the known material stress/strain relationships, or their idealised relationship, can be derived the stress profile as shown in Fig. 3.28(c). The concrete stress profile is often considered as rectangular when the concrete has reached the crushing strain ϵ_c , however any shape according to the national code can be used; it is common practice

to ignore the tensile strength of the concrete in ultimate strength analyses due to the very large strains associated with failure but this can be easily incorporated if thought necessary. Integrating the stresses over the areas in which they act gives the resultant forces F and their positions y in the force profile in Fig. 3.28(d). The position y can be measured from any level in the cross-section and is often measured from the extreme compression fibre at B for convenience. If the longitudinal forces F sum to zero, for this beam with no externally applied axial load which is often the case, then there is longitudinal equilibrium and the guess for the neutral axis position and hence the strain profile is correct. Otherwise the strain profile can be swung around the pivotal point as shown in Fig. 3.28(b) to find a strain profile in which there is longitudinal equilibrium.

Let us assume that the profile A in Fig. 3.28(b) is the correct strain profile at failure as it is in longitudinal equilibrium; that is the longitudinal forces in Fig. 3.28(d) sum to zero. The moment capacity can be derived from the force distribution in Fig. 3.28(d) by taking moments about some convenient point such as the extreme compressive fibre at point B; however for a beam with no externally applied axial load taking moments at any level will give the same answer. Furthermore, the curvature at failure χ can be determined from Fig. 3.28(b) and even the maximum strain in the tension reinforcing ε_b in Fig. 3.28(b) at concrete failure.

As a matter of interest, if the strain in the tension reinforcing ε_b in Fig. 3.28(b) is greater than the fracture strain of the bar ε_{rebar} , which is unlikely but may occur particularly with the introduction of higher-strength/lower-ductility reinforcing steel in RC structures, then the assumption that concrete crushing at ε_c causes failure has been proved to be incorrect and the analysis has to be repeated, but this time with the pivotal point at ε_b which is now the fracture strain of the reinforcing steel. However, in this case the idealised rectangular stress block distribution for the concrete cannot be used as it only applies when ε_c is achieved so that the 'true' stress distribution should be used. The procedure can also be used to determine the behaviour at first yield, in which case the pivotal point is at ε_b which is now equal to the yield strain of the bar ε_y . Hence this procedure can be used to derive the whole moment/curvature relationship of an RC beam such as those shown in Figs 3.17 and 3.18 and which are required for the flexural rigidity approach for moment redistribution.

3.4.1.2 Adhesively bonded tension face plated beams

The flexural analysis for a tension face plated beam is shown in Fig. 3.29. As shown by the possible pivotal strains in Fig. 3.29(b), failure of the beam can be caused by either the concrete crushing at a strain ε_c , the plate IC debonding at a strain ε_{db} , the plate fracturing at ε_{frac} , or the reinforcing bars fracturing at ε_{rebar} . Hence, the pivotal point in the analysis can occur at either ε_c , ε_{db} , ε_{frac} or ε_{rebar} , whichever occurs first. It is simply a question of guessing which of these strains is reached first and pivoting about this strain. If the results show that the other strains have not been reached then the initial assumption is correct, otherwise, the analysis has to be repeated by pivoting about the strain that has been exceeded.

For pultruded carbon FRP plates, the IC debonding strain ε_{IC} , as listed in Table 2.2, is generally much smaller than the plate fracture strain ε_{frac} , and certainly much smaller than the reinforcing bar fracture strain ε_{rebar} . Hence in the region of the tension face, the first strain to be reached is generally the IC debonding strain, although this may not be the case with very thin wet lay up plates or if glass FRP plates are used. Experience has shown that with carbon FRP plates, the concrete rarely reaches its

failure strain of ϵ_c and quite often remains in the pseudo elastic range. Hence for carbon FRP plates, a good initial assumption for the pivotal point is the IC debonding strain $\epsilon_{IC} = \epsilon_{db}$ as shown in Fig. 3.29(c). It needs to be emphasised that even if the pivotal point is incorrectly chosen, the ensuing analyses will show this to be the case so that the pivotal point can be eventually changed to the correct value.

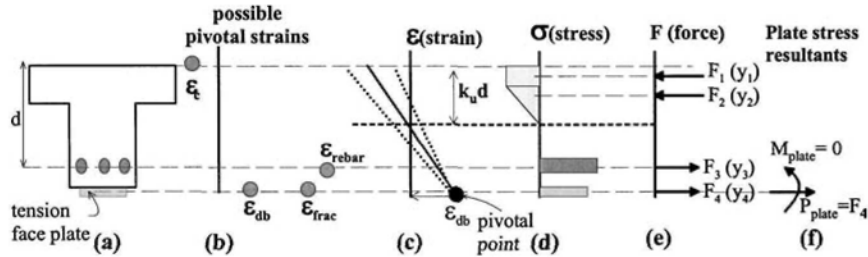


Figure 3.29 Flexural analysis of a tension face plated beam

Having chosen the pivotal point in Fig. 3.29(c), the analysis follows the standard procedure described in Section 3.4.1.1. For a given strain profile in Fig. 3.29(c), can be derived the stress profile in Fig. 3.29(d). The concrete stress has been shown as elastic/plastic in Fig. 3.29(d); however, any national variation will do, just as long as it allows for low stresses in the pseudo elastic range as IC debonding can occur when the concrete stresses at the compression face are very low. From the stress profile can be derived the force profile in Fig. 3.29(e), and if these forces are in longitudinal equilibrium, that is they sum to zero for a beam with no externally applied axial load, then the strain profile is correct. The strain profile in Fig. 3.29(c) is now known and can be used to see if any of the other possible pivotal points in Fig. 3.29(b) have been exceeded. If a possible pivotal point strain has been exceeded, then the position of the pivotal point should be changed to that pivotal strain and the process continued until no possible pivotal point strains are exceeded. Once the correct strain profile in Fig. 3.29(c) has been found, then the curvature at failure is given by the slope of the strain profile in Fig. 3.29(c), and the moment capacity by taking moments of the longitudinal forces in Fig. 3.29(e). These results will give the end of the plastic zone in Fig. 3.18.

The analysis procedure described in Fig. 3.29 can be used to find the whole moment/curvature relationship such as that shown in Fig. 3.18. However it may be more straightforward to find the flexural rigidity of the cracked section and possibly the moment at first yield of the reinforcing bars from elementary linear elastic analyses. If not, the start of the plastic zone such as B_s in Fig. 3.18 can be derived from Fig. 3.29 by this time pivoting about the yield strain of the reinforcing bars ϵ_y at the level of the reinforcing bars.

Also of interest are the stress resultants in the plate, as shown in Fig. 3.29(f), as it is these stress resultants that have to be transferred across the plate/beam interface. For example, it may have been decided to bolt the plates as well as adhesively bond the plates, as in Figs. 2.8 and 2.9, so that the bolts will take over if the adhesive bond deteriorated such as might occur in a fire or due to rusting at the interface in steel plated structures. In which case, the bolts would have to be designed to resist the stress resultants in Fig. 3.29(f). For tension face plates, the major stress resultant is the axial force $P_{plate} = F_4$, so that the bolts would have to be designed to

resist this axial force as described in Section 3.4.1.5. The moment in the plate M_{plate} is not actually zero as shown in Fig. 3.29(f) because the strain through the plate is inclined as shown in Fig. 3.29(c). However, because the plate is very thin compared with the depth of the beam, the moment in the plate is considerably smaller than the moment in the beam and usually ignored; that is the inclination of the strain in the plate is usually ignored.

Exactly the same procedure as outlined in Fig. 3.29 can be applied to metal plates. However, if they have been designed to yield before debonding, then a better starting position for the pivotal point may be at the concrete crushing strain ϵ_c , as shown in Fig. 3.28(b), and then check to ensure that IC debonding has not preceded concrete crushing. If this is the case, then the ductility of the metal plated section can be assumed to be governed by the neutral axis depth factor k_u as described in Section 3.3.1, otherwise, the flexural rigidity approach in Section 3.3.2 may have to be applied if moment redistribution is required.

3.4.1.3 Adhesively bonded shallow FRP side plated beams

The flexural analysis of a fairly shallow FRP side plated beam, in which the plate has been placed in the tension zone of the beam, is shown in Fig. 3.30. IC debonding occurs at the level of the largest tensile strain in the plate, that is at the level of the plate furthest from the neutral axis; which is where the pivotal point is shown in Fig. 3.30(b). The usual iterative procedure is applied to determine longitudinal equilibrium and to then check that the choice of the pivotal point is correct. The strain profile in Fig. 3.30(b) also gives the strain in the reinforcing bars ϵ_{bar} . If the reinforcing bars have not yielded, this may be considered to be very inefficient, as far as the strengthening procedure is concerned, and it also leads to a brittle section which is undesirable. If debonding prior to bar yielding does occur, then a solution would be to move the plate upwards towards the compression zone. For example, having the bottom of the plate above the level of the reinforcing bars will ensure that the reinforcing bar strains are always larger than the plate strains and, hence, the reinforcing bars are more likely to yield before the plates debond.

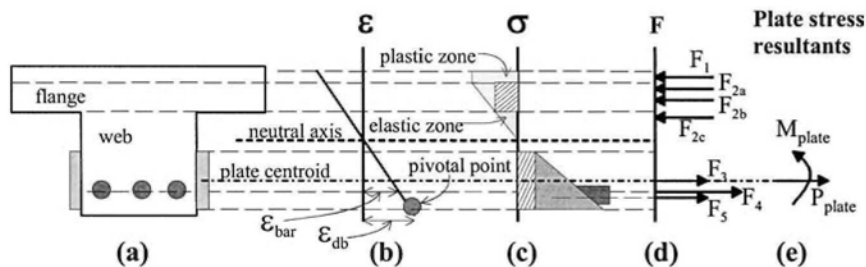


Figure 3.30 Flexural analysis of an FRP side plated beam

From the strain profile in Fig. 3.30(b), can be derived the stress profile in Fig. 3.30(c); the tensile strength of the concrete can be easily incorporated if desired. Invariably for carbon FRP plated specimens, much of the concrete in compression is within the elastic or pseudo elastic zone as shown in Fig. 3.30(c). This is because the IC debonding strains of carbon FRP pultruded plates are quite small as shown in Table 2.2. This can also be deduced from Eq. 1.2 which shows that the debonding strain is inversely proportional to the stiffness of the plate material, which for carbon

FRP is generally quite large. As FRP is a linear elastic material, the stresses within the plate are linearly distributed as shown in Fig. 3.30(c). The forces in Fig. 3.30(d) can be derived from both the stress distributions in Fig. 3.30(c) and the cross-sectional areas over which they act in Fig. 3.30(a); bearing in mind that, in this example, the plate forces F_3 and F_5 are the forces in both of the plates shown in Fig. 3.30(a). It is convenient to divide the stress profiles into distributions that can be conveniently integrated over the cross-sectional area such as triangular and rectangular components. For example, the concrete stress distribution in Fig. 3.30(c) has been separated into: the plastic zone in the flange to give the force F_1 at the mid-depth of the plastic zone; the elastic zone in the web which has a stress resultant of F_{2c} acting a third the way down the triangular stress distribution in the web; and the elastic zone in the flange which has been broken down into a rectangular stress and triangular stress distributions with the resultant forces F_{2a} and F_{2b} . Similarly, the FRP plate stress distribution has been divided into the rectangular portion shown hatched that acts over the whole of the plate area and whose force F_3 acts through the plate centroid, and the triangular distribution that also acts over the whole of the plate area but the resultant F_5 acts one-third the way up the plate.

In Fig. 3.30(e) is the resultant axial force in the plate P_{plate} and the moment in the plate about the plate centroid M_{plate} . These stress resultants are not required in the design of adhesively bonded plates but would be required if it was decided to bolt the adhesively bonded plate as an additional safeguard. It must be emphasised that the adhesive bonded system should be considered to act independently of the bolted system and, hence, the two systems should be designed independently of each other; it is suggested that the bolts should not be considered to enhance the adhesively bonded system and vice versa, as an adhesive bond is brittle whilst a bolted bond is ductile as it needs interface slip. The resultant axial force in the plate P_{plate} is simply the sum of the plate forces F_3 and F_5 in Fig. 3.30(d), and the resultant moment M_{plate} is simply determined by taking moments of the plate forces F_3 and F_5 about the plate centroid. The bolts have to resist these stress resultants as explained in Section 3.4.1.5.

3.4.1.4 Adhesively bonded deep metal side plated beams

It is well known that the addition of tension reinforcement such as the tension face plate in Fig. 3.29(a) will always reduce the sectional ductility, and it is often this reduction in ductility that limits the increase in flexural strength that can be achieved by plating. Extending the adhesively bonded side plates in Fig. 3.30(a) into the compression zone as shown in Fig. 3.31(a) can increase the flexural capacity whilst maintaining and sometimes even increasing the ductility.

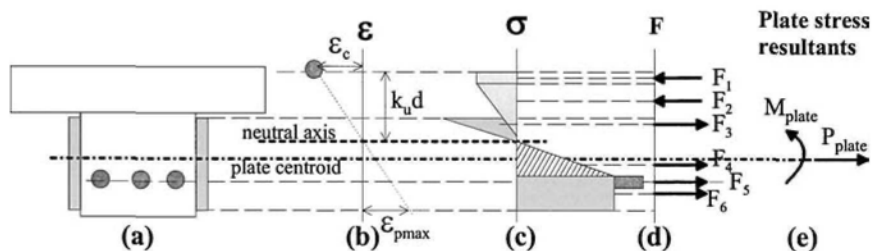


Figure 3.31 Flexural analysis of a deep metal side plated beam

For an ultimate limit strength analysis, the metal side plates in Fig. 3.31 would probably be designed to yield before debonding. In which case, the assumption that the pivotal point is at the concrete crushing strain ϵ_c , as shown in Fig. 3.31(b), would be a reasonable start to the analysis, with the usual checks for debonding after the analysis is complete. If the concrete crushing strain ϵ_c did control the analysis at ultimate, then the neutral axis depth factor k_u in Fig. 3.31(b) would control moment redistribution. For a serviceability analysis, thick plates would probably have been used to increase the flexural rigidity and reduce deflections and crack widths and would have been designed not to yield at the low serviceability loads. In this case, the debonding strain would control the analysis, that is ϵ_{pmax} in Fig. 3.31(b) would be ϵ_{db} and the pivotal point would be at this position.

The stress resultants in the plate are shown in Fig. 3.31(e) and as mentioned previously, if the plates were bolted so that the bolts took over totally if the adhesive bond deteriorated, then the bolts would have to be designed to resist these stress resultants. It is worth comparing the stress resultants in Figs. 3.29(f) for the tension face plate which occupies a small vertical dimension, with Fig. 3.30(e) for the shallow side plate, and with Fig. 3.31(e) for the deep side plate which occupies a large vertical dimension. It is worth noting that as a general rule that as the vertical dimension of the plate increases, the axial force in the plate P_{plate} reduces and the moment in the plate M_{plate} increases. Let us consider an FRP plated beam as an example, when the vertical dimension of the plate is simply the plate thickness as in the tension face plate in Fig. 3.29(a), then $M_{plate} \rightarrow 0$ and P_{plate} is at its maximum which is the product of the cross-sectional area of the plate and the debonding stress. As the vertical height of the plate increases as in Fig. 3.31(a), the tensile component in the plate, that is F_3 increases reducing the overall axial force P_{plate} and increasing the moment M_{plate} . Hence for shallow plates the bolt forces tend to be governed by P_{plate} whereas for deep plates they tend to be governed by M_{plate} .

3.4.1.5 Bolted side plated beams

The analysis for bolting a metal or FRP plate to the sides of a beam is illustrated in Fig. 3.32; the analysis follows the same general procedure that was used for adhesively bonded plates. Unlike adhesively bonded connections, bolted connections are highly ductile and are unlikely to fail in a brittle fashion. Hence, a standard analysis for RC structures can be followed by pivoting about ϵ_c , as shown in Fig. 3.32(b); after which for an FRP plate, the strain in the plate can be checked to ensure that it has not fractured.

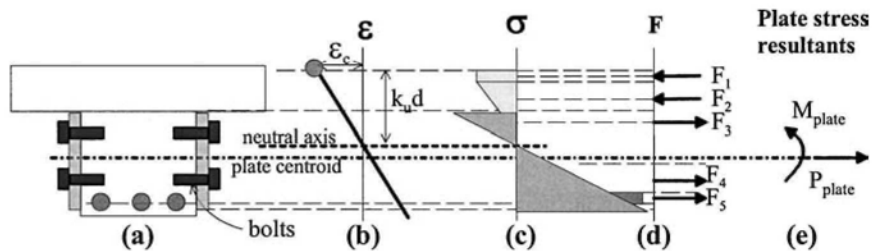


Figure 3.32 Bolted FRP side plate

Consider the forces in the plates in Fig. 3.32(d); from the forces F_3 and F_4 , can be derived the axial force in the two plates P_{plate} and the moment about the plate

centroid M_{plate} for the two plates. Similar analyses have already been illustrated in Figs 3.29 to 3.31. These stress resultants in the plates are transferred from the RC beam to the plate through the bolt shear connectors shown in Figs 3.32(a) and 3.33(a).

Figure 3.33 is a longitudinal view of the beam over either the hogging region or the sagging region of length L ; that is, between the points of contraflexure which also represent the supports of a simple supported beam. This portion of a beam will be referred to as a *region*, as it refers to either the hogging region or the sagging region. This region can be considered to consist of two parts on either side of the position of maximum moment, which will be referred to as the left and right *shear spans* and which have plates of length $(L_{sh-sp})_{left}$ and $(L_{sh-sp})_{right}$. It is important to realise that the plates in each shear span resist both P_{plate} and M_{plate} ; that is, both the plate and the bolts in each shear span resist P_{plate} and M_{plate} . It is also worth noting that if P_{plate} and M_{plate} represent the forces in two plates as would be the case in the side plate analyses in Figs.3.30 to 3.32, then the number of bolts required is the total number of bolts in a shear span and should be spread equally between the plates on either side of a beam as in Fig. 3.32(a) and uniformly along a shear span as in Fig. 3.33.

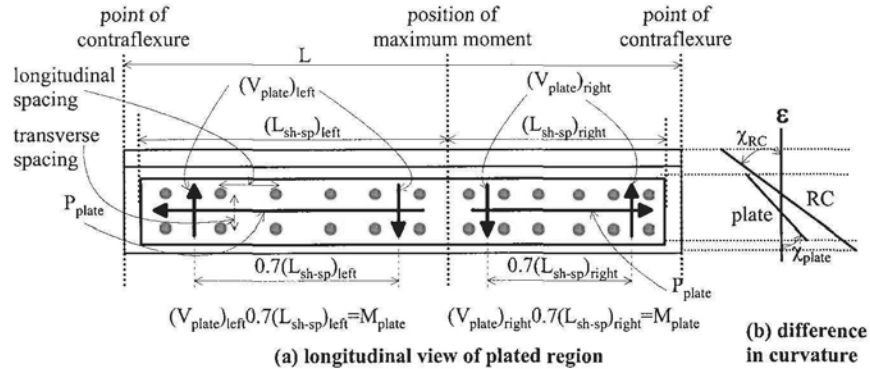


Figure 3.33 Design forces in bolted plates

On either side of the position of maximum moment in Fig. 3.33(a), the bolts have to resist the stress resultants in the plate, that is M_{plate} and P_{plate} as shown in Fig. 3.32(e) (similarly in Figs 3.29(f), 3.30(e), and 3.31(e)). It is a safe design to simply determine the number of bolts that are required to resist the longitudinal force P_{plate} by itself (N_{long}) and then add the number of bolts required to resist the vertical force in the bolts induced by M_{plate} (N_{vert}) as shown in Fig. 3.33(a). Let us assume that the shear capacity of a single bolt in a bolted plated joint is P_{sh} , which can, if need be, be determined directly from push tests in the same way as the capacity of shear connectors for composite steel and concrete beams is determined.

The number of bolts required to resist the longitudinal force P_{plate} in each shear span L_{sh-sp} in Fig. 3.33(a) is $N_{long} = P_{plate}/P_{sh}$. Tests and numerical simulations (Oehlers et al 2000) have found that the moment M_{plate} is resisted by a vertical force couple V_{plate} in Fig. 3.33(a) that have a lever arm of $0.7L_{sh-sp}$ where L_{sh-sp} is the length of the plate in a shear span. Hence $V_{plate} = M_{plate}/0.7L_{sh-sp}$, so that the number of bolts required to resist both vertical forces in a shear span is $N_{vert} = 2(M_{plate}/0.7L_{sh-sp})/P_{sh}$. Therefore, the number of bolts required in a shear span is $N_{long} + N_{vert} = P_{plate}/P_{sh} + 2(M_{plate}/0.7L_{sh-sp})/P_{sh}$. Mechanical shear connectors, such as bolt shear connectors, are ductile connections and, hence, they can be spread uniformly along a shear span as

shown in Fig. 3.33(a); that is the longitudinal and lateral spacings are the same throughout a shear span. If the shear span plates are of equal length, $(L_{sh-sp})_{left} = (L_{sh-sp})_{right}$, then the number of bolts and their distribution in each shear span will be the same, so that the total number of bolts in a region will be twice that in a shear span. If the shear span plates are of different lengths, then the number of bolts in each shear span will be different due to the difference in V_{plate} between shear spans and their spacings will also be different; the shorter right shear span plate in Fig. 3.33(a) will require more bolts than in the left and will, therefore, require a closer longitudinal spacing of the bolts.

It is worth bearing in mind that the analyses shown in Figs. 3.29 to 3.33 assume full interaction between the plate and the beam which occurs in adhesively bonded plates as an adhesive bond is a very rigid joint. However, for bolted connections to work, slip is required between the plate and the beam to induce the shear forces in the bolts. Hence, a bolted joint is a partial interaction joint in which there is longitudinal and vertical slip between the plate and the beam and, therefore, the curvature in the plate χ_{plate} is less than that in the beam χ_{RC} as shown in Fig. 3.33(b). The strains in the plate, therefore, lag behind those in the beam, so that this difference in curvature can reduce the strength slightly. Tests on bolted plated beams have shown (Oehlers et al 2000) that, in general, the reduction in the increase in strength due to plating is about 8% with one beam recording a 15% reduction. This is the reduction in the *increase in strength due to plating* and not the reduction of the total strength. It is, therefore, recommended that a safe design, to allow for partial interaction, would be to reduce *the increase in strength due to plating* derived from a full interaction analysis by 15%.

It is also worth bearing in mind that the analysis in Fig. 3.32 is a full shear connection analysis which means that sufficient bolts are provided to resist P_{plate} and M_{plate} . Fewer bolts can be provided, in which case the stress resultants P_{plate} and M_{plate} are now governed by the number of bolts provided, and this is referred to as a partial shear connection analysis and details of this analysis can be found elsewhere (Oehlers and Bradford 1995). However, when a partial shear connection analysis is used, the ductility of the shear connectors now becomes very important in order to prevent the bolt shear connectors from fracturing due to excessive slip as shown in Fig. 1.31(a). Hence, it is recommended that a full shear connection analysis is applied as depicted in Fig. 3.32.

Bolted plates when placed in the compression zone such as in Figs 3.32 and 1.31(b) can buckle and there are guidelines for positioning the bolts to prevent buckling for steel plated members (Smith et al 1999, 2000 and 2001). However, restricting the bolted plates to the tension zones such as in Figs 3.29 and 3.30 will overcome this problem. Buckling is not a problem with adhesively bonded plates. It is also worth bearing in mind that bolted FRP plates are not susceptible to premature debonding or premature failure so that they can generally be designed to attain a high stress in the FRP, whereas, the maximum stress in adhesively bonded FRP plates is generally quite small and may only be 20% to 30% of their fracture stress.

The design of the bolt shear connectors is illustrated in Fig. 3.34. Bolt shear connectors behave in a similar fashion to stud shear connectors in composite steel and concrete design. Hence, it is recommended that rules for the design of stud shear connectors (Oehlers and Bradford 1995, 1999) can be applied directly and which are given in national codes for composite steel and concrete beams. The bolts act as dowels in transferring the shear from the RC member to the plate; the top bolt marked as *bolt shear connector* in Fig. 3.35 has broken by dowel action with the characteristic

small zone of crushed concrete just visible adjacent to the bolt on the left side. A minimum length of bolt embedded in the concrete in Fig. 3.34 is required to prevent embedment failure (that is to prevent the bolts from pulling out). The stirrups act as transverse reinforcement. The shear planes in the RC beam have to be able to resist the imposed dowel forces. There must be sufficient cover to the bolt to prevent the dowel forces from splitting the concrete as shown in Fig. 3.35. The transverse spacing and longitudinal spacing of the bolts in Fig. 3.33 must be sufficiently large to allow the full dowel strength to be achieved. Design rules for all these failure mechanisms are available from the design of stud shear connectors.

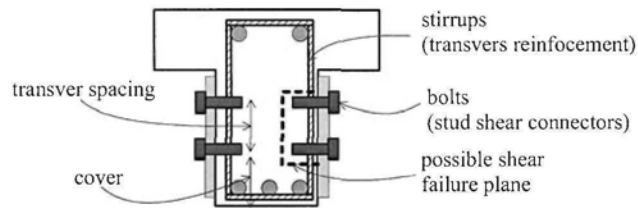


Figure 3.34 Design of bolt shear connectors

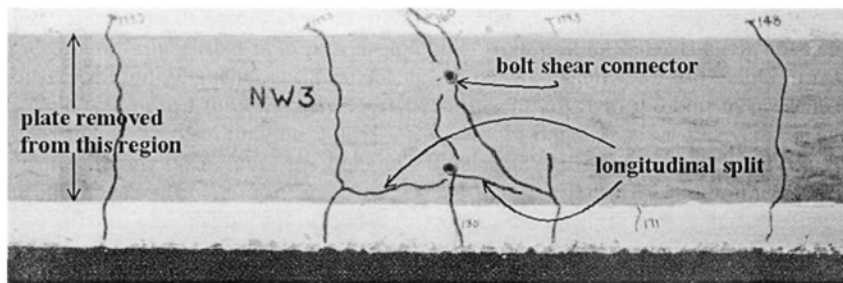


Figure 3.35 Failure of bolt shear connectors

It is often much easier to bolt the sides of beams as in Fig. 3.35 where only the stirrups have to be avoided, than to bolt the tension face of beams, where the congestion of the tension reinforcing bars may make it impossible to extend the bolt well past the concrete cover to ensure that embedment failure does not occur.

3.4.2 Unpropped structure

3.4.2.1 Adhesively bonded tension face plated beam

The problem with FRP plating in particular, is that the IC debonding strains as determined from tests, as shown in rows 1-2 and 5-6 in Table 2.2, are about the same magnitude as the yield strain of high yield tension reinforcing bars and, because the tension face plate is further from the neutral axis than the tension reinforcing bars, as shown in Fig. 3.36(b), there is a very good chance that the tension face plate will debond before the reinforcing bars yield which would produce a very brittle sectional and beam behaviour. One way of overcoming this problem is to plate the beam when it is unpropped, so the beam is preloaded with at least its own weight prior to plating. Hence, the plate will only help resist the additional live load whilst the tension reinforcing bars are resisting all of the dead and live load. If this is still not sufficient

to prevent IC debonding prior to the reinforcing bars yielding, then it is theoretically possible to pre-load the beam prior to plating to further increase the difference between the reinforcing bar strains and the plate strains.

The flexural analysis of a propped beam in Fig. 3.36(A) is compared with that of an unpropped beam in Fig. 3.36(B). The propped analysis in Fig. 3.36(A) follows the procedures already described in Section 3.4.1; at plate debonding, at a plate strain of ϵ_{db} in Fig. 3.36(b), the strain in the tension reinforcing bars is $(\epsilon_{bar})_{propped}$ is less than the IC debonding plate strain of $\epsilon_{IC} = \epsilon_{db}$.

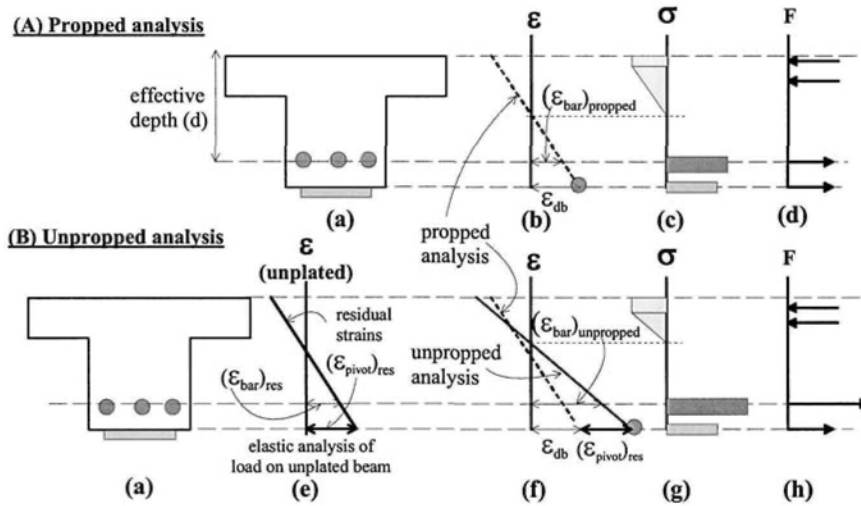


Figure 3.36 Flexural analysis of an unpropped plated beam

When the unplated beam is unpropped or preloaded, then there are already strains within the section which will be referred to as the *residual strains* and which are shown in Fig. 3.36(e). These strains can be determined from a straightforward linear elastic analysis of the section under the serviceability loads that are acting; depending on the state of the beam and the loads that are acting and have acted, will determine whether an uncracked or cracked sectional analysis is appropriate. The residual strain in the tension reinforcing bars is shown as $(\epsilon_{bar})_{res}$ in Fig. 3.36(e). The residual strain at the tension face of the concrete is shown as $(\epsilon_{pivot})_{res}$ and it is the residual strain at the level of the future pivotal point; the strain $(\epsilon_{pivot})_{res}$ is really an effective strain as it defines the strain profile but it may not be the actual strain in the concrete due to flexural cracking. When the unpropped beam is plated, and prior to any further increase in load, the plate strain is zero and the concrete strain adjacent to it is $(\epsilon_{pivot})_{res}$, so that this strain difference between the plate and the adjacent concrete will always exist upon loading. This is similar to the signature strain difference $\Delta\epsilon_p$ between prestressing tendons and the concrete at the level of the tendons in prestressed concrete which is fixed at the time of stressing.

On loading the plated beam, the plate will eventually debond at a plate strain of $\epsilon_{db} = \epsilon_{IC}$. Therefore the strain in the adjacent concrete is $\epsilon_{db} + (\epsilon_{pivot})_{res}$ as shown in Fig. 3.36(f). This is the pivotal point for the strain profile in the RC beam as shown in Fig. 3.36(f). Having fixed the pivotal point, the analysis follows the standard

procedure already described in Section 3.4.1. By comparing Figs. 3.36(b) and (f), it can be seen that as the pivotal point strain has increased, the strain in the reinforcing bars has increased from $(\epsilon_{\text{bar}})_{\text{propped}}$ to $(\epsilon_{\text{bar}})_{\text{unpropped}}$ at failure. This increase may be sufficient to allow the reinforcing bars to yield.

3.4.2.2 Adhesively bonded side plated beam

The analysis of an unpropped side plated beam is shown in Fig. 3.37 and follows the same procedure as for the tension face plated beam in Fig. 3.36. The residual stresses in the unplated beam prior to plating have first to be determined as shown in Fig. 3.37(b). When the side plates are adhesively bonded to the beam and prior to any further loading, the plate will not have any stresses and, therefore, the difference between the plate strain and the RC beam strain will be given by the strain profile in Fig. 3.37(b). Any two points need to be known to fix this strain difference. For convenience these will be chosen at the level of the compression edge of the plate where the residual strain is $(\epsilon_{\text{comp.edge}})_{\text{res}}$ and at the tension edge of the plate where the residual strain is $(\epsilon_{\text{pivot}})_{\text{res}}$, where the tensile strain in the plate will eventually be its highest and, therefore, where debonding will eventually initiate.

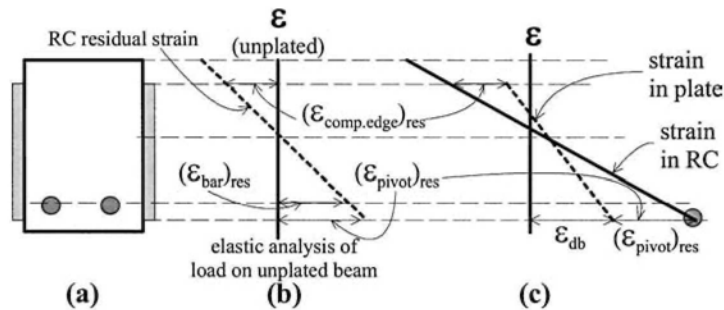


Figure 3.37 Flexural analysis of an unpropped side plated beam

As the beam is loaded, the strain profile in the RC beam will change but the plate strains will always lag behind the RC strains by a value of $(\epsilon_{\text{comp.edge}})_{\text{res}}$ at the top of the plate and $(\epsilon_{\text{pivot}})_{\text{res}}$ at the bottom of the plate, until just prior to plate debonding the pivotal strain is $\epsilon_{\text{db}} + (\epsilon_{\text{pivot}})_{\text{res}}$ as shown in Fig. 3.37(c). To find a solution, the strain profile in the RC beam is swung around the pivotal point in Fig. 3.37(c), bearing in mind that the plate strain profile lags behind by the values $(\epsilon_{\text{comp.edge}})_{\text{res}}$ and $(\epsilon_{\text{pivot}})_{\text{res}}$ as shown in Fig. 3.37(c), until longitudinal equilibrium is achieved. As with the tension face plate in Fig. 3.36, the strains in the reinforcing bars at plate debonding will increase. If this is not sufficient to allow the bars to yield, then either a pre-load can be applied to the beam prior to plating or the bottom level of the FRP plate in Fig. 3.37(a) could be raised, thereby, raising the pivotal point in Fig. 3.37(c), which will cause the strains in the reinforcing bars to increase prior to debonding.

3.5 Analyses and parametric studies

The design procedure for flexural strengthening based on IC debonding will be illustrated for adhesive bonding tension FRP face plates, adhesive bonding steel side

plates and bolting steel, aluminium or FRP plates to either slab structures or beam structures. These analyses supplement a comprehensive set of worked examples fully described in Chapter 7 that covers all forms of debonding. All safety factors and load factors have been removed from the analyses as it is assumed the designers will apply their own national values.

The design procedure for flexural strengthening based on IC debonding applies to both the hinge approach described in Section 2.5.2 and the anchorage approach in Section 2.5.1. However, the IC debonding resistances from pull tests are used in the following analyses, which means that the results are typical of the hinge approach. The anchorage approach allows the use of higher debonding strains and examples of analyses with these higher strains are given in Chapter 7.

3.5.1 Slab structure with adhesively bonded FRP plates in sagging region

A slab is strengthened along one span by adhesive bonding carbon FRP plates to the sagging region. Brief specifications are first given (the full specifications are given in Chapter 7), then moment redistribution is considered to determine the theoretical maximum increase in the strength of the sagging region to achieve the maximum increase in overall strength. The slab is then plated as propped and unpropped for comparison.

3.5.1.1 Slab specifications

An internal bay of a continuous slab has been chosen to illustrate the design procedure. Details of a 1 meter width of the slab are shown in Fig. 3.38. The slab spans 5m, as shown in Fig. 3.38(a) and the cross-sectional details for both the hogging (-ve) and sagging (+ve) regions are shown in Fig. 3.38(d). The unplated slab has a hogging strength of 41 kNm and a sagging strength of 31 kNm, as shown in Fig. 3.38(b), such that the static moment at failure is 72 kNm which converts to a uniformly distributed load at failure of 22.9 kN/m as shown in Fig. 3.38(a). The elastic distribution for the static moment is shown as the dashed line in Fig. 3.38(b) and it can be seen that the slab has been designed for a moment redistribution from the hogging region of 15%; that is the strength of the hogging region is 15% less than its elastic moment. The maximum vertical shear load is 57 kN as shown in Fig. 3.38(c).

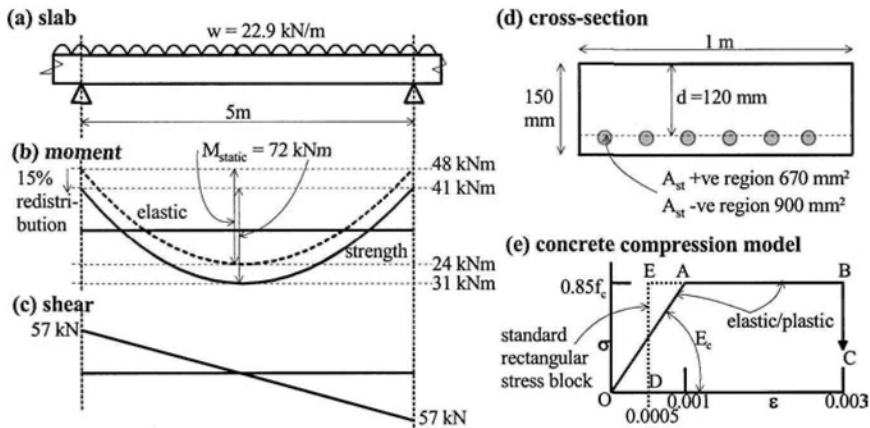


Figure 3.38 Slab structure

For convenience, the concrete compressive constitutive model has been assumed to have a pseudo linear-elastic/perfectly-plastic variation O-A-B-C, as shown in Fig. 3.38(e), with a strain capacity of $\epsilon_c = 0.003$. Any variation can be used in the following calculations such as the well-known parabolic/rectangular shape. However, the pseudo elastic/plastic variation has been used here to help to illustrate to the reader, in the following calculations, how IC debonding can occur well before the concrete crushes at its ultimate strain ϵ_c and whilst the concrete is pseudo-elastic. For interest, the elastic/plastic relationship O-A-B-C has been compared in Fig. 3.38(e) with the standard rectangular stress block at ultimate (which is only applicable when the maximum concrete strain has reached ϵ_c) used in Australia and elsewhere of O-D-E-B-C. The depth of the standard rectangular stress block D-E-B-C is typically defined by a factor γ of the neutral axis depth $k_u d$ and is a function of f_c . It may also be worth noting that in design examples, where the concrete crushing strain ϵ_c is reached, the difference in the ultimate flexural strength between using the perfectly plastic rectangular distribution O-D-E-B-C and the pseudo elastic/plastic distribution O-A-B-C was very small, more often less than 1%. Hence, the elastic/plastic variation O-A-B-C can be used at all stages of loading, such as when all the concrete is in the pseudo-elastic region O-A. Whereas the rectangular variation O-D-E-B-C cannot cope with any stress distribution other than that at ultimate when ϵ_c has been reached.

In the following examples, the concrete cylinder compressive strength $f_c = 30$ MPa, the yield strength of the reinforcing bars $f_y = 400$ MPa and their yield strain $\epsilon_y = 0.002$, the Young's modulus of the concrete $E_c = 25.5$ GPa, and the Brazilian tensile strength of the concrete $f_{cb} = 2.7$ MPa. Hence for the value of f_c and E_c used in the following examples, the strain at point A in Fig. 3.38(e), that is the transition from elastic to plastic behaviour, is 0.001. For the hogging region, the neutral axis depth factor $k_u = 0.14$ and the vertical shear capacity of the slab, from a national standard, is $V_c = 119$ kN. For the sagging region, $k_u = 0.10$ and $V_c = 108$ kN. It can be seen that the shear load on the slab of 57 kN in Fig. 3.38(c) is well within its shear capacity of 119 kN. The slab is to be plated with 1.2 mm thick carbon FRP plates of Young's modulus $E_p = 160$ GPa, which from Eq. 2.1 and Table 2.2 has a characteristic IC debonding strain of $\epsilon_{IC} = 0.00267$, a characteristic debonding stress of $\sigma_{IC} = 427$ MPa (for convenience it has been assumed that $b_p/b_c = 0.5$ throughout) and from Eq. 2.3 an anchorage length of $L_c = 187$ mm.

3.5.1.2 Moment redistribution

In this example, we are only allowed to plate the sagging region with FRP plates as shown in Fig. 3.39(a). The first stage of the design is to determine if there are any limits to increasing the load on the continuous slab when strengthening the sagging region only with FRP plates. The moment distribution at failure of the unplated beam is shown as line A in Fig. 3.39(b); the static moment, being the sum of the hogging and sagging strengths of 41 kNm and 31 kNm, is 72 kNm. The sagging region is to be plated with carbon FRP plates and, therefore, it will be assumed that a plastic hinge cannot form in the sagging region for the reasons given in Section 3.3.1. The hogging regions are unplated and have a small neutral axis factor $k_u = 0.14$ which for some codes in Fig. 3.14 allows 30% redistribution which will be assumed.

The largest increase in the overall strength of the continuous beam, that is the largest increase in the load that can be applied to the continuous beam, occurs when the maximum moment is redistributed from the hogging region to the sagging region. As the hogging hinges in Fig. 3.39(a) can redistribute 30% of their elastic moment, the elastic moments at the hogging hinges are $(M_h)_u/0.7 = 59$ kNm which are shown

as points E in Fig. 3.39. As a check, 30% redistribution from 59 kNm gives the hogging strength of 41 kNm. As the hogging moments at points E are part of the elastic distribution, the elastic sagging moment must be half the hogging moment and is shown as point F of magnitude $(M_h)_u/0.7/2 = 29$ kNm. Hence, the maximum static moment that can be achieved by allowing for 30% redistribution from the hogging region to the sagging region is $59 + 29 = 88$ kNm which is shown as $(M_{static})_{pl}$; the subscript *pl* has been used as this static moment can only be achieved after plating. The static moment has been increased from 72 kNm to 88 kNm, that is a 22% increase in strength. Moment redistribution will allow the elastic moment distribution E-F-E (line B in Fig. 3.39(b)) to drop to H-G-H (line C), such that the hogging moment has reduced by 18 kNm (30%) and is now that of the unplated structure $(M_h)_u$. Hence, the sagging elastic moment has increased by the same magnitude from 29 kNm to 47 kNm. Therefore, the maximum increase in the strength of the continuous beam occurs when the sagging strength has been increased from 31 kNm to 47 kNm. The next stage in the design is to see if this increase in strength can be achieved by plating.

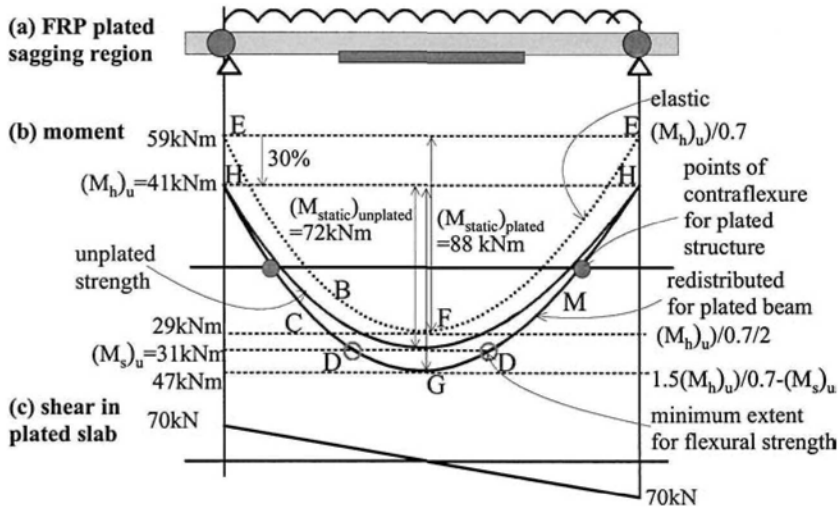


Figure 3.39 FRP plating sagging region of slab

It is worth considering what would happen if the sagging strength capacity is increased above this theoretical maximum value 47 kNm. If, for example, the sagging strength is increased to say 61 kNm, then the theoretical static moment at failure is $41 + 61 = 102$ kNm. The elastic distribution of this static moment would require a hogging moment of two-thirds of 102 kN that is 68 kN. The capacity of the hogging region is 41 kNm. Hence the redistribution required is $(68 - 41)/68 = 40\%$ which is greater than the 30% the k_u value of the hogging region allows.

3.5.1.3 Propped flexural analysis

The flexural analysis is shown in Fig. 3.40. The pivotal point $(\epsilon_{pivot})_{RC}$ in Fig. 3.40(b) always represents the strain in the concrete adjacent to the plate. Hence, the strain profile that extends from the pivotal point is the strain profile in the RC structure. As this is a propped analysis, the pivotal strain is the plate debonding strain $(\epsilon_{pivot})_{RC} = \epsilon_{db}$

= 0.00267. The strain $(\epsilon_c)_{max}$ is the maximum strain in the concrete at debonding; χ is the curvature at debonding; ϵ_{bar} is the strain in the reinforcing bars at plate debonding; d_y is the depth of the pseudo plastic zone in the concrete and is negative in the following analyses when the concrete remains fully in the elastic zone; F_{c1} and F_{c2} are the resultant forces in the plastic zone and elastic zone of the concrete respectively; F_s is the force in the steel reinforcing bars which yield at a strain of 0.002; F_p is the axial tensile force in the plate required for longitudinal equilibrium; and b_p is the width of 1.2 mm CFRP plate required.

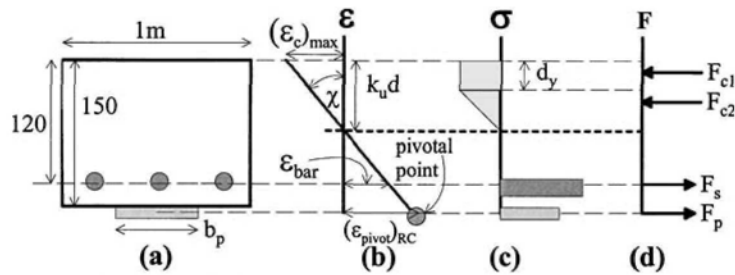


Figure 3.40 Flexural analysis: CFRP tension face plate in sagging region

The results of the spreadsheet analyses are summarised in Table 3.2. The spreadsheet procedure used here was to determine the plate size required for a specific neutral axis depth. As an example, let us consider the first row of results in Table 3.2. The pivotal strain $(\epsilon_{pivot})_{RC}$ in the reinforced concrete slab is the plate IC debonding strain 0.00267; the neutral axis depth has been fixed at 48 mm, this gives a curvature of $2.6 \times 10^{-5} \text{ mm}^{-1}$; a reinforcing bar strain of 0.00187; a maximum concrete strain of 0.00125; and a depth of the concrete plastic zone of 9.6 mm. From the forces in Fig. 3.40(d), the force in the plate required for longitudinal equilibrium is 483 kN; as the stress in the plate at debonding is 427 MPa and the plate thickness is 1.2mm, the width of plate required is 942 mm. By taking moments of the forces in Fig. 3.40(d) can be determined the moment capacity 91 kNm; this capacity is greater than the required value of 47 kNm and hence the neutral axis depth is reduced until the required capacity is reached in row 4 which is shown highlighted.

Table 3.2 Summary of propped flexural analysis: CFRP tfp in sagging region

	$(\epsilon_{pivot})_{RC}$	$k_u d$ [mm]	χ (10^{-5}) [mm^{-1}]	ϵ_{bar}	$(\epsilon_c)_{max}$	d_y [mm]	F_p [kN]	b_p [mm]	k_u	M_{cap} [kNm]
1	0.00267	48	2.6	0.00187	0.00125	9.6	483	942	0.40	91
2	0.00267	45	2.5	0.00190	0.00114	5.4	389	759	0.38	79
3	0.00267	40	2.4	0.00193	0.00097	-1.4	234	458	0.33	60
4	0.00267	36	2.3	0.00196	0.00085	-6.4	132	257	0.30	47

It can be seen in row 4 of Table 3.2 that the reinforcing bars have not quite yielded prior to debonding and even if they had just managed to yield the section would still be very brittle. It can also be seen that the maximum concrete stress is still in the elastic zone and, hence, the negative value of d_y . The width of plate required is 257 mm per meter width of slab. The length of plate required has to cover the region D-D in Fig. 3.39 where the applied moment, for the strengthened structure, exceeds

the strength of the unplated section. The plates should at least be extended beyond this region by their anchorage length of $L_c = 187$ mm. It is also worth noting that the neutral axis depth factor is 0.30 but as the maximum strains in the concrete have not reached their crushing strain, then this factor cannot be used for moment redistribution even though it would appear from Fig. 3.14 that some redistribution could be allowed.

3.5.1.4 Unpropped flexural analysis

The unpropped analysis is also depicted in Fig. 3.40. From an elastic cracked sectional analysis of the unplated beam under serviceability loads, it was determined that the residual stress in the unplated beam just prior to plating was $(\epsilon_{pivot})_{res} = 0.00139$ so that the pivotal point $(\epsilon_{pivot})_{RC} = 0.00267 + 0.00139 = 0.00406$ as shown in column 2 in Table 3.3. As mentioned previously, $(\epsilon_{pivot})_{RC}$ is the strain in the RC beam, the strain in the plate is ϵ_{db} , so that the plate strain lags behind the concrete strain by $(\epsilon_{pivot})_{res}$. The steps in the analyses have already been described in Section 3.5.1.3.

The final result is summarised in row 5 in Table 3.3. It is worth comparing these results with those for the propped analysis in Table 3.2. Plating the unpropped beam as compared to the propped beam, has increased the curvatures by 48%, the strains in the reinforcing bars are now well above the yield strain and have increased by 55%, the concrete strains are still very low and barely within the plastic zone and have only increased by 19%, the force in the plate has reduced slightly by 8% so that slightly less FRP is required. Importantly from these analyses, plating the unpropped beam has increased the ductility.

Table 3.3 Summary of unpropped flexural analysis: CFRP tfp in sagging region

	$(\epsilon_{pivot})_{RC}$	$k_u d$ [mm]	χ (10^{-5}) [mm ⁻¹]	ϵ_{bar}	$(\epsilon_c)_{max}$	d_y [mm]	F_p [kN]	b_p [mm]	k_u	M_{cap} [kNm]
1	0.00406	48	4.0	0.00285	0.00190	22.7	634	1104	0.40	111
2	0.00406	45	3.8	0.00288	0.00173	19.0	548	954	0.38	101
3	0.00406	40	3.7	0.00294	0.00147	12.8	405	704	0.33	83
4	0.00406	35	3.5	0.00299	0.00123	6.5	261	455	0.29	65
5	0.00406	30	3.4	0.00303	0.00101	0.4	121	211	0.25	47

3.5.2 Beam structure with adhesively bonded plates

In this example, we will only be concerned with strengthening the hogging sections of a continuous beam and not with the overall behaviour of the continuous beam as in Section 3.5.1, and propped construction will only be considered.

3.5.2.1 Beam specifications

The details of the continuous beam are given in Fig. 3.41. The hogging flexural capacity is 339 kNm. The variation of the moment distribution at failure, that is the strength, is very close to the elastic distribution so that the beam has been designed without moment redistribution. The concrete, reinforcing bar, and FRP plate material properties are the same as those described in Section 3.5.1. The hogging region of the beam has $k_u = 0.29$ and $V_c = 134$ kN and the sagging region $k_u = 0.14$ and $V_c = 104$ kN.

3.5.2.2 Tension face plates on underside of flange in hogging region

Plating the tension face of a beam can sometimes be a problem as the strains in the plate ($\epsilon_{pivot}RC$ in Fig. 3.40(a) will generally be greater than that in the reinforcing bars ϵ_{bar} as shown in Fig. 3.40(b) for a propped analysis. This may not be the case for an unpropped analysis where the residual stresses in the reinforcing bars increase their strains relative to that of the plate. In a propped analysis, this may lead to debonding of the plate prior to yielding of the reinforcing bars. One solution is to plate the underside of the flange as shown in Fig. 3.42(a), as this will drop the pivotal point below the tension reinforcing bars which will ensure that the reinforcing bar strains are higher than those in the plates.

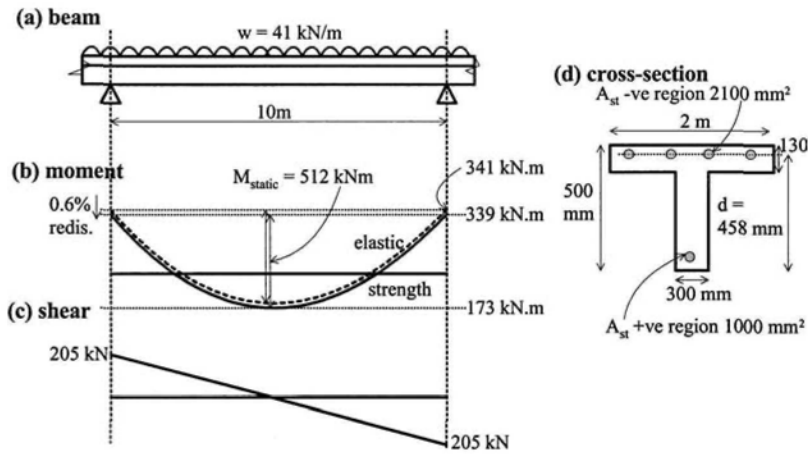


Figure 3.41 Beam structure

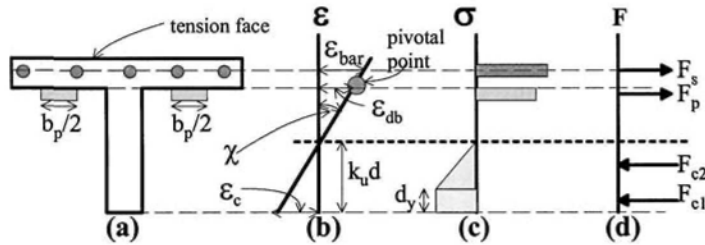


Figure 3.42 Propped balanced flexural analysis of plating underside of flange in hogging region

A practical upper limit to the strengthening technique is to use a balanced analysis as shown in Fig. 3.42(b) where the concrete reaches its ultimate strain capacity $\epsilon_c = 0.003$ at the same time as the plate reaches its debonding strain ϵ_{db} . In which case, the strain profile and, hence, the stress profile in Fig. 3.42(c) are now fixed, so that it is just a question of finding a cross-sectional area of plate in which the resulting force F_p in Fig. 3.42(d) provides longitudinal equilibrium, that is the sum of the forces is zero. The results of the analyses are summarised in Table 3.4 for CFRP plates with thicknesses varying from 0.6 mm to 3.6 mm. The cross-section area of the

plate required for longitudinal equilibrium A_p is given in column 8 and in the last column $\% \Delta M$ is the percentage increase in strength over that of the unplated section.

It can be seen in column 5 in Table 3.4 that plating the underside of the flange has ensured that the reinforcing bars yield prior to debonding even for the very thick plate of 3.6 mm in row 4. For the thinner plates, the reinforcing bar strains are much greater than their yield strain of 0.002 which suggests a nice ductile behaviour as the moment increases gradually along the plastic zone in Fig. 3.18. It can be seen in column 3, that as the plate thickness is increased the stress at debonding reduces quite substantially. However, the force in the plate does increase as shown in column (8) but only because the cross-sectional area of plates in column 7 increases significantly. For example, let us compare the results for the 0.6 mm plate in row 1 with the 3.6 mm plate in row 4. Increasing the plate thickness from 0.6 mm to 3.6 mm has increased the moment capacity by 31% but the cross-sectional area of plate required has increased by 770%. It would appear that using thick FRP plates is not economical.

Table 3.4 Summary of *propped* balanced flexural analysis: CFRP plating underside of flange in hogging region

	t_p [mm]	ϵ_{db}	σ_{db} [MPa]	χ (10^{-5}) [mm $^{-1}$]	ϵ_{bar}	F_p [kN]	A_{p2} [mm 2]	M_{cap} [kNm]	ΔM [%]
	(1)	(2)	(3)	(4)	(5)	(6)	(7)	(8)	(9)
1	0.6	0.0038	605	1.83	0.0054	203	336	388	14
2	1.2	0.0027	427	1.53	0.0040	408	955	436	29
3	2.4	0.0019	302	1.32	0.0031	607	2007	471	39
4	3.6	0.0015	246	1.23	0.0026	719	2917	490	45

3.5.2.3 Side plates over full depth of web in hogging region

Let us consider plating the full depth of the web in the hogging region as shown in Fig. 3.43(a). From Eq. 2.1 and also shown in Table 2.3, it can be derived that for a steel plate of Young's modulus 200GPa and yield strength $f_y = 300$ MPa, the plate thickness at which yield and debonding occur simultaneously is 3.0 mm. This is a transition thickness between IC debonding and yield.

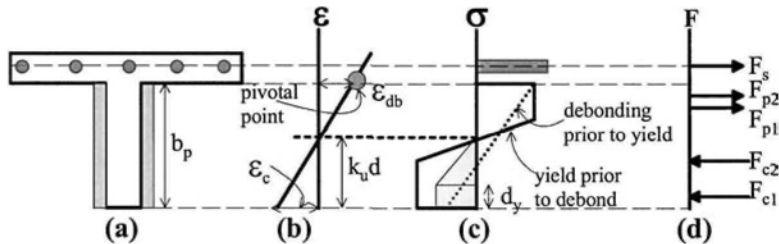


Figure 3.43 Propped flexural analysis of full depth web plate in hogging region

If the plate thickness is just above the transition thickness of 3 mm, then the plate will debond prior to yielding. The analysis is shown in Fig. 3.43(b) where the pivotal point is at ϵ_{db} , and in Fig. 3.43(c) for the plate stress distribution given by the broken line where yield in the plate can only occur at the pivotal point. In this case, the moment capacity is 374 kNm which is 10% more than that of the unplated structure of 339 kNm. However, if the plate thickness is just below 3mm so that debonding does not occur, then the beam can be reanalysed with the pivotal point at ϵ_c

= 0.003. This allows the steel to yield through the plate depth as shown by the solid line plate stress distribution in Fig. 3.43(c), in which case the moment capacity increases to 403 kNm, that is by 19%. The curvature also increases three fold from 7.8×10^{-6} to $20.0 \times 10^{-6} \text{ mm}^{-1}$. In the latter analysis where yielding preceded debonding, it was assumed that debonding never occurred. However tests have shown, such as those in rows 8 and 9 in Table 2.2 and rows 1 to 3 in Table 3.1, that metal plates do eventually debond even if designed to yield prior to debonding. Therefore when the analysis is complete, it will be necessary to ensure that the debonding strain capacity after yield, as given in Tables 2.2 and 3.1, has not been exceeded and if so then this will be the new pivotal point.

The transition thickness between yield and debonding for aluminium of yield strength 215 MPa and Young's modulus 63 GPa is about 1.8 mm. At this thickness, the yield and debonding strains are 0.00341. When debonding controls, the moment capacity is 355 kNm which gives a 5% increase in strength. When the aluminium can yield prior to debonding, so that concrete crushing controls the pivotal point at $\epsilon_c = 0.003$, then the moment capacity is 362 kNm which is only a 7% increase in strength. In this example, there is little benefit in using aluminium plates.

3.5.3 Beam structure with bolted plates

3.5.3.1 Full interaction flexural analysis

A comparison is made of bolting different types of plates to the sides of the web as in Fig. 3.44(a). The plates considered are of steel of Young's modulus 200 GPa and yield strength 300 MPa, aluminium of Young's modulus 63 GPa and yield strength 125 MPa, and glass/carbon FRP plates of Young's modulus 51 GPa and a fracture strength of 600 MPa. The plate thicknesses have been adjusted so that the moment capacities are almost equal.

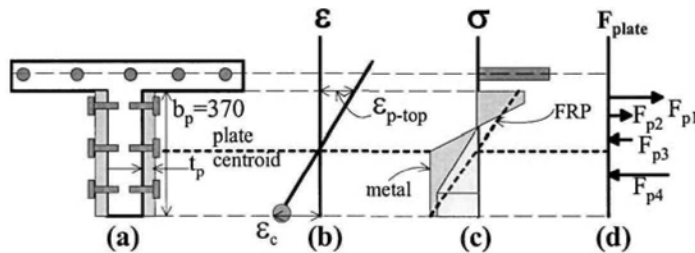


Figure 3.44 Full interaction flexural analysis of bolted plated section

A full interaction flexural analysis of a bolted plated beam is shown in Fig. 3.44. This analysis is referred to as full interaction as it assumes that there is no slip between the plate and the RC beam. Hence, the strain profile shown in Fig. 3.44(b) applies to both the plate and to the reinforced concrete beam. As this is a bolted structure and not an adhesively bonded structure, IC debonding does not occur. For the metal plates, only one pivotal point at the concrete crushing strain, as shown in Fig. 3.44(b), needs to be considered. For the FRP plate, this is also a good starting position for the pivotal point. However from this analysis, an additional check has to be made to ensure that the FRP fracture strain has not been exceeded. If it has been exceeded, then this fracture strain should be the new pivotal point. The analyses started with 10 mm thick steel plates over the full depth of the web, after which the

thicknesses of the aluminium and FRP plates were adjusted to achieve the same capacity. The results of the analyses are summarised in Table 3.5.

The 10 mm thick steel plates increased the capacity from 339 kNm to 542 kNm, in column 4 of Table 3.5, which is a 60% increase in strength. The maximum tensile strain in the plate at concrete crushing is 0.0037, in column 3, which suggests a ductile behaviour; this is the hallmark of bolted plated RC structures as there is not much, if anything at all, that can fail in a brittle fashion. To achieve the same capacity as the steel plated beams, 20 mm thick aluminium and 25 mm thick carbon/glass FRP plates are required. Because the real bolted structure will have slip between the plate and the beam, there will be a difference in curvature between the plate and the beam as shown in Fig. 3.33(b). It was recommended in Section 3.4.1.5 that the increase in the flexural capacity be reduced by 15%. Hence the increase in the flexural capacity, given by ΔM_{cap} in column 5 in Table 3.5, has been reduced by 15% in column 6 to give the design strength of the plated beam in column 7.

Table 3.5 Summary of full interaction flexural analysis: Side bolted plates

t_p [mm]	material	ϵ_{p-top}	M_{cap} [kNm]	ΔM_{cap} [kNm]	85% ΔM_{cap} [kNm]	Design M_{cap} [kNm]	P_{plate} [kN]	M_{plate} [kNm]
(1)	(2)	(3)	(4)	(5)	(6)	(7)	(8)	(9)
10	steel	0.0037	542	203	173	512	220	190
20	aluminium	0.0035	551	212	180	519	256	188
25	C/G FRP	0.0035	543	204	173	512	250	190

3.5.3.2 Bolt forces

In order to design the bolt shear connectors, we need to know the length of the hogging region L , as shown in Fig. 3.33, and in particular the length of the plate in each shear span in the hogging region L_{sh-sp} . Let us assume that the left shear span plate $(L_{sh-sp})_{left} = 1.5$ m and the right shear span plate $(L_{sh-sp})_{right} = 2.0$ m. We also need to know the axial force in the plate P_{plate} and the moment in the plate M_{plate} . These stress resultants can be derived from the stress distribution in the plate as shown in Figs 3.44(c) and (d). It is easiest to determine the resultant force in each rectangular and triangular portion of the stress distribution. For the metal plate in Fig. 3.44(c), these are shown as F_{p1} to F_{p4} in Fig. 3.44(d). The longitudinal sum of these forces is equal to P_{plate} and the moment of these forces about the centroid of the plate is equal to M_{plate} . These have been determined for all the plates in columns 8 and 9 in Table 3.5 where M_{plate} and P_{plate} are the stress resultants in both side plates in a shear span as in Fig. 3.44..

As an example, let us determine the bolts required for the carbon/glass FRP plate of 25 mm thickness in Table 3.5. For the left shear span in Fig. 3.33, the bolt shear connectors have to resist a longitudinal force of $P_{plate} = 250$ kN. The vertical shear force in both plates on the left shear span is $(V_{plate})_{left} = M_{plate}/0.7(L_{sh-sp})_{left} = 190/(0.7 \times 1.5) = 181$ kN. Therefore, the total vertical shear force in the left shear span is $2(V_{plate})_{left} = 2 \times 181 = 362$ kN; there being two vertical forces in each shear span. Therefore, the total shear force that the bolts have to resist in the left shear span is $250 + 362 = 612$ kN. The shear capacity of bolt shear connectors can be determined from the manufacturer's recommendations or from simple push tests. If we assume that the strength of the bolt shear connectors for the carbon/glass plate is 20 kN, then the number of bolts required in the left shear span is $612/20 = 30.6$. The number required on one side of the left shear span is $30.6/2 = 15.3$. If we assume that there are two

rows of bolts, then the number per row is $15.3/2 = 8$. Therefore, the longitudinal spacing in Fig.3.33 in the left shear span is $1500/8 = 188$ mm.

The number of bolts in the right shear span will be slightly less than the left shear span as the right shear span is longer and, hence, there is a larger lever arm to resist M_{plate} . The right shear span has to resist the same longitudinal force of $P_{plate} = 250$ kN. $(V_{plate})_{right} = M_{plate}/0.7(L_{sh-sp})_{right} = 190/(0.7 \times 2.0) = 136$ kN. Therefore, the total vertical shear force is $2(V_{plate})_{right} = 2 \times 136 = 272$ kN. The total shear force is $250 + 272 = 522$ kN. The number of bolts required in the right shear span is $522/20 = 26.1$, the number on one side is 13.0, and assuming two rows gives 7 bolts per row. Therefore, the longitudinal spacing in the right shear span is $2000/7 = 286$ mm.

3.5.4 Moment redistribution in metal plated hinges: flexural rigidity approach

The slab in Fig. 3.45(a) has the same amount of tension reinforcing bars in the hogging and sagging regions as shown in Fig. 3.45(d); the flexural capacity of the unplated section is 31 kNm. The slab is to be strengthened using the same mild steel plates in the hogging and sagging regions as shown in Fig. 3.45(d) where A_p is the cross-sectional area of the plate, so that the moment capacity increases to 55 kNm. These plates are to be designed so that they yield before they debond; but it is worth bearing in mind that the steel plates will definitely debond after yielding but at a much higher plate strain ϵ_{db} given in Tables 2.2 and 3.1. As the strength of the plated hogging region is the same as that of the plated sagging region as shown in Fig.3.45(b), the variation of the moment at failure, the *strength* line in Fig. 3.45(b), is different from the *elastic* distribution as shown. To reduce the hogging moment from 73 kNm to 55 kNm requires a moment redistribution of 25% of the hogging moment; this will allow both the hogging and sagging capacities to be reached in the continuous beam. It needs to be determined what is the minimum debonding strain that will allow sufficient ductility for full moment redistribution. Once this debonding strain is determined, then the plate thickness can be chosen from, for example, those in rows 1 to 3 in Table 3.1 and rows 8 and 9 in Table 2.2.

The flexural rigidity approach described in Section 3.3.2 will be used to determine the required debonding strain capacity. To apply this technique, we need the moment/curvature relationship for the plated sections, such as those shown in Fig. 3.17, as well as the variation in the plate strain with the curvature. These relationships can be determined directly from the iterative analyses described in Fig. 3.29 where the pivotal point is now the plate strain ϵ_p instead of ϵ_{db} in Fig. 3.29(c). Pivoting about a specific plate strain ϵ_p will give the moment M and curvature χ and, hence, the following secant flexural rigidity for that specific plate strain ϵ_p .

$$EI = \frac{M}{\chi} = \frac{M(1 - k_u)d}{\epsilon_p} \quad 3.6$$

where for convenience the effective depth d is taken as the full depth of the beam as in Fig. 3.15. The complete M/χ relationship and χ/ϵ_p relationship can be determined by changing the magnitude of ϵ_p . Alternatively, the relationships can be approximated as follows.

The M/χ variation has been approximated to the bi-linear relationship shown in Fig. 3.46. The flexural capacity $M_u = 55$ kNm can be determined from standard analyses of RC beams with steel reinforcement that can yield if required and in which debonding is ignored. The flexural rigidity of the cracked plated section $EI_{hcr} = EI_{scr} =$

$EI_{cr} = 2.84 \times 10^{12} \text{ Nmm}^2$ was calculated from a linear elastic analysis that assumed that the tensile strength of the concrete was zero. Knowing M_u and EI_{cr} , the curvature at point A can be determined as $\chi_A = 1.9 \times 10^{-5} \text{ mm}^{-1}$, and the plate strain as $(\epsilon_p)_A = 0.0021$. As we are dealing with metal plates that yield, the plastic zone DF can be assumed to be horizontal and failure occurs when the concrete crushes at point C at $\epsilon_c = 0.003$. The curvature at point C is $\chi_C = 14.4 \times 10^{-5} \text{ mm}^{-1}$ and $(\epsilon_p)_C = 0.0185$. The problem is to define what is happening between points D and F, that is, to relate the flexural rigidity, such as at point E, of EI_{ep} with the strain in the plate ϵ_p .

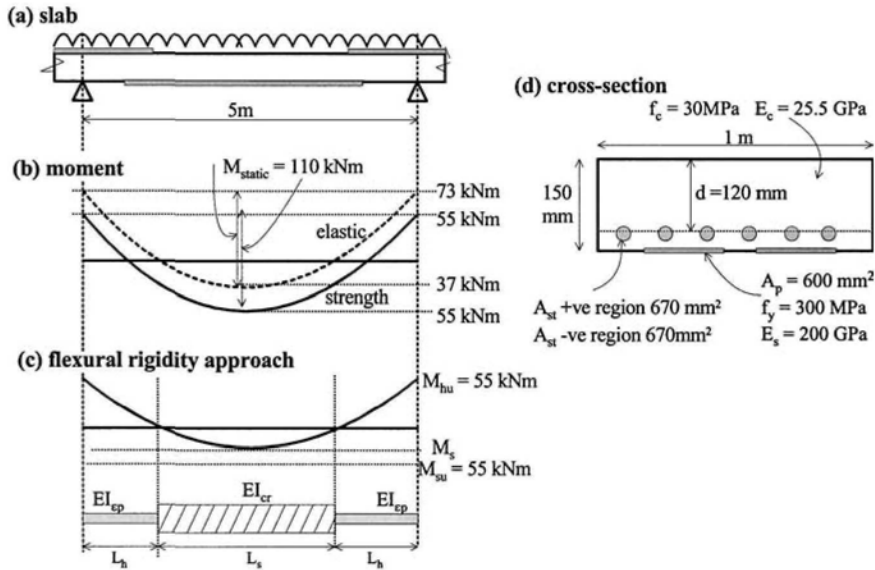


Figure 3.45 Moment redistribution in a steel plated slab

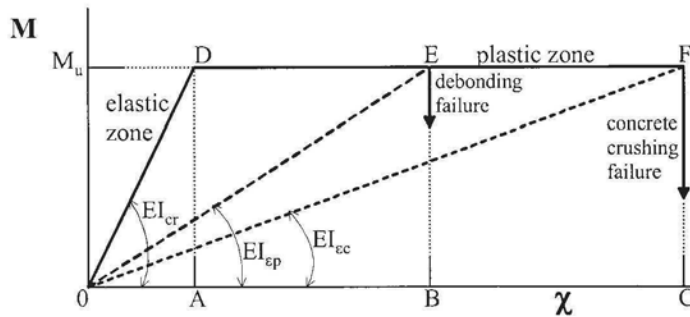


Figure 3.46 Idealised moment/curvature relationship

The method of approximating the flexural rigidity for a given plate strain is illustrated in Fig. 3.47. The depth of the slab is d in Fig. 3.47(a) and the distance from the reinforcing bars to the tension face is c . In the strain profile in Fig. 3.47(b), the plate strain is ϵ_p and this is used as the pivotal point as in the propped construction;

otherwise, the residual stress will have to be added to ε_p to get the pivotal point as explained in Section 3.4.2. The strain in the concrete at the transition from the elastic zone to the plastic zone is ε_e which, in this example, has a value of 0.001 as shown in Fig. 3.38(e). The vertical position of ε_e in Fig. 3.47(b) is given in terms of β as shown. The stress profile is given in Fig. 3.47(c). It is assumed that the reinforcing bars have yielded and as the strain in the plate is known as it is the pivotal point, the stress in the plate is also known. The resulting forces are given in Fig. 3.47(d) and their distance from the top compressive fibre in Fig. 3.47(e).

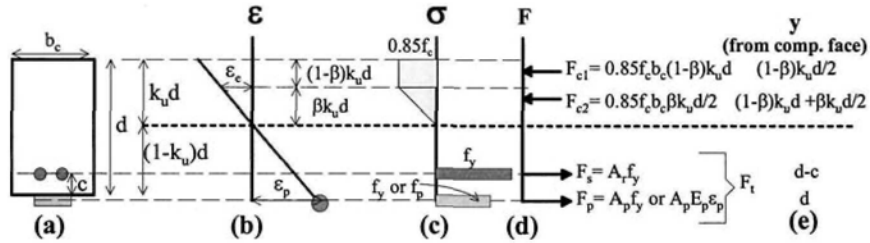


Figure 3.47 Flexural rigidity

From compatibility in Fig. 3.47(b), the position of the transition strain ε_e is given by the following α term

$$\beta = \frac{\varepsilon_e}{\varepsilon_p} \frac{1 - k_u}{k_u} \quad 3.7$$

Note that the following equations are derived for the case shown in Fig. 3.47(b), that is for $\beta \leq 1$. From equilibrium of the longitudinal forces in Fig. 3.47(d)

$$F_t = 0.85 f_c b_c k_u d (1 - 0.5\beta) \quad 3.8$$

where F_t is the total tensile force and in which it is assumed that the reinforcing bars have yielded. If this cannot be assumed, then the standard iterative procedure as described in Section 3.4 has to be applied. Eliminating β from Eqs 3.7 and 3.8 gives the neutral axis depth factor as

$$k_u = \frac{(2F_t \varepsilon_p) + (0.85 f_c b_c d \varepsilon_e)}{0.85 f_c b_c d (2\varepsilon_p + \varepsilon_e)} \quad 3.9$$

Hence the flexural rigidity at a plate strain of ε_p can now be derived from Eq. 3.6, where d is the depth of the beam and M is the moment in the beam when the plate strain is ε_p . For metal plates the moment M can be assumed to be the ultimate moment capacity M_u as the plastic zone is generally considered horizontal. However, if a more accurate value is preferred, then the moment can be determined by taking moments of the forces in Fig. 3.47(d) where their lever arm from the compression face is given in Fig. 3.47(e).

Having determined the M/χ relationship in Fig. 3.46 and in particular its dependence on the plate strain ϵ_p , the analysis procedure can follow the steps described in Section 3.3.2 and illustrated in Fig. 3.45(c). As the hogging moment is redistributing its moment to the sagging region, the flexural rigidity of the sagging region will remain at EI_{cr} in Fig. 3.46 whilst the hogging region moves along the plastic zone D-F in Fig. 3.46 with varying secant flexural rigidities EI_{ep} , depending on the strain in the plate. For a given plate strain ϵ_p , we know the flexural rigidity EI_{ep} from Fig. 3.46 and as we already know the sagging flexural rigidity, these can be inserted into the beam in Fig. 3.45(c). Any magnitude of load can be applied and the analysis iterated until the step changes in the EI variations along the beam coincide with the points of contraflexure. When they do coincide, the analysis will give the ratio of the maximum hogging to maximum sagging moments M_h/M_s . As the hogging joint is redistributing moment $M_h = M_u$, this will give M_s . If $M_s < M_u$ then the debonding strain will have to be increased to reduce the flexural rigidity of the hogging region to try to achieve the moment redistribution required that is when $M_s = M_u$.

The analysis described in the previous paragraph was carried out for the slab structure shown in Fig. 3.45. The results are summarised in Table 3.6 for a range of plate debonding strains ϵ_p within the plastic zone D-F in Fig. 3.46. The values for the length of the hogging L_h , shown in Fig. 3.45(c), and M_h/M_s in Table 3.6 were determined using a basic plane frame analysis program. An iterative solution technique was required to solve for L_h such that L_h is located at the point of contraflexure, that is the moment is zero. To coincide with the example slab shown in Fig. 3.45 a uniformly distributed load of 35.2 kN/m was used in the plane frame analysis so that $M_{static} = 110$ kNm. The corresponding percent moment redistribution, %MR, for the given plate strain is given in the last column of Table 3.6 and is shown graphically in Fig. 3.48 where it can clearly be seen that the required debonding strain for increasing moment redistribution increases at an increasing rate.

Table 3.6 Summary of the moment redistribution analysis using the flexural rigidity approach

ϵ_p ($\times 10^{-3}$)	k_u (Eq. 3.9)	β (Eq. 3.7)	EI_{ep} ($\times 10^{12}$) [Nmm ²] (Eq. 3.6)	L_h [mm]	M_h/M_s	%MR
4	0.215	0.912	1.619	900	1.450	10.8
5	0.197	0.813	1.324	850	1.296	14.9
6	0.185	0.734	1.121	800	1.178	18.5
7	0.176	0.669	0.971	760	1.091	21.4
8	0.169	0.614	0.857	730	1.016	24.0
9	0.164	0.568	0.767	710	0.957	26.3
10	0.159	0.528	0.694	690	0.905	28.4
11	0.156	0.494	0.633	670	0.861	30.3
12	0.152	0.463	0.583	650	0.821	32.1
13	0.150	0.437	0.540	630	0.789	33.6
14	0.148	0.413	0.502	610	0.759	34.9
15	0.146	0.391	0.470	600	0.732	36.3
16	0.144	0.372	0.441	590	0.708	37.5
17	0.142	0.354	0.416	580	0.685	38.8
18	0.141	0.338	0.394	570	0.664	39.9

Figure 3.48 is used to determine that the minimum required debonding strain for the steel plates proposed to strengthen the slab in Fig. 3.45 and achieve the 25%

moment redistribution of the hogging moment is 0.0085. From row 9 in Table 2.2 and rows 1 to 3 in Table 3.1 the steel plate thickness required to achieve this debonding strain is less than 2 mm.

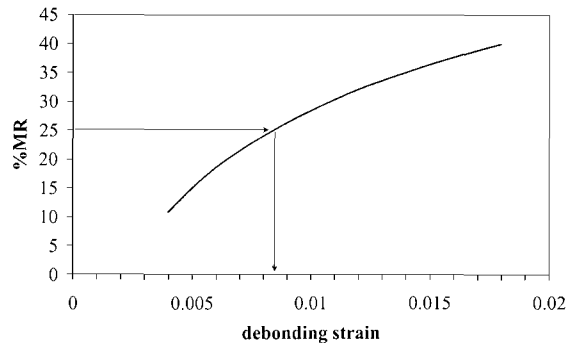


Figure 3.48 Minimum required debonding strain for steel plates

3.6 Conclusions

IC debonding affects both the sectional flexural strength and ductility, as well as the ability of a beam to redistribute moment. Generic analysis techniques have been described for determining the flexural strength and ductility for any type of plated structures as well as determining the amount of moment redistribution that IC debonding allows. We have now covered IC debonding at positions of maximum moment such as those shown in Fig. 2.1. The next stage of the analysis is to ensure that critical diagonal crack (CDC) debonding does not weaken the structure and this is covered in Chapters 4 and 5.

3.7 References

- Oehlers, D. J. and Bradford, M. A. (1995). *Composite Steel and Concrete Structural Members: Fundamental Behaviour*. Pergamon Press, Oxford.
- Oehlers, D.J. and Bradford, M.A. (1999). *Elementary behaviour of Composite Steel and Concrete Structural Members*. Butterworth Heinemann, Oxford.
- Oehlers, D.J., Ahmed, M., Bradford, M.A and Nguyen, N.T. (2000) "Retrofitting reinforced concrete beams by bolting steel plates to their sides. Part 2: Transverse interaction and rigid plastic design." *Journal of Structural Engineering and Mechanics*, An International Journal, September, Vol.10, No.3.
- Oehlers, D.J., Ju, G., Liu, I., and Seracino, R., (2003a) "Moment redistribution in continuous plated RC beams. Part 1 Tests". Submitted for publication.
- Oehlers, D.J., Liu, I., Ju, G., and Seracino, R., (2003b) "Moment redistribution in continuous plated RC beams. Part 1 Design". Submitted for publication.
- Smith, S.T., Bradford, M.A. and Oehlers, D.J. (1999) "Local buckling of side-plated reinforced concrete beams. Part 1: Theoretical study. *ASCE Structural division, Journal of Structural Engineering*, June, 622-634.
- Smith, S.T., Bradford M.A. and Oehlers, D.J. (2000) "Unilateral buckling of elastically restrained rectangular mild steel plates". *Journal of Computational Mechanics*, Vol.26, No.4, 317-324.
- Smith, S.T., Bradford, M.A., and Oehlers, D.J. (2001) "Buckling tests on steel plates restrained at discrete points in the retrofit of reinforced concrete beams", *Proc. ICE, Structs. & Bldgs*, 146(2), 115-127, May.

Chapter 4: CDC Debonding of Tension Face Plates

4.1 Introduction

Chapter 3 is concerned with the effect of IC debonding on the flexural strength, flexural stiffness and flexural ductility of adhesively bonded plated beams and slabs. It was shown that the IC debonding resistance controls the initial stages of the design as it determines: the size, type and position of the adhesively bonded plate; the region where adhesive bonding can be applied; the amount of moment redistribution that can occur; and the maximum increase in the overall strength of the beam that can be attained. Hence at this stage, the beam or slab has been designed at the positions of maximum moment, as in Fig. 2.1, and this is based on the IC debonding resistance. The longitudinal extent of the plate, that is the length of plate beyond the position of maximum moment in Fig. 2.1, depends on the region of the beam where the flexural strength has to be increased over that of the unplated beam such as the region D-D in Fig. 3.39. Furthermore, the extent of plating depends on the IC debonding design philosophy that has been applied, as described in Section 2.5. For the anchorage philosophy described in Section 2.5.1, the plate has to be extended to at least the points of contraflexure. Whereas for the hinge philosophy in Section 2.5.2, the plates can be terminated short of the points of contraflexure.

Having designed for IC debonding, the next step in the design procedure is to ensure that the plate does not debond due to the rigid body displacement induced by the formation of a critical diagonal crack (CDC) as shown in Figs. 1.17 to 1.19, which is the subject of this chapter. An example of CDC debonding in a tension face plated beam in which the plate ends are trapped by the supports is shown in Fig. 4.1. As the plate ends were trapped by the supports, plate end debonding as explained in Section 1.3.3 could not have occurred. Furthermore, IC debonding needs flexural or flexural-shear cracks which are not present. This leaves CDC debonding which requires a rigid body displacement on either side of the critical diagonal crack which is clearly visible.

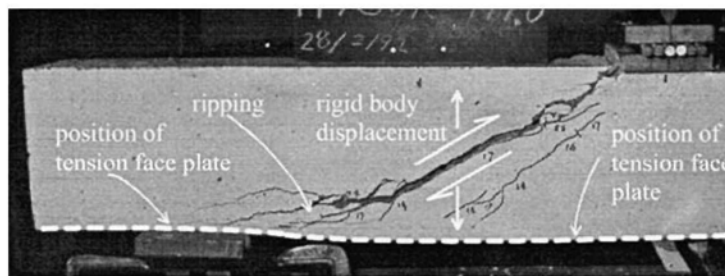


Figure 4.1 CDC debonding of tension face plate trapped by supports

It must be emphasised that a CDC is not the inclined crack associated with flexural-shear cracks such as those in Fig. 1.15. A CDC is the diagonal crack that extends virtually through the depth of the beam or slab as shown diagrammatically in Fig. 2.1 and can clearly be seen in Figs. 1.18, 1.19, 1.38, 1.39 and 4.1. It is the rigid body displacement across this CDC, in the form of sliding and/or rotation, that

governs the shear capacity of the beam or slab without stirrups V_c . The position of the CDC also controls the extent of plating. As CDC debonding depends on the formation of the critical diagonal crack, CDC debonding is rarely a problem in plated slabs as the vast majority of slabs are designed without stirrups and, hence, are designed for V_c so that a CDC does not occur. However, most beams have stirrups and, therefore, rely on both the concrete shear capacity V_c and the shear resisted by the stirrups V_s . Hence beams are prone to CDC debonding when the shear load exceeds V_c which may be well before the shear capacity of the beam V_c+V_s has been attained. Beams are particularly prone to CDC debonding in the hogging regions where the vertical shear force is at its largest, as shown in Fig. 2.1(a). Hence in some beams, it may not be possible to adhesively bond plates in the hogging region due to CDC debonding, in which case the plates can be bolted. However, it may be possible to adhesively bond plates to the sagging regions where the vertical shear is less and because plates inhibit the formation of the CDC, that is increase V_c .

As the design guidelines listed in Table 1.1 only cover tension face plates as in Fig. 2.1(b), this chapter has been restricted to CDC debonding of tension face plates so that a comparison between the different design guidelines can be made. The CDC debonding of all the other types of plates and positions, as in Figs. 2.1(c) and (d), is covered in Chapter 5. It will be shown that CDC debonding depends on the IC debonding resistance of the plate spanning the CDC, that the CDC debonding resistance is the same mechanism as that which controls the vertical shear capacity of beams without stirrups, and that stirrups do not inhibit CDC debonding.

4.2 CDC debonding mechanism

4.2.1 CDC debonding mechanism

The rigid body displacement across a critical diagonal crack that induces CDC debonding has already been described in Section 1.3.2 and illustrated in Fig. 1.17. The sliding action across the CDC A-B in Fig. 1.17, accompanied by some rotation as shown, causes the plate to peel away, starting from the root of the crack at B, and propagating towards the plate end at C. Numerous tests with metal plates and pultruded FRP plates have shown that the presence of stirrups has virtually no effect on CDC debonding; probably because the plates debond at the very early stage of the rigid body displacement which is not sufficient to stretch the stirrups to resist shear. Therefore, CDC debonding is not a function of the shear resisted by stirrups V_s , but it is a function of the shear capacity of the beam without stirrups V_c .

The ability of a reinforced concrete element without stirrups to transfer shear across a crack, V_c , is illustrated in Fig. 4.2 for a cracked concrete element with longitudinal reinforcing bars that span the crack. Shear is directly transferred across the crack by the dowel action of the reinforcing bars P_{dowel} ; this dowel action is induced by the shear displacement across the crack which causes these bars to transfer the shear by bearing against the concrete, in much the same way as stud shear connectors transfer shear in composite steel and concrete beams. Shear is also transferred by the mechanism of aggregate interlock. The aggregate interlock mechanism requires that the crack surface is very uneven with numerous protrusions and indentations formed by the individual aggregates, so that any shear displacement across the crack causes the crack surfaces to separate by riding over each other which induces tensile forces in the reinforcing bars P_{bar} as shown. These tensile forces require compressive forces P_{inter} across the interface to maintain equilibrium, as

shown. They are referred to in Fig. 4.2 as passive normal forces as they disappear when the shear force is removed. These passive normal forces induce the passive shear resistance which transfers the shear and which is much larger than a frictional force because of aggregate interlock. Hence the reinforcing bars resist the interface shear by dowel action directly and provide the normal interface force for the shear transferred by aggregate interlock.

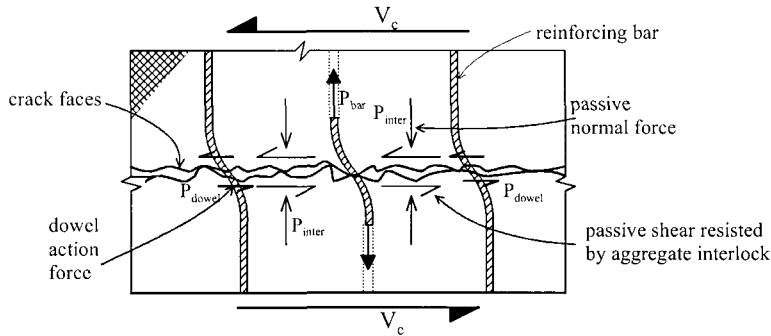


Figure 4.2 Passive aggregate interlock forces

The mechanism of transferring shear across a pre-existing crack, described in Fig. 4.2, also transfers some of the shear across a critical diagonal crack. Consider the critical diagonal crack at B in Fig. 4.3 which has been shown as a smooth straight interface but in reality is very rough with protrusions and indentations and also curved which further enhances the shear transferred by aggregate interlock. The sliding action across this crack, due to the shear rigid body displacement, is resisted directly by the dowel force P_{dowel} ; although this dowel contribution may be quite small as the reinforcement is close to the concrete surface at a distance c and, hence, the dowel strength will probably be reduced considerably due to ripping along the level of the longitudinal reinforcing bars as shown in Fig. 4.1. However, the bars can still resist the opening of the diagonal crack induced by the aggregate interlock mechanism. The bars resist the aggregate interlock crack opening mechanism by going into tension with a force shown as P_{bar} which has an upper limit of the axial capacity of the bar $A_s f_y$. The tensile force in the bar P_{bar} must induce a compressive force across the interface P_{inter} for equilibrium, which then transfers the shear through aggregate interlock. The same can be said for the plate spanning the diagonal crack, where the dowel force contribution is probably even less than that contributed by the longitudinal bars particularly for FRP plates which are generally very thin. However, the tensile force in the plate, which depends on the IC debonding resistance P_{IC} can be quite substantial, and also contributes to the interface force P_{inter} and, hence, to the shear transferred by aggregate interlock.

It can be seen in Fig. 4.3 that the plate can be considered to act as additional longitudinal reinforcing bars by providing an additional passive compressive interface force P_{inter} across the crack. Alternatively, the plate can be considered to directly provide a passive prestress P_{inter} across the crack that is induced by the aggregate interlock mechanism. It can also be seen in Fig. 4.3 that the IC debonding resistance provided by the plate P_{IC} depends on the bonded anchorage length L_p between the root of the CDC and the plate end; the anchorage length required to achieve full anchorage L_c is quantified in Eq. 2.3 and, hence, P_{IC} also depends on the position of the diagonal